Roles of PPARγ and Lactate Metabolism in The Hypoxic Response of Trophoblasts

by

Tiffany Marie Bernardo

BS, The Pennsylvania State University, 2014

Submitted to the Graduate Faculty of the

School of Medicine in partial fulfillment

of the requirements for the degree of

Doctor of Philosophy

University of Pittsburgh

2020

UNIVERSITY OF PITTSBURGH

SCHOOL OF MEDICINE

This dissertation was presented

by

Tiffany Marie Bernardo

It was defended on

December 18, 2019

and approved by

Donna Beer Stolz, PhD, Department of Cell Biology

Yoel Sadovsky, MD, Department of OBGYN and Reproductive Sciences

Wendy M. Mars, PhD, Department of Pathology

Jon D. Piganelli, PhD, Department of Surgery

Dissertation Director: Yaacov Barak, PhD, Department of OBGYN and Reproductive Sciences

Roles of PPARγ and Lactate Metabolism in The Hypoxic Response of Trophoblasts

Tiffany Marie Bernardo, PhD

University of Pittsburgh, 2020

Normal placental development and function is critical for the viability and growth of the developing embryo. Oxygen gradients are a key determinant in normal placental development, as evidenced by the severe defects in placentas deficient for the transcription factor Hypoxia-Inducible Factor α (*Hif1a*) and its regulators. Additionally, aberrant oxygenation is a frequent driver of placental pathologies, including intrauterine growth restriction and preeclampsia. Placentas deficient for the nuclear receptor Peroxisome Proliferator-Activated Receptor γ (*Pparg*) exhibit severe, lethal vascular defects that strongly resemble those in knockouts of HIF1α pathway genes. This dissertation establishes that PPARγ is essential for sustained HIF1α activation and survival of trophoblasts during acute hypoxic exposure. Hypoxia necessitates a switch from aerobic respiration to glycolytic metabolism, which is largely mediated by HIF1α target genes, augmenting lactate synthesis. Importantly, placental PPARγ strongly regulates Lactate Dehydrogenase B (*Ldhb*) and Pyruvate Carboxylase (*Pcx*), two enzymes whose tandem action converts lactate to oxaloacetate. Metabolomic profiling revealed significantly elevated levels of both L-lactate and pyruvate in PPARγ-null trophoblast stem cells cultured under acute hypoxic conditions. Moreover, pharmacological manipulation of anaerobic glycolysis inhibited the sustained activation of HIF1α, PPARγ and additional downstream proteins in hypoxic trophoblast cultures. Stable human trophoblast cell lines engineered to lack key hypoxia regulatory proteins were used to further delineate the PPARγ-HIF1α axis. *In vivo,* analyses of the effect of *Ldhb* deficiency on vascular development of placentas subject to hypoxic stress found that whereas

Ldhb-null and WT placentas are grossly similar in normoxic pregnancies, *Ldhb* deficiency ameliorated vascular anomalies in placentas from hypoxic pregnancies. These data implicate PPARγ as a crucial player in the hypoxic adaptation of trophoblasts. We further hypothesize that PPARγ regulates the HIF1α axis, in part, by controlling the intracellular levels of lactate and its metabolites.

Abbreviations

α – anti
129 – 129S1/SvlmJ
AH – Armenian hamster
AR – AR-C155858
ARNT – aryl hydrocarbon receptor nuclear translocator
ANOVA – analysis of variance
ATP – adenosine triphosphate
B6 – C57BL/6J
CP – chorionic plate
CT-2 – cytoplasmic tail of Muc1
Dec – decidua
DNA – deoxyribonucleic acid
dox - doxycycline
E – embryonic day
EC – endothelial cell
EPC – ectoplacental cone
ESC – embryonic stem cell
EtOH - ethanol
EVT – endovascular extravillous cytotrophoblasts
ExE – extraembryonic ectoderm
FGF4 – human fibroblast growth factor-4
FGR – fetal growth restriction
FLAG – polypeptide protein tag
FSK – forskolin
FWD – forward
FX – FX11
GLUT – glucose transporter
GlyT – glycogen trophoblast
h - hour
H&E - Hematoxylin and eosin
HIF – hypoxia-inducible factor
HRE – hypoxia response element
ICM – inner cell mass
ICP – intrahepatic cholestasis of pregnancy
IF – immunofluorescence
JEG-3 – human choriocarcinoma cell line
JEG 5.1 – JEG-3 with rtTa-Cas9 stable integration
JZ – junctional zone
Kb - kilobase
kD, kDa – kilodalton
KO – knock out
Lab - labyrinth
LDHA – lactate dehydrogenase A
LDHB – lactate dehydrogenase B

mAb – monoclonal antibody
MCT – monocarboxylate transporter
MEF – mouse embryonic fibroblasts
MEM – minimum essential medium
MeOH - methanol
mRNA – messenger RNA
MW – molecular weight
ND – not determined
NDRG – N-myc downregulated gene
neo – neomycin resistance gene
OAA – oxaloacetate
OCT – optimal cutting temperature compound
ODD – oxygen-dependent degradation domain
Oligo - oligonucleotide
O/N – overnight
Ox – sodium oxamate
PA – phenylacetic acid
PBS – phosphate buffered saliene
PCR – polymerase chain reaction
PCX – pyruvate carboxylase
PDHC – pyruvate dehydrogenase complex
PDK1 – pyruvate dehydrogenase kinase 1
PFA – paraformaldehyde
PGK1 – phosphoglycerate kinase 1
PHD – prolyl hydroxylase domain-containing protein
PMSF - phenylmethylsulfonyl fluoride
pO_2 – partial pressure of oxygen
PPARγ – peroxisome proliferator-activated receptor gamma
puro - puromycin
qPCR – quantitative PCR
Rev – reverse
RNA – ribonucleic acid
Rosi – rosiglitazone
RT – room temperature
RPMI 1640 – Roswell Park Memorial Institute medium
RT-PCR – reverse transcriptase-PCR
RXRα – retinoid X receptor α
sd – standard deviation
SDS – sodium dodecyl sulfate
SDS-PAGE – SDS-polyacrylamide gel electrophoresis
sgRNA – single guide RNA
SpT - spongiotrophoblast
sTGCs – sinusoidal trophoblast giant cells
synT – syncytial trophoblast
TCA – tricarboxylic acid
TE – trophectoderm

TF – transcription factor
TGCs – trophoblast giant cells
TSCs – trophoblast stem cells
VEGF – vascular endothelial growth factor
vCTB – villous cytotrophoblasts
VHL – von Hippel-Lindau
WT – wild type

Table of Contents

List of Tables

List of Figures

Preface

The basis for the dissertation before you set out to answer one simple question – why do *Pparg*-null embryos die? What started out as a relatively straightforward path rapidly devolved into a labyrinth (*no pun intended*) of seemingly endless alternative routes, side projects, and exciting possibilities. Oftentimes, it felt as though there were more questions than answers, which solidified the idea that we had uncovered just the tip of a massively intricate and complex iceberg. While this dissertation certainly doesn't contain all the answers, I hope it enlightens the reader on the critical role of a PPARγ-HIF1α axis in placental development, and inspires future research on the topic.

To all of my friends and family - Thank you for your unwavering support, love, and laughter through all the years of this crazy ride. I wouldn't have been able to do it without you.

Tali and Fran – Thank you for being so many wonderful things. You both have acted as my mentor, problem-solver, shoulder to cry on, and support system. It meant the world to me.

To my committee members – Thank you for all of the thoughtful conversations and helpful discussions. You all have helped shape this project into something I'm extremely proud of.

Yaki – There aren't enough words. Thank you so very much for all of your guidance, support, patience, advice, and ultimately, friendship. You've made me a better person.

Though the course may change sometimes,
rivers always reach the sea.
–*Led Zeppelin*

1.0 Introduction

1.1 The placenta is essential for mammalian embryogenesis

The evolution of a maternal-fetal transport interface is a recent pregnancy adaptation that is critical for prolonged intrauterine mammalian embryogenesis (Maltepe and Fisher, 2015). Early in gestation, the developing conceptus fulfills its bioenergetic requirements via facilitated diffusion of glucose, pyruvate, and lactate (Gardner and Leese, 1988). As gestation progresses, the nutritional demands of the developing embryo exceed the limits of diffusion and necessitates the formation of an efficient transport interface (Brett et al., 2014). The placenta functions as bridge between maternal and fetal vascular compartments, and facilitates the bilateral exchange of gases, nutrients, and waste (Lewis RM et al., 2012). In addition to its transport functions, the placenta secretes hormones essential for pregnancy maintenance, and confers immune protection to the developing fetus (Delorme-Axford et al., 2014).

Accordingly, defects in placental development or function have dire consequences, and often result in fetal growth restriction (FGR), preterm labor, stillbirth, and/or death. It has been hypothesized that placental defects are the underlying cause of first and second trimester non-chromosomal human pregnancy losses, which affect approximately 20-30% of all pregnancies (Ornoy A et al., 1981). These data were validated by analysis of genetic mutations that cause embryonic lethality in mice, confirming that ~60% of all gene knock outs (KOs) that result in embryonic death contain placental pathologies (Hemberger M et al, 2001). Furthermore, of the ~2.6 million third trimester human stillbirths that occur annually worldwide, it has been estimated that as low as 11% or as high as 65% of cases display contributory or causative placental pathology

(Kidron D et al., 2009; Ptacek I et al., 2014; Lawn JE et al., 2016). While mild placenta dysfunction in response to environmental conditions can support fetal survival, pregnancies are often accompanied by complications such as preeclampsia and FGR. FGR has been shown to increase long-term cardiovascular, neurocognitive, and metabolic disease susceptibility in adulthood, illustrating the programming power of placental responses to the intrauterine environment (Barker DJ, 2004; Sferruzzi-Perri AN and Camm EJ, 2016;). Indeed, defects in placental development and function represent a major public health problem with a substantial economic burden, and efforts to understand the placenta's role in these disease processes is of the utmost importance.

1.2 Placental development and structure

Our understanding of placental development and its role in normal pregnancy maintenance has vastly expanded over the past few decades, largely due to the advance of gene editing technologies (for in-depth reviews, see Rossant and Cross, 2001; Cross JC, 2005; Simmons DG and Cross JC, 2005;l Woods L et al., 2018). Mouse placentation begins on the third day of development (E3.5) with the formation of the outermost layer of the preimplantation blastocyst - the trophectoderm (TE). The TE is the first cell type to differentiate in the early embryo and will eventually give rise to all trophoblast lineages, which provide the primary functional and structural components of the mature placenta. The inner cell mass (ICM) forms the second of two distinct pluripotent lineages in the blastocyst and is comprised of embryonic stem cells (ESCs) that will ultimately form all tissues of the embryo proper, including the allantois and fetal vessels (Rossant J and Tam PP, 2009).

By the time of implantation (E4.5), the TE can be subdivided based on its position relative to the ICM. The mural TE, which lies in opposition to the embryonic pole, terminally differentiates and enters into endoreduplicative cycles to form primary trophoblast giant cells (TGCs) that are essential for implantation. In contrast, the polar TE borders the epiblast and continues to proliferate in response to ICM-derived fibroblast growth factor (FGF-4), to form the diploid extraembryonic ectoderm (ExE) and ectoplacental cone (EPC) of the early postimplantation conceptus (Christodoulou N et al., 2019). A secondary wave of invasive TGCs differentiate from the EPC margins post-implantation and drive maternal spiral artery remodeling, while cells of the ExE differentiate and expand to form the chorionic epithelium.

At E8.5 the allantois extends from the posterior end of the embryo and makes contact with the chorionic plate, a critical first step in establishment of the maternal-fetal vascular interface. Expression of the transcription factor (TF) *Gcm1* increases hours after chorioallantoic attachment and drives the formation of folds in the chorion. These folds act as a road map, effectively guiding the invading allantoic vessels into a structure that will form the fetal component of the placental vascular tree. As gestation progresses, the fetal vessels and intertwining maternal blood sinuses are constantly expanded and refined to produce the *labyrinth*. For the purposes of this dissertation, the labyrinth is the most relevant layer of the placenta and contains the maternal and fetal circulations, which can be likened to oil and vinegar – touching, yet never fully mixed. Both the human and mouse placenta are hemochorial, meaning that the maternal blood directly bathes the fetal trophoblasts, yet the maternal and embryonic vasculatures remains separated by a multi-layer cell barrier composed of trophoblasts. In the placenta of the mouse and most other rodents, the fetal endothelium is separated from the maternal vascular space by a total of 3 layers - two layers of multinucleate syncytial trophoblasts (synT) directly line the fetal endothelium, while an

additional layer of polyploid mononuclear cells, aptly termed the sinusoidal trophoblast giant cells (sTGCs), line the maternal blood sinuses (Rossant J and Cross JC, 2001; Woods L, 2018). The basic structure of the human placental barrier is referred to as the villus and is comprised of a two cell-layer barrier – mononucleated villous cytotrophoblasts (vCTB) directly line the fetal endothelium, while a single layer synTs are in contact with the maternal blood (Blundell C et al., 2016).

The labyrinth is structurally supported by the more distal junctional zone (JZ) - a compact layer primarily composed of spongiotrophoblasts (SpTs) that are thought to originate from the EPC of the early embryo, but whose function is still poorly understood. Intermixed in a sea of SpTs are islands of glycogen trophoblasts (GlyTs) whose name accurately implies that they store glucose in the form of glycogen, potentially as a fuel source for the embryo during times of rapid development (Tesser RB et al., 2010; Knott JG and Paul S, 2014). Finally, the entire placenta is surrounded by a one- to two-cell layer of secondary TGCs that separate it from the maternal decidua (*see diagram below*).

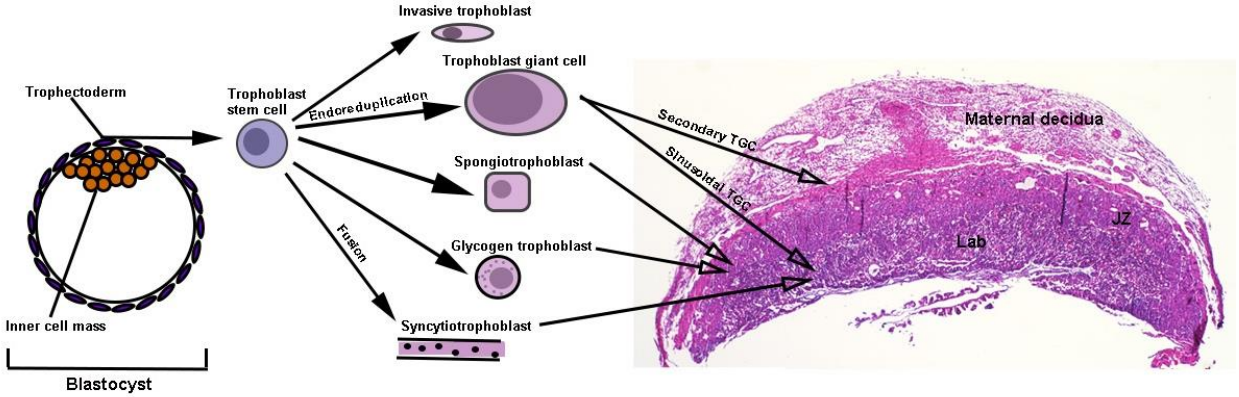

Placenta diagram

Schematic representation of the mature mouse placenta

1.3 The role of oxygen in placental development

Although the placenta develops into a highly vascularized, well-oxygenated tissue by term, early placental development occurs in a hypoxic niche that has been shown to be crucial for both fetal organogenesis and proper placentation (Dunwoodie SL, 2009). Hypoxia is defined as a decrease in the partial pressure of oxygen (pO_2) relative to the normal saturation level. Physiologically normoxic levels in most mammalian tissues range from 2-9% pO_2 although certain tissues, such as the bone marrow, kidney medulla, and thymus, often endure oxygen tensions below 1% (Simon MC and Keith B, 2008). However, oxygen tension is not absolute, and dynamic intra-tissue oxygen gradients have been demonstrated to instruct stem cell proliferation, differentiation, and maintenance to coordinate embryonic and placental development (Genbacev O et al, 1997; Tuuli MG et al., 2001).

During the first trimester of human pregnancy, the endovascular extravillous cytotrophoblasts (EVT) invade the uterine spiral arteries where they degrade resident smooth muscle and endothelial cells (ECs) and replace them with a trophoblast lining. This remodeling event converts reactive, high-resistance vessels into passive, high-capacity conduits to establish adequate perfusion of the feto-placental unit. Initially, the remodeled vessels are plugged with the endovascular trophoblasts to ensure that the conceptus develops in a relatively low oxygen environment (2.5% pO_2) (Maltepe E et al, 2015; Weiss H et al, 2016). This hypoxic niche supports embryonic organogenesis and placental angiogenesis, promotes cytotrophoblast proliferation, and suppresses trophoblast differentiation, largely due to the activity of oxygen-regulated TFs (*see sections 1.4 and 1.5*) that mediate physiological adaptation to changes in oxygen tension (Genbacev O et al, 1997; Simon MC et al, 2008; Tuuli MG et al, 2011). During this time the maternal plasma and endometrial secretions nourish the embryo, but a major switch in oxygen

tension occurs at 10-12 weeks as the demand for fuel and oxygen increases. The endovascular EVT plugs disintegrate, blood flow resumes, and the subsequent rise in oxygen tension (8.6% pO_2) drives cytotrophoblast differentiation and invasion (Rodesch F et al., 1992; Genbacev O et al., 1997). There is less information regarding trophoblast plugs in rodent models, however a similar remodeling event occurs in the maternal spiral arteries (Rossant J et al., 2001; Dunwoodie SL, 2018).

The extensive vascular network is established by E10.5-11.5 in the mouse, and its initial formation and continuous expansion throughout gestation is critically dependent on placental oxygen sensing mechanisms (Rossant J et al, 2001; Chen DB et al., 2014; Maltepe E et al., 2015;). The dependence on the morphogenetic properties of oxygen for proper placentation is also discernible in numerous mouse models, as evidenced by the abnormal placental architecture and embryonic lethality in numerous KOs of oxygen-regulated genes. Importantly, mice carrying deletions of *Hif1α/Hif2α, Arnt, Phd2, Vhl,* and *Pparg* exhibit reduced progenitor cell proliferation, impaired vascularization of the presumptive labyrinth, and a drastic decrease in total labyrinth volume (Cowden Dahl KD et al., 2005; Kozak KR et al., 1997; Takeda K et al., 2006; Gnarra JR et al., 1997; Barak Y et al., 1999). While embryonic lethality is generally attributed to the arrest of fetal vessel invasion, the primary defects often lie in the trophoblast compartment. The labyrinthine trophoblasts are thought to provide a structure into which the invading fetal vessels grow, and cross-talk between the mesoderm and trophoblasts further refines feto-placental vascularization. In the absence of proper trophoblast differentiation, i.e., without the road map for fetal vessel invasion, the labyrinth fails to vascularize.

While areas of micro-hypoxia are essential for driving trophoblast differentiation and vessel morphogenesis, chronic placental hypoxia in the absence of re-oxygenation severely

impairs placental development and function. Chronic hypoxia is the most common placental injury during human pregnancy, with effects that range from FGR to third trimester miscarriage, stillbirth, and maternal preeclampsia. Defects in maternal spiral artery remodeling, arrest of fetal vessel invasion, maternal anemia, and/or high altitude pregnancies (elevation >2700m) contributes to trophoblast dysfunction and placental hypoxic lesions including villous hypervascularity, compensatory placental overgrowth, and reduced remodeling of the maternal vessels (Hung TH et al., 2002; Stanek J, 2013). The increased expression of hypoxia-inducible factor α (HIF1α; see below) at the mRNA and protein level, as well as elevated vascular endothelial growth factor (VEGF) release from human hypoxic placentas corroborate these findings and implicates oxygen gradients and the downstream transcriptional events as key mediators of trophoblast proliferation, differentiation, and placental development (Zamudio S et al., 2007).

1.4 HIFs in placental development

Hypoxia, whether injurious or developmental, induces rapid, transient changes in carbohydrate and lipid metabolism that results in the cessation of oxygen-dependent ATP production and a sharp increase in glycolysis. The increased glycolytic capacity of hypoxic trophoblasts is due, in part, to the activity of the HIF family of TFs (Firth JD et al., 1994; Semenza GL et al., 1994). HIF proteins function as heterodimers and are composed of one of three oxygen-sensitive alpha subunits (HIF1α, HIF2α, or HIF3α), and the constitutively active subunit HIF1β/aryl hydrocarbon nuclear translocator (ARNT) (Wang GL et al., 1995; Koh MY et al., 2012). HIF1α normally resides in the cytoplasm where its expression is tightly regulated in an oxygen-dependent manner. In the presence of oxygen, HIF1α is hydroxylated by specific prolyl

hydroxylase domain-containing proteins (PHD) on two conserved proline residues located within the oxygen-dependent degradation domain (ODD) to form two hydroxyprolines, which facilitates the binding of von Hippel-Lindeau syndrome protein (VHL). VHL functions as the substrate recognition module of an E3 ubiquitin ligase, and directs HIF1α for polyubiquitination and proteasomal degradation (Ohh M et al., 2000; Jaakkola P et al., 2001). Therefore, under normal oxygen tension α subunits of HIFs are degraded. Under hypoxic conditions, the PHDs are unable to hydroxylate HIF1α and the protein is free to translocate to the nucleus. HIF1α binds its cognate hypoxia response element (HRE) as an obligate heterodimer with ARNT to positively regulate the expression of numerous hypoxia-responsive gene networks (Koh MY et al., 2012).

Both HIF1α and ARNT are abundantly expressed in both the human and mouse placenta and have been shown to have critical roles in regulating placental development, where oxygen gradients play a role in the determination of cell fate (Dunwoodie SL, 2018). Interestingly, the placental architecture in *Arnt*$^{-/-}$ embryos is severly disrupted. The null placentas display a smaller chorionic plate, decreased progenitor cell proliferation, and decreased vessel density and tortuosity in the labyrinth as compared to their WT counterparts. Embryos die by E10.5 presumably due to failure in placental vascularization (Kozak KR et al., 1997). While the placental defects in HIF1α KO embryos are less severe, placental malformations are observed as early as E9.5, and null embryos die by E11.0 (Iyer NV et al., 1998; Cowden Dahl KD et al., 2005). The allantois and chorion fail to make contact by E9.5 in 31% of *Hif1*$^{-/-}$ embryos. In the remaining 69% of *Hif1a*-null embryos that had undergone proper chorioallantoic fusion, the fetal vascular density is significantly decreased relative to WT placentas, and the vessels appear dilated. Additionally, the pool of SpTs is reduced by about 50% in the *Hif1*$^{-/-}$ placentas, suggesting that cellular differentiation programs are affected (Cowden Dahl KD et al., 2005). Conversely, *Hif2*$^{-/-}$ placentas

appeared relatively normal when compared to their WT counterparts. Most notably, they display typical fetal vessel invasion patterns, vascular density, and SpT compartment. However, when both *Hif1a* and *Hif2a* are absent, the resulting mutants display an identical phenotype to the ARNT-deficient embryos suggesting redundancy between the two HIF proteins (Cowden Dahl KD et al., 2005; Maltepe E et al., 2015). The role of oxygen in cell fate determination was also interrogated using mouse trophoblast stem cells (TSCs) - a pluripotent, self-renewing population of trophoblast cells derived from the TE of the blastocyst. In the absence of genetic manipulation, WT TSCs cells will differentiate primarily into TGCs, although SynTs and SpTs are present in the culture, and differentiation is enhanced when cells are cultured in hypoxic conditions (Tanaka S et al., 1998). Notably, $ARNT^{-/-}$, $Hif1a^{-/-}$, and $HIF2^{-/-}$ TSCs were unable to differentiate into TGCs or SpTs when cultured under standard or hypoxic conditions. Rather, these cells primarily differentiated into SynTs, confirming that oxygen is a major player in trophoblast differentiation (Cowden Dahl KD et al., 2005).

In addition, $Phd2^{-/-}$ and $VHL^{-/-}$ embryos also exhibit gross placental abnormalities. These mutations result in constitutively active HIF, and subsequent embryonic lethality. *Vhl*-null embryos were indistinguishable from their WT counterparts at E9.5, but viable embryos were not recovered past E12.5. The fetal vessels from *Vhl*-null embryos failed to invade the presumptive labyrinth, and null placentas displayed severe hemorrhaging and necrosis at the implantation site. Additionally, there was no evidence of SynT differentiation (Gnarra JR et al., 1997). Moreover, *Phd2* KO also resulted in embryonic lethality by E14.5, owing to decreased labyrinth vascularization and abnormal invasion of SpTs into the labyrinth (Takeda K et al., 2006). These findings demonstrate that both induction and inhibition of HIF levels are equally deleterious to

placental development, and therefore must be tightly regulated to ensure proper trophoblast differentiation and placentation.

1.5 Metabolic adaptations to hypoxia

While multiple gene networks are activated in response to decreased oxygen tension, the pathways that control metabolic adaptation, particularly those that control the synthesis and transport of lactate, are the most relevant to this project. Importantly, placental glucose transporters (GLUTs) and glycolytic enzymes increased in response to acute hypoxic injury are influenced by HIF1α stabilization. Studies in transformed human placental cell lines and whole villous explants have shown that the expression levels of GLUT1 and GLUT3 are increased during acute hypoxic exposure in a HIF1α-dependent manner. Baumann et al. (2007) confirmed the increase in expression correlated to increased transepithelial glucose transport in a time- and dose-dependent manner in BeWo cells, consistent with previous reports, and demonstrated that anti-sense oligonucleotides (oligos) directed against HIF1α prevented the induction of GLUT1 and GLUT3 in hypoxia. However, the induction of GLUT1 and GLUT3 was minimal in hypoxic human villous explants, possibly owing to their heterogenous nature or the short lifespan of placental explants in culture (Hayashi M et al., 2004; Baumann ME et al., 2007). Additionally, Esterman et al. (1997) reported an increase in GLUT1 expression and a subsequent decrease in the uptake of [^{3}H] 2-deoxyglucose when trophoblasts were exposed to hypoxic conditions. This discrepancy could be attributed to differences in transepithelial *transport* versus *total cellular uptake* of glucose, respectively.

The elevated uptake of glucose dictates that glycolytic flux must also be increased to keep up with cellular demand of energy. Accordingly, it was discovered that placental HIF1α regulates phosphoglycerate kinase 1 (PGK1) in human placental villous samples of pregnancies complicated by intrahepatic cholestasis of pregnancy (ICP). PGK1 catalyzes the first ATP-generating step in glycolysis, and its increased expression in complicated pregnancies suggests an increased flux through the glycolytic pathway in response to acute hypoxia, the primary suspect in the underlying pathophysiology of ICP (Wei W et al., 2014). This increased glycolytic flux is further enhanced by HIF1α-mediated upregulation of pyruvate dehydrogenase kinase 1 (*PDK1*). PDK1 phosphorylates and effectively inactivates the pyruvate dehydrogenase complex (PDHC), thereby shutting down mitochondrial respiration and diverting pyruvate for use in other pathways (Kim JW et al., 2006).

Moreover, heightened glycolytic activity is often commensurate with an increase in lactate generation. Indeed, studies have shown a HIF1α-dependent increase in expression and activity of the lactate dehydrogenase (LDH) isozyme A_4 (LDHA) in response to acute oxygen deprivation in transformed human placental cell lines and in the fetal ECs of preeclamptic villi (Tsoi SC et al., 2001; Kay HH et al., 2007). LDHA catalyzes the conversion of pyruvate to lactate and, in turn, generates the reducing equivalents required for sustained glycolysis and energy generation (Adams MJ et al., 1973). However, excessive lactate is extremely cytotoxic and is exported from the cell through HIF1α-dependent upregulation of the proton-coupled monocarboxylate transporter 4 (MCT4). MCT4 is localized to the basal plasma membrane of the second SynT layer in the mouse placenta, proximal to the fetal endothelium, suggesting that lactate is transported from either the maternal circulation or placenta to the fetus. Conversely, MCT4 is localized to the microvillus member of the SynT layer in human placentas (maternal-facing), indicating lactate flux from the

embryo into the maternal blood pools. This dichotomy between mice and humans may be attributed to the bi-directional transport capacity of the MCTs depending on the concentration gradient of lactate in the mother and fetus (Settle P et al., 2004; Nagi A et al., 2010).

1.5.1 A new role for lactate?

Traditionally, lactate is viewed as a dead-end product of glycolysis that is eliminated as waste or exported to the liver as a carbon substrate for gluconeogenesis, yet has recently been promoted to a *bona fide* signaling molecule. Accumulating evidence suggests that hypoxia-driven shifts in fuel utilization play a pivotal role in normal microvascular development, where localized hypoxic areas promote EC proliferation, migration, vessel morphogenesis, and subsequent reoxygenation of the adjacent tissue. In fact, it has been shown that migratory, hypoxic ECs primarily utilize anaerobic glycolysis to generate their ATP supply. Pyruvate, the end product of glycolysis, is reduced to lactate to generate the reducing equivalents for sustained glycolytic flux. In addition, lactate functions as a competitive antagonist for α-ketogluterate, a key intermediate of the TCA cycle, which inactivates the PHD proteins, and, in turn, promotes HIF-dependent VEGF expression. This mechanism effectively generates a positive feedback loop for enhanced angiogenesis (Lu H et al., 2002; Kumar EB et al., 2007; Fraisl P et al., 2009).

Furthermore, Lee et al. demonstrated that HIF1α-mediated induction of *Ldha* generates the increased lactate load required to bind to and physically stabilize the oxygen-regulated protein N-myc downregulated gene 3 (NDRG3) during chronic hypoxic exposure. Stable NDRG3 can then signal through the Raf-ERK pathway to promote angiogenesis and subsequent reperfusion (Lee DC et al., 2015). Interestingly, human trophoblasts express the close homolog NDRG1, an oxygen-responsive protein that protects human term trophoblasts from hypoxic insult (Chen B et al., 2006).

NDRG1 can also be detected in placentas from pregnancies complicated by FGR and preeclampsia, both of which are thought to have pathophysiological roots in abnormal placental perfusion (Choi SH et al., 2007). In addition, it has been demonstrated that *Ndrg1*$^{-/-}$ female embryos exposed to hypoxic conditions are more susceptible to lethality than their male counterparts, suggesting that NDRG1 may regulate a sex-specific response to hypoxic injury (Larkin J et al., 2014). NDRG1 can be found in the nucleus within 24 h of hypoxic exposure in human term trophoblasts, yet the function, regulation, and termination of this pathway are unclear (Shi XH et al., 2013).

1.6 PPARγ and placental development

Peroxisome proliferator-activated receptors (PPARs) are ligand-activated TFs with fundamental roles in energy homeostasis, cellular differentiation, and inflammation. Three PPAR isotypes encoded by distinct single-copy genes have been identified: PPARα, PPARβ/δ, and PPARγ (Kliewer SA et al, 1994). Alternative splicing and promoter utilization gives rise to two primary PPARγ transcripts in the human and mouse; PPARγ1 is expressed in many tissues and is the predominant isotype in the placenta, whereas PPARγ2 is localized to adipocytes and the liver, and contains a 30 amino acid N-terminal extension via an alternate transcription start site (Tontonoz et al., 1995; Lavery DN et al., 2005; Schaiff WT et al., 2006; Fournier T et al., 2007). PPARs bind to their cognate response element in the promoters of regulated genes as an obligate heterodimer with the retinoid X receptor and activate transcription in response to ligand stimulation (Kliewer SA et al., 1994). As early as E8.5, PPARγ1 expression is exclusively detected in the murine trophoblast lineages, including the SpT, SynT, and secondary TGCs, and its

expression is not present in the embryo proper until E13.5 (Barak Y et al., 1999). PPARγ is abundantly expressed in human trophoblasts starting at the 7th week of gestation, but information regarding the prevalence and significance of PPARγ deficiency in complicated pregnancies remains controversial (Meirhaeghe A et al., 2007; Barak Y et al., 2008; McCarthy FP et al., 2013).

The regulatory functions of PPARγ are critical for extraembryonic tissue development as *Pparg*-null mouse embryos die by E10.0 and are rescued by tetraploid chimeras, confirming that death is due to placental malformation (Barak Y et al., 1999). In normal pregnancy, the chorionic basement membrane forms a tight association between the fetal ECs and trophoblast layers, which is necessary for embryonic vessel invasion and nutrient exchange. The basement membrane is severely disrupted in *Pparg*-null placentas, and consequent lack of cohesion between the two cell types results in failed fetal vessel permeation and transport through the feto-placental unit. While all layers of the placenta (TGCs, SpTs, labyrinth, and chorion) are intact, the labyrinthine trophoblast precursors fail to mature and form the multinucleate barrier essential for efficient nutrient exchange and immune protection of the developing embryo. In addition, null placentas are entirely devoid of the lipid droplets that typify WT placentas (Barak Y et al., 1999). In pursuit of the mechanisms underlying the developmental arrest of *Pparg*-null placentas, transcriptional profiling revealed that the mucin gene *Muc1* is a robust target of placental PPARγ. The MUC1 protein is localized to the apical surface of the sTGCs that line maternal blood pools, and its expression is upregulated upon PPARγ agonist stimulation in mouse TSCs. However, Muc1$^{-/-}$ embryos are viable, and mutant placentas infrequently display minor maternal blood sinus dilation at worst (Shalom-Barak T et al., 2004). While compelling, these findings suggest that the relevant PPARγ target genes whose expression is indispensable for placental development remain unknown.

1.6.1 Transcriptional regulation by placental PPARγ

PPARγ is a well-established transcriptional regulator of lipid metabolism and glucose homeostasis in multiple tissues, including liver, adipose, skeletal muscle, and leukocytes. However, the metabolic functions of placental PPARγ have not been fully established (Desvergne B et al., 1999; Wahli W, 2002). Gene microarrays identified numerous PPARγ target genes in the mouse placenta, many of which are metabolic enzymes (Shalom-Barak T et al., 2012). Importantly, two of the most differentially regulated genes encode lactate dehydrogenase B (*Ldhb*), an enzyme implicated in the conversion of lactate to pyruvate, and pyruvate carboxylase (*Pcx*), an enzyme that converts the pyruvate product of LDHB to oxaloacetate (OAA) and has proven functions in lactate clearance, oxidative phosphorylation, and fatty acid (FA) synthesis (Takeno T et al., 1989; Jitrapakdee S et al., 1999; Shalom-Barak T et al., 2012). *In situ* hybridization of WT and *Pparg*-null E9.5 placentas showed that *Ldhb* expression is lost in the labyrinth and SpT layers of the null placentas as opposed to its retention in the chorion and secondary TGC layers, indicating that *Ldhb* is developmentally regulated by PPARγ in a cell-type specific manner (Shalom-Barak T et al., 2012). In the human placenta, *LDHB* expression is localized to SynTs, but its function during pregnancy is unclear (Tsoi SCM et al., 2001). Despite its evolutionary conservation across plant, fungi, and animal kingdoms, the molecular regulation and physiological importance of the LDH isozyme B_4 remains unclear (Nash WG et al., 1982). To date, at least 15 distinct mutations in the human *Ldhb* gene are known to cause lactate dehydrogenase deficiency, but patients are asymptomatic even though the enzymatic activity is significantly decreased in cardiac muscle cells (Maekawa M et al., 1994; Sudo K et al., 1994; Wakabayashi H et al., 1996; Tanis RJ et al., 1997; Takatani T et al., 2001).

Conversely, *Pcx* deficiency is an autosomal recessive rare inborn error of metabolism with three unique clinical presentations: Type A ("North American"/infantile form), Type B ("French"/neonatal form), and Type C ("Mild" form). Types A and B present in infancy or shortly after birth, respectively, and are characterized by lactic acidosis, hyperammononemia, liver failure, hypomyelination of axons, and neurocognitive delays. Patients succumb to the disease during the neonatal period or early childhood due to multi-system organ failure as a result of severe metabolic acidosis (Arnold GL et al., 2001; Garcia-Cazorla A et al., 2006). Type C, often referred to as the benign form, is characterized by intermittent attacks of lactic acidosis and moderate neurocognitive delays. The mild clinical presentation is attributed to increased residual PCX enzymatic activities permitting patient survival to at least the third decade (Stern HJ et al., 1995; Arnold GL et al., 2001). The activity of PCX was shown to increase during the fourth and final months of pregnancy in sheep placentas, but little is known regarding the distribution or relative contribution of *Pcx* to placental metabolic homeostasis (Edwards EM et al., 1977). It is tempting to postulate that these enzymes instruct placentation via trophoblast metabolic regulation, as none of the targets of placental PPARγ are conventional developmental regulators.

1.7 Thesis hypothesis and major findings

Given the phenotypic similarity between *Pparg*-null and *Hif1a*-null placentas, this study was developed to determine if (I) PPARγ and its transcriptional targets modulate key developmental and pathological adaptations to placental hypoxia, including the function of signaling proteins and tissue vascularization and (II) Enzymes that metabolize lactate play important, quantitative roles in these functions. At the onset of this study the connection between

PPARγ and HIF1α in trophoblast hypoxic signaling were yet to be explored. This thesis demonstrates that PPARγ is essential for both sustained HIF1α activation and survival of trophoblasts during acute hypoxia. Interestingly, subsequent studies elucidated a central role of lactate metabolism in the hypoxic response of trophoblasts. The remainder of the dissertation explores the intimate details of the PPARγ-HIF1α-lactate axis in trophoblasts.

2.0 Materials and Methods

2.1 Animals

Adult (6-8 week old) WT C57Bl/6 (B6) and 129SvlmJ (129) male and female mice used here were from in-house colonies propagated off of stocks purchased from Jackson Laboratories. All procedures for animal care and experimental use were in accordance with the Institutional Animal Care and Use Committees of the University of Pittsburgh and Magee-Womens Research Institute.

2.1.1 *In vivo analyses*

Ldhb-null mice were generated before the start of this project. $Ldhb^{\Delta/+}$ founders were backcrossed onto both B6 and 129 background for several generations before phenotypic analysis. $Ldhb^{\Delta/+}$ B6 dams and sires were crossed to obtain matched WT, mutant, and null placentas. Copulation plugs were used to determine the date of pregnancy (noon on the day of the plug = E0.5). Where applicable, dams pregnant with the product of heterozygous crosses were randomly allocated to either hypoxic (12% O_2) or standard (21% O_2) conditions starting at E9.5 To induce placental hypoxia, pregnant dams were reared in an O_2- and CO_2-controlled hypoxic glove box equipped with a purge airlock system, humidity control, and gaseous waste removal (Coy Laboratory Products) at 6-day intervals between mid-gestation and term. Placentas were collected at various times and separated from embryos. Excess decidual tissue was carefully removed, and yolk sac tissue was collected for genotyping. DNA was extracted from yolk sacs and the target

allele PCR-amplified with Taqman (Life Technologies) to determine embryo genotype. *Genotyping oligos*:

Table 1 - Genotyping oligos

Name	Sequence
Cre FWD	GCATTACCGGTCGATGCAACGAGTG
Cre Rev	GAACGCTAGAGCCTGTTTTGCACGTTC
WT *Ldhb* FWD	CTCCAGGTCTGCAGCTGTATCATCAG
WT *Ldhb* Rev	TGTGCACCTGTTAGCACAATCTCCA
Ldhb Δ	TTCCCGTACAGACCGTCATGGC

2.2 Generation of JEG-3 monoclonal cell lines

pCW-Cas9 (Addgene) was used to generate a doxycycline (dox)-inducible Cas9 stable cell line. A puromycin (puro)-resistant vector expressing the Dox-dependent activator, rtTa, and a Tet response element driven FLAG-tagged Cas9 (Flag-Cas9) was transfected into JEG-3 cells. Individual puro-resistant clones were selected, expanded, and incubated in the presence or absence of 1 μM dox for two days. Clones were screened for the expression of Flag-Cas9 upon dox stimulation with an α-FLAG M2 antibody (Millipore Sigma). Clone 5.1 (JEG 5.1) produced high levels of Flag-Cas9 when stimulated as compared to undetectable levels at baseline, and therefore was selected as the parent clone for all subsequent genetic modifications.

Next, a neomycin (neo)-resistant single guide RNA (sgRNA) vector was generated by subcloning the guide portion from pLKO5.sgRNA.EFS.GFP (Addgene) into Bluescript using the NotI/SalI restriction sites. Mutant monoclonal cell lines were generated by first priming JEG 5.1 with 1 μM dox for two days to induce Cas9 expression. Once primed, multiple sgRNAs directed

against the target gene were transfected into JEG 5.1 and selected with neo (400 µg/ml) such that a single cell that had undergone successful Cas9-mediated gene excision was isolated and propagated to generate individual colonies. Clones were screened via PCR, expanded, and further validated by probing with antibodies directed against the protein of interest. All plasmids and sgRNAs used are included in Appendices A and B, respectively. Antibodies used for validation are included in Appendix D. pCW-Cas9 and pLKO5.sgRNA.EFS.GFP were kind gifts from the Sadovsky lab.

2.3 TSC culture

Undifferentiated WT and *Pparg*-null mouse TSCs were maintained on a feeder layer of mitotically inactivated mouse embryonic fibroblasts (MEFs) in RPMI-1640 medium containing 20% serum, 1% sodium pyruvate, FGF4 (25 ng/ml; Sigma) and heparin (1 µg/ml). Media was changed every other day until colonies reached adequate size and subsequently passaged for various experiments. For all experiments, TSCs were cultured in feeder-free conditions with MEF-conditioned TS media supplemented with 20% serum, FGF4 and heparin. To induce differentiation, the FGF4 and heparin pressure was removed, and cells were cultured for three days in the presence or absence of various ligand combinations before experimental manipulation. Ligand concentrations are detailed in Appendix E.

2.4 *In vitro* hypoxia exposure

JEG-3 and differentiated TSCs were cultured under hypoxic conditions (<1% O_2) for 6-72 hours in the presence or absence of various ligands or inhibitors of lactate metabolism as described. For pharmacological studies, cells were first pre-treated with inhibitors and/or exogenous L-lactate for 1 hour under standard tissue culture conditions before hypoxic exposure. When necessary, cell culture media was equilibrated for 24 hours in the hypoxia chamber. Media was changed every other day until cells were collected for further processing. All chemicals and the concentrations used are listed in Appendix E.

2.5 Preparation of whole cell lysates and Western blotting

Placentas were collected from WT, heterozygous, and *Ldhb*-null mice, immediately snap-frozen in liquid nitrogen, and stored at –80°C. Cells were washed, scraped in ice-cold PBS, pelleted, and stored at –80°C. Whole placentas and cell pellets were extracted in lysis buffer (50 mM Tris pH 8.0, 150 mM NaCl, 5 mM EDTA, 0.5% NP-40, 25 µg/ml aprotinin and leupeptin, 1.25 mM phenylmethylsulfonyl fluoride [PMSF]), and cleared by centrifugation.

For Western blotting, all samples were diluted, supplemented with 4x Laemmli buffer containing β-mercaptoethanol, and fractionated on a 10% denaturing acrylamide gel. Proteins were transferred onto a nitrocellulose membrane and probed with various antibodies. Bands of interest were detected by chemiluminescence according to manufacturer's instructions (ThermoFisher Scientific). β-actin was used as a loading control. All primary antibodies and their dilutions are listed in Appendix E.

2.6 Expression analyses

RNA was extracted from TSCs using the Trizol method. RNA quality and purity were confirmed by a formaldehyde gel and nanodrop analysis, respectively, prior to quantitative complementary DNA (cDNA) synthesis. RT and quantitative PCR (qPCR) were performed with qPCR kits from Applied Biosystems according to manufacturer's instructions, and samples were run on a CFX96 Touch thermocycler from Bio-Rad Laboratories. Oligo pairs for each gene of interest were based on Primer Bank whenever available or designed using the Primer3 shareware. qPCR reactions were normalized to the *Dazap1* gene, which was relatively unchanged over the course of TSC differentiation and Rosi treatment as identified in the lab's extensive screens. Relative expression levels were transformed to a linear scale by the ΔΔCT method and analyzed with a one-way analysis of variance (ANOVA) and Tukey's *post hoc* test (Livak et al., 2001). Expression under standard tissue culture conditions in the absence of Rosi was assigned a relative value of 1.0. *Pparg*, *Muc1*, and *Dazap1* oligo pairs used were described previously (Shalom-Barak T et al., 2012). Additional oligo pair sequences are as follows:

Table 2 - qPCR oligos

Name	Ref #	Sequence
mHif1a FWD qPCR	2018	ACCTTCATCGGAAACTCCAAAG
mHif1a Rev qPCR	2019	CTGTTAGGCTGGGAAAAGTTAGG
mNdrg1 FWD qPCR	2020	ATGTCCCGAGAGCTACATGAC
mNdrg1 Rev qPCR	2021	CCTGCTCCTGAACATCGAACT

2.7 Gross morphology

Whole placentas were fixed overnight (O/N) at 4°C in neutralized 4% paraformaldehyde (PFA), transferred to 70% ethanol (EtOH) O/N at room temperature (RT), dehydrated in a graded EtOH series, and embedded in paraffin wax. Midline cross sections (5 µm) were stained with hematoxylin and eosin (H&E).

2.8 Immunofluorescence

Dams pregnant with *Ldhb*$^{\Delta/+}$ intercrosses were reared in 12% O_2 from E9.5-15.5. Whole placentas were harvested, fixed in neutralized 4% PFA O/N at 4°C, transferred to 30% sucrose O/N at 4°C, and embedded in OCT. Midline sections (10 µm) were permeabilized with neutralized 4% PFA for 15 minutes at RT and stained with mouse α-CD31 (eBioscience) and Armenian hamster (AH) α-MUC1 (ThermoFisher Scientific). The following day, slides were washed and stained with Rat α-mouse AlexaFluor555 and goat α-AH AlexaFluor488 for 1 hour at RT. Slides were washed, counterstained with DAPI, and mounted for fluorescence.

Images were acquired on a Nikon A1 (s216.3) confocal microscope equipped with a motorized stage and 20x objective to collect stepwise images. The acquired image tiles were stitched together to generate a comprehensive overview of the vascular structures. The total labyrinth area was quantified on whole area scans in the program Nis Elements (Nikon Instruments Inc.). Briefly, binary masks were generated by defining thresholds on each individual channel. Masks were overlaid to calculate the proportion of the labyrinth, comprised of the maternal blood

spaces (green) and fetal vessels (red), to the total placental area. Values were analyzed for significance with a two-way ANOVA and Tukey's multiple comparisons test.

2.9 Lactate analysis

Samples were washed with ice-cold PBS, scraped in ice-cold 8% perchloric acid to quench metabolic processes, and cleared by centrifugation. Supernatants were collected, neutralized with dropwise addition of 3 mM potassium carbonate, and cleared by an additional round of centrifugation. Supernatants were aliquoted, snap-frozen in liquid nitrogen and stored at –80°C. Undiluted samples were analyzed using the Amplite Fluorimetric assay kit exactly according to manufacturer's instructions (AAT Bioquest). Values were analyzed with either a one-way ANOVA and Dunnett's *post hoc* test or two-way ANOVA and Tukey's multiple comparisons test, as described in the text.

2.10 Metabolomics

Differentiated WT and PPARγ-null TSCs were cultured in triplicate under standard conditions and < 1% O_2 for 12 hours as described. Plates were subsequently washed with ice-cold PBS, scraped in ice-cold 80% methanol (MeOH) to quench metabolic processes, and cleared by centrifugation. The cell pellets were re-extracted, cleared by another round of centrifugation, and pooled. Samples were sent to the University of Minnesota for untargeted metabolomics using LC-MS/MS Selective Reaction Monitoring (SRM) analysis of compounds. Samples (10 µl) for SRM

analysis were subjected to separation using a Shimazo column to an analytical SeQuant ZIC-pHILIC (150mmx4.6mm at 30°C) connected to the Applied Biosystem 5500 iontrap fitted with a turbo V electrospray source run in negative mode with declustering potential (DP) and collision energies (CE) in table 3. The samples were subjected to a linear gradient of 80%B to 25%B over a 18 minute gradient (A: 10mm ammonium acetate pH7, 20% acetonitrile 0 B: Acetonitrile) at a column flow rate of 400 µl /min. The column was cleared with 25 % B for 2 minutes and then equilibrated to 80% B for 10 minutes. Transitions monitored as in table 3 were established using the instrument's compound optimization mode with direct injection for each compound. The data was analyzed using MultiQuant™ (ABI Sciex Framingham, MA) providing the peak area. A standard curve was constructed using in 10 µl. Samples were run once and concentrations determined from the standard curve. Values were analyzed using a two-way ANOVA and Tukey's multiple comparisons test.

Table 3 - Seperation and detection specifics for measured analytes

ID	Q1	Q3	DP	CE
ACoA_408	808	408	-45	-40
ACoA_461	808	461	-45	-40
alphaKeto_101_Q	145	101	-50	-21
alphaKetp_57_V	145	57	-50	-25
ATP_159	506	159	-50	-45
ATP_408	506	408	-45	-30
Lactate_41V	89	41	-70	-16
Lactate_43Q	89	43	-50	-16
Malic Acid 7_V	133	71	-50	-14
Malic Acid_Q	133	115	-50	-20
PEP_63_V	166.9	63	-30	-30
PEP_79_Q	166.9	79	-75	-35
Pyruvate_Q	87	43	-50	-12
Succinic Acid_100	117	100	-65	-26
Succinic Acid_73	117	73	-65	-16

2.11 Statistics

One- and two-way ANOVA were used to determine *P*-values in Graphpad Prism. A *P* value of <0.05 was considered significant in all experiments. Error bars designate standard deviation (sd).

3.0 Results

3.1 PPARγ is required for sustained HIF1α protein expression in hypoxic trophoblasts

The positive regulation of Ldhb and Pcx by placental PPARγ, and the absence of conventional developmental regulators or differentiation target genes, raises the intriguing possibility that lactate metabolism may play a role in proper placentation. Although lactate can be produced under steady-state conditions, the bulk of lactate is generated in the absence of oxygen, during which the TCA cycle is shut off and the conversion of pyruvate to lactate is required for generating the reducing equivalents for sustained glycolysis and ATP production (Ferguson BS et al., 2018). This metabolic switch is largely achieved through the activity of stabilized HIF1α and its target gene regulation. HIF1α increases the expression of PDK1 and LDHA, which are responsible for inactivating the TCA cycle and promoting lactate production, respectively. Given the essential role of HIF1α in the cellular response to hypoxia, and phenotypic similarities shared by Pparg-null and Hif1a-null placentas, studies were initiated to determine if there was a relationship between these two proteins.

3.1.1 *Pparg* is required for sustained expression of HIF1α protein in hypoxic TSCs

Because placental development occurs in a relatively hypoxic environment prior to the formation of the labyrinthine vascular tree, WT and *Pparg*-null TSC lines were used to determine if there is a relationship between PPARγ and HIF1α in hypoxic trophoblasts. TSCs were differentiated for 3 days in the presence or absence of the PPARγ agonist Rosiglitazone (Rosi; 1

μM) and cultured under either standard (21% O_2) or hypoxic (<1% O_2) conditions. In WT TSCs HIF1α expression was increased dramatically at 24 h post hypoxia exposure and this induction was further enhanced by Rosi (Figure 1A lanes 5 and 6).

Concomitant with a decline in PPARγ levels at 48 h post hypoxic exposure, HIF1α levels also decreased (lane 7). This decrease was mitigated by the addition of Rosi (lane 8), suggesting that PPARγ positively regulates HIF1α induction in hypoxia. As shown previously, PPARγ levels declined slightly in WT cells treated with Rosi (lane 3), possibly reflecting negative feedback regulation (Shalom-Barak T et al., 2004; 2012). Compared to the WT counterpart, HIF1α expression was completely absent in *Pparg*-null TSCs within 24 h of exposure to hypoxia (lane 4). *Pparg*-null TSCs exhibited variable lethality throughout the course of this project, ranging from complete death by 24 h to survival past 48 h in hypoxia. While the intimate details of this phenomenon were not explored, the overall trends in the expression of hypoxia-regulated proteins remained the same. By 48 h in hypoxia, *Pparg*-null cells have all died, possibly due to a lack of HIF1α at that time point, obviating protein analyses. Importantly, an inverse relationship between PPARγ and NDRG1 was observed. NDRG1 levels were maintained at near-zero in normoxic

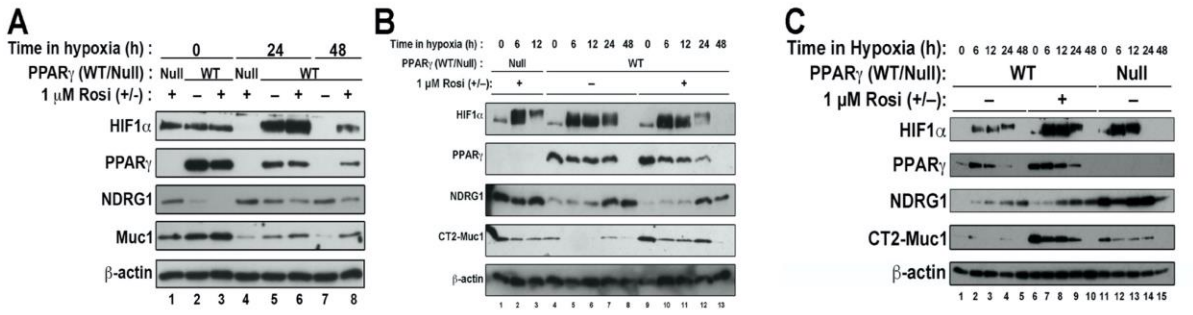

Figure 3-1 - PPARγ is required for sustained HIF1α expression.

WT (GY11) and *Pparg*-null (GY9) TSCs were differentiated for 3 days and cultured under standard or hypoxic conditions for (A) 24 or 48 h or (B) and (C) 0 – 6-48 h in the presence or absence of the PPARγ agonist Rosi (1 μM). (A) HIF1α expression levels at 24 and 48 h post hypoxic exposure respond to Rosi and are completely absent in *Pparg*-null TSCs. (B) and (C) PPARγ is required for sustained HIF1α expression between 12 and 48 h post hypoxic exposure. Additionally, PPARγ appears to negatively regulate the hypoxia response protein NDRG1. β-actin confirms equal sample loading in all lanes.

trophoblasts (lane 2), as previously reported (Shi XH et al., 2013), and were further suppressed by Rosi (lanes 3, 6, 8). In contrast, the absence of PPARγ promoted NDRG1 expression in normoxic TSCs (lane 1), and further augmented NDRG1 levels in hypoxic cultures relative to WT TSCs (lane 4). Both results are consistent with negative regulation of NDRG1 by PPARγ. Expression of the intracellular C-terminal 2 (CT2) domain of the PPARγ target MUC1 declined over time in both WT and *Pparg*-null hypoxic TSCs.

It has been previously shown that HIF1α protein can be detected in cancer cell lines as early as 4 h post hypoxia exposure, rapidly declines starting at 24 h, and is nearly undetectable in most cells around 48 h (Lee DC et al., 2015). This raised the question whether HIF1α absence from *Pparg*-null TSCs at the 24 h time point reflects total failure to induce HIF1α or a different induction and decay kinetics. Figures 1B and 1C roughly recapitulated this reported kinetics in WT TSCs (1B lanes 4-14; 1C lanes 1-10). In contrast, although *Pparg*-null TSCs strongly expressed HIF1α at 6 h post-hypoxia (1B lane 2; 1C lane 12), its levels sharply declined by 12 h (1B lane 3; 1C lane 13). Although in the experiment shown in Figure 1B, no TSCs survived by

24h, and therefore, protein kinetics could not be analyzed, in the one shown in Figure 1C the cells survived for over 48h, enabling analysis at a later time point; here, HIF1α was completely absent by the 24 h time point (1C lane 14).

It is noteworthy to highlight the shift in HIF1α doublet formation in Rosi-treated WT (1B lanes 10, 11; 1C lanes 7, 8) and *Pparg*-null (1B lane 2; 1C lane 12) hypoxic TSCs to a singlet protein (1B lane 3, 12; 1C lanes 9, 13). Although the exact nature and composition of this doublet is has not been analyzed by us or others, its differential behavior in the context of TSCs and PPARγ suggests a potential functional significance.

These extended protein kinetics experiments further validated the direct relationship between PPARγ and HIF1α and confirmed the decline of Muc11 in hypoxia.

3.1.1.1 Validation of the PPARγ-HIF1α axis

TSCs are a primary pluripotent mouse cell line derived from the TE of individual blastocysts and, due to the stochastic nature of their derivation, carry the hypothetical risk of being highly variable in their molecular and biochemical responses. The hypoxic responses of one additional *Pparg*-null clone (GY20) and two additional WT lines (Clone 2 and TRF) were interrogated to rule out the possibility of clonal artifacts (Figure 2). By 6 h in hypoxia both WT cell lines had increased HIF1α expression (lanes 5, 18, 21). By 12 h post hypoxia, HIF1α levels were sustained in the WT TRF line (lane 21) but nearly diminished in Clone 2 (lane 8), highlighting the variable hypoxic response of TSCs. In both WT lines, HIF1α levels declined significantly by 24 h in hypoxia (lanes 10-13, 23-26). Nevertheless, this decrease was mitigated by the addition of

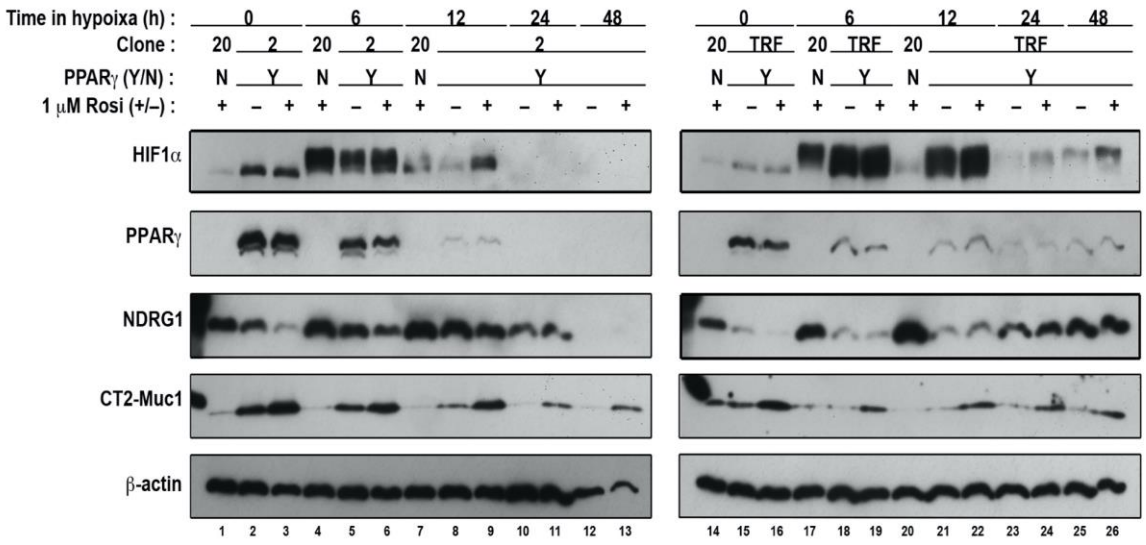

Figure 3-2 - Additional clones validate PPARγ-HIF1α axis in hypoxic trophoblasts.

WT (Clone 2 and TRF) and *Pparg*-null (GY20) TSCs were differentiated for 3 days in the presence or absence of Rosi (1 μM) and cultured under standard or hypoxic (< 1% O_2) conditions for 6-48 h. HIF1α expression levels at 12 h (Clone 2) and 24 and 48 h (TRF) respond to Rosi and are absent in *Pparg*-null TSCs. NDRG1 expression is elevated in the absence of PPARγ in normoxic trophoblasts. β-actin confirms equal sample loading in all lanes.

Rosi (lanes 9, 24, 26) consistent with our earlier interpretation that the extent of PPARγ activation correlates positively with the extent of sustained HIF1α expression. PPARγ protein expression declined by 12 h post hypoxic exposure in both WT lines (lanes 8-13, 21-26). This decline in PPARγ protein was accompanied by a rise in NDRG1 levels by 12 h in hypoxia (lanes 8, 21), whereas treatment with Rosi mitigated this increase (lanes 9, 11). Here too, Muc1 expression declined over time in hypoxia.

In *Pparg*-null TSCs, HIF1α was strongly induced by 6 h post hypoxia in *Pparg*-null TSCs (lanes 4, 17), yet rapidly declined by 12 h (lanes 7, 20). By 24 h cell death was near-complete, precluding protein analysis. The inverse relationship between PPARγ and NDRG1 was evident in GY20 as well. The absence of PPARγ enhanced NDRG1 expression at baseline (lanes 1, 14) and augmented NDRG1 levels in hypoxia relative to WT (lanes 4, 7, 17, 20), consistent with results shown in Figure 1. This confirms that PPARγ plays a role in the negative regulation of NDRG1.

It is worthwhile to point out that while PPARγ and HIF1α protein decay kinetics in both WT clones were accelerated compared to the clone GY11 counterpart, the requirement of PPARγ, the positive effect of Rosi, and the overall trend of NDRG1 remained the same. All further experiments were carried out with GY 11 (WT) and GY9 (*Pparg*-null) as these clones were consistent and robust in the expression of key proteins of interest.

3.1.1.2 The influence of oxygen

Early in gestation, the hypoxic uterine environment facilitates placentation by promoting trophoblast proliferation and providing the necessary stimulus for fetal vessel angiogenesis (Adelman DM et al., 2000). Once the labyrinthine vascular tree is fully established, blood that flows through the feto-placental unit contains ~8.6% oxygen in humans (Rodesch F et al., 1992). Culture of TSCs under "standard" tissue culture conditions, i.e., ambient air or 21% oxygen, therefore represents hyper-oxic conditions and may not be representative of the *in vivo* baseline expression of key hypoxia-regulated proteins.

To ensure validation of the established model, WT TSCs were cultured under standard tissue culture conditions or 8% oxygen for 24 and 48 h. PPARγ expression did not change with respect to oxygen saturation, hypoxia duration, or ligand stimulation (Figure 3). Importantly, PPARγ levels were similar at 21% and 8% oxygen and did not decline under reduced oxygen conditions, as seen in Figures 1 and 2. It was concluded that TSCs cultured under physiologically relevant versus standard conditions did not influence baseline expression of PPARγ protein. All normoxic conditions in subsequent studies were carried out in 21% oxygen for convenience and simplicity.

The emerging relationship between placental PPARγ and HIF1α during acute oxygen deprivation raised the question whether artificial HIF1α stabilization in normoxia would mimic the effect and

provide insight into the regulation of key hypoxia-responsive proteins. Cobalt chloride ($CoCl_2$), a transition metal salt and PHD inhibitor, was used to manipulate HIF1α levels *in vivo*. PHD2 is a non-heme requiring enzyme and, in the presence of oxygen, catalyzes hydroxylation of proline residues in the ODD of HIF. These hydroxyprolines function as docking sites for VHL, which recruits an E3 ligase that targets HIF for polyubiquitination and subsequent proteasomal degradation (Maxwell PH et al., 1999). $CoCl_2$ is a competitive inhibitor of iron and prevents the interaction between PHD2 and the ODD of HIF1α by occupying an iron-binding site on PDH2, thus preventing HIF degradation in the presence of oxygen (Epstein AC et al., 2001).

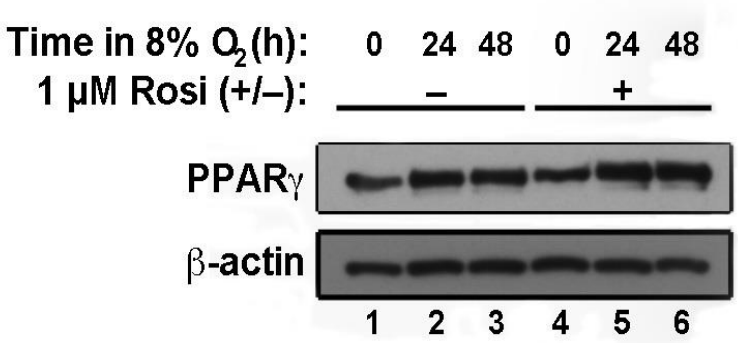

Figure 3-3- 8% oxygen does not alter PPARγ levels.

WT TSCs (GY11) were differentiated for 3 days and cultured under 21% or 8% O_2 for an additional 24 and 48 h in the presence or absence of Rosi (1 μM). The expression of PPARγ in TSCs reared 8% O_2 does not change relative to control.

Initially, WT and *Pparg*-null TSCs were incubated with varying concentrations of $CoCl_2$ for 24 h to determine a suitable working range (Figure 4A). HIF1α levels increased in a dose-dependent manner in WT and *Pparg*-null TSCs (lanes 1-10). In contrast, PPARγ protein levels were unchanged (lanes 1-5). NDRG1 was increased in WT cells only in the presence of >200μM $CoCl_2$ a dose-dependent manner in WT cells (lanes 4,5), yet was consistently elevated in *Pparg*-null TSCs irrespective of $CoCl_2$ concentration (lanes 6-10). Because 200 μM $CoCl_2$ was sufficient

for maximal HIF1α stabilization both in WT and *Pparg*-null TSCs and NDRG1 activation in WT TSCs, this concentration was subsequently used to investigate the expression kinetics pattern of hypoxia-regulatory proteins of interest. In Figure 4B, WT and *Pparg*-null TSCs were incubated with 200μM $CoCl_2$ for 6-48 h in the presence or absence of Rosi. HIF1α levels remained stable up to 48 h in both WT TSCs and *Pparg*-null TSCs and did not respond to Rosi. Similarily, the expression of PPARγ in WT TSCs was relatively unchanged over time and upon ligand stimulation. Collectively, these data indicate that PPARγ and HIF1α induction and decay patterns are driven by the complex effect of oxygen deprivation, and cannot be mimicked simply by $CoCl_2$-mediated HIF1α stabilization. Therefore, $CoCl_2$ treatment is an unsuitable replacement for oxygen deprivation in this system.

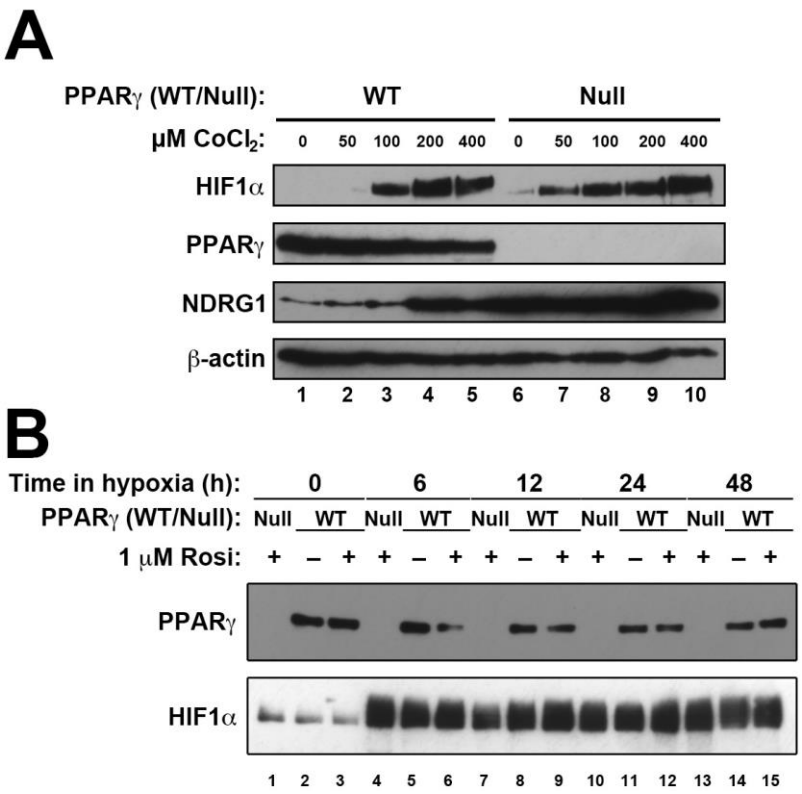

Figure 3-4- Cobalt chloride does not mimic the effect of oxygen deprivation in TSCs.

WT (GY11) or *Pparg*-null TSCs were differentiated for 3 days and (A) incubated with varying concentrations of $CoCl2_2$ for 24 h or (B) incubated with $CoCl_2$ (200 μM) for 6-48 h in the presence or absence of Rosi (1 μM). (A) HIF1α and NDRG1 levels increased in a dose-dependent manner in WT TSCs, but PPARγ levels were unchanged. NDRG1 levels were elevated in *Pparg*-null TSCs as compared to WT irrespective of $CoCl_2$ concentration. (B) PPARγ and HIF1α levels were unchanged over the course of $CoCl_2$ exposure in both WT and null cell lines.

3.1.2 PPARγ-NDRG1 regulation occurs at the RNA level

The requirement of PPARγ to sustain HIF1α protein levels (Figures 1 and 2) in hypoxic TSCs prompted a search for the potential mechanism. Because PPARγ is a TF, regulation at the gene level was a logical starting point. WT and *Pparg*-null TSCs were cultured under standard or hypoxic conditions and the temporal expression patterns of key hypoxia-responsive transcripts were analyzed (Figure 5).

Hif1a mRNA levels steadily declined over time and plateaued by 12 h in both hypoxic WT and *Pparg*-null TSCs. All *Pparg*-null TSCs had died by 24 h in hypoxia, obviating gene

expression analysis. The addition of Rosi had no effect on *Hif1a* mRNA at any time point in WT TSCs. These findings are consistent with previous reports that HIF1α regulation primarily occurs post-translationally (Koh MY et al., 2012).

Conversely, *Pparg* transcripts in WT TSCs increased by 6 h in hypoxia, declined to near baseline levels by 12 h, and plateaued thereafter. The overall trend indicates that the increase in PPARγ protein in the early stages of hypoxia (Figure 1C, lane 2) may be regulated at the transcriptional level, whereas its later decline may occur, at least in part, at the post-transcriptional level. *Pparg* levels steadily declined in WT TSCs stimulated with Rosi, as shown previously at the protein level (Figure 1A), consistent with a putative negative feedback loop (Shalom-Barak T et al., 2004; 2012). *Pparg* expression was undetected in null TSCs as expected.

Importantly, the data revealed that NDRG1 regulation by placental PPARγ occurs primarily at the transcriptional level. The baseline expression of *Ndrg1* was higher in normoxic *Pparg*-null TSCs relative to WT, although more power would be required for statistical significance. *Ndrg1* levels steadily rose in hypoxic *Pparg*-null TSCs and peaked at 12 h, the last time point at which samples could be collected. *Ndrg1* levels also increased in hypoxic WT TSCs, albeit to a lesser degree, and the addition of Rosi mitigated the increase at 6 and 12 in hypoxia. By 24 h hypoxic exposure *Ndrg1* expression in WT TSCs began to decline and converge with WT TSCs treated with Rosi. Whereas protein levels of NDRG1 in WT TSCs steadily increased over time in hypoxia (Figures 1 and 2) transcriptional upregulation appeared to cease at 12 h, suggesting a potential switch to post-translational regulation during chronic hypoxic exposure.

Muc1, the most robust target of placental PPARγ (Shalom-Barak T et al., 2004; 2012), followed "bowl-shaped" expression kinetics over the course of hypoxic treatment in both WT and *Pparg*-null TSCs. *Muc1* mRNA levels steadily declined, bottomed out at 12 h, and slightly

recovered by 24 h in hypoxia. The expression of *Muc1* remained highest in WT TSCs treated with Rosi. Unsurprisingly, *Muc1* transcript levels were substantially lower in *Pparg*-null TSCs, as previously reported (Shalom-Barak T et al., 2004; 2012). The overall timeline of *Muc1* decay in hypoxic *Pparg*-null TSCs was accelerated, yet still recapitulated the overall trend. Every time point analyzed had varying degrees of statistical significance, except WT TSCs ± Rosi at 24 h, yet were excluded from the figure for the sake of clarity. Although the exact role of Muc1 in the placenta is yet to be defined, it is tempting to speculate a possible role in the hypoxic signaling of trophoblasts, especially in light of recent reports to this effect in other cell types (Pastor-Soler NM et al., 2015; Shukla SK et al., 2017).

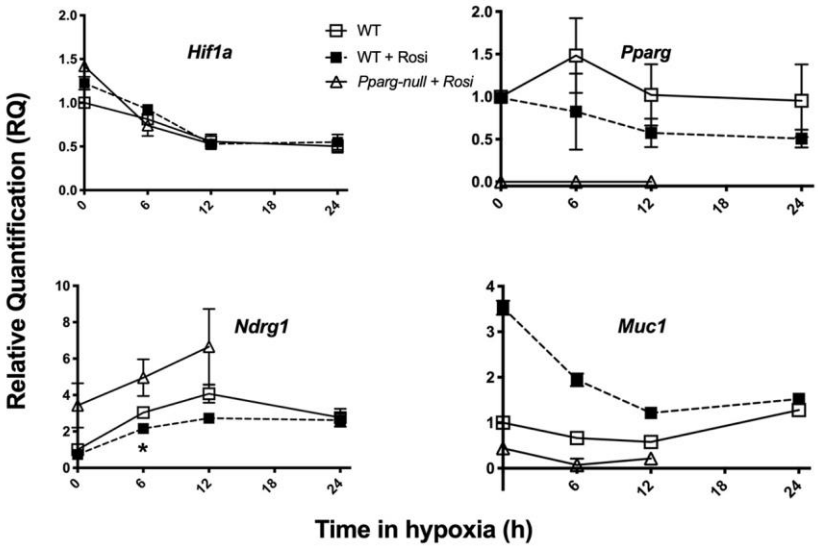

Figure 3-5- PPARγ negatively regulates NDRG1 transcription

Expression of four hypoxia-regulated genes in WT (GY11; solid lines, squares) and *Pparg*-null (GY9; solid lines, triangles) TSCs over the course of acute oxygen deprivation in the absence (open squares) or presence (filled squares, dashed lines) of 1 μM Rosi. Each qPCR measurement was performed in duplicate, normalized to the *Dazap1* gene, and analyzed with the ΔΔCT method. Expression under standard tissue culture conditions in the absence of Rosi was assigned a relative value of 1.0. Values were analyzed with a one-way ANOVA and Tukey's *post hoc* test. $P < 0.05$ was considered significant. Error bars designate sd. NDRG1 RNA is elevated in the absence of *Pparg*.

3.2 A new role for lactate?

In the absence of direct transcriptional regulation of HIF1α by PPARγ, the focus of this thesis shifted back to the known targets of placental PPARγ. PPARγ regulates multiple metabolic enzymes in the mouse placenta, with two of the strongest targets being LDHB and PCX (Shalom-Barak T et al., 2012). LDHB is responsible for converting lactate to pyruvate, and PCX converts the pyruvate product of LDHB to OAA, a pleiotropic intermediate that replenishes numerous metabolic pathways (Takeno T et al., 1998; Jitrapakdee S et al., 1999). Given the intimate association of lactate production and oxygen deprivation, the idea that PPARγ and its transcriptional targets modulate the expression of key hypoxia-regulated proteins via lactate metabolism began to form. This chapter explores the role of lactate and its metabolites in the hypoxic signaling of trophoblasts.

3.2.1 *Pparg*-null TSCs accumulate lactate in hypoxic conditions

Non-targeted metabolomics were used to characterize the intracellular metabolite pools of WT and *Pparg*-null TSCs reared in standard and acute hypoxic conditions for 12 h (Figure 6). The greatest differential between HIF1α protein expression in WT and *Pparg*-null TSCs was observed at the 12th h of hypoxic exposure (Figures 1 and 2), and therefore, was chosen for interrogation.

In WT TSCs, intracellular pyruvate concentrations were relatively unchanged after 12 h of hypoxic exposure compared to normoxia. In contrast, while the intracellular pyruvate of normoxic *Pparg*-null TSCs were below the detection threshold, they increased dramatically in hypoxia, although fell short of attaining statistical significance due to wide data distribution.

Similar to pyruvate, 12 h of hypoxic treatment did not alter intracellular lactate concentrations in WT TSCs. However, intracellular lactate significantly accumulated in hypoxic relative to normoxic *Pparg*-null TSCs. *Pparg*-null TSCs also accumulated more intracellular lactate by 12 h in hypoxia compared to WT TSCs. These data demonstrate a central role for PPARγ and by proxy, its target genes, in trophoblast lactate clearance, under acute hypoxic conditions.

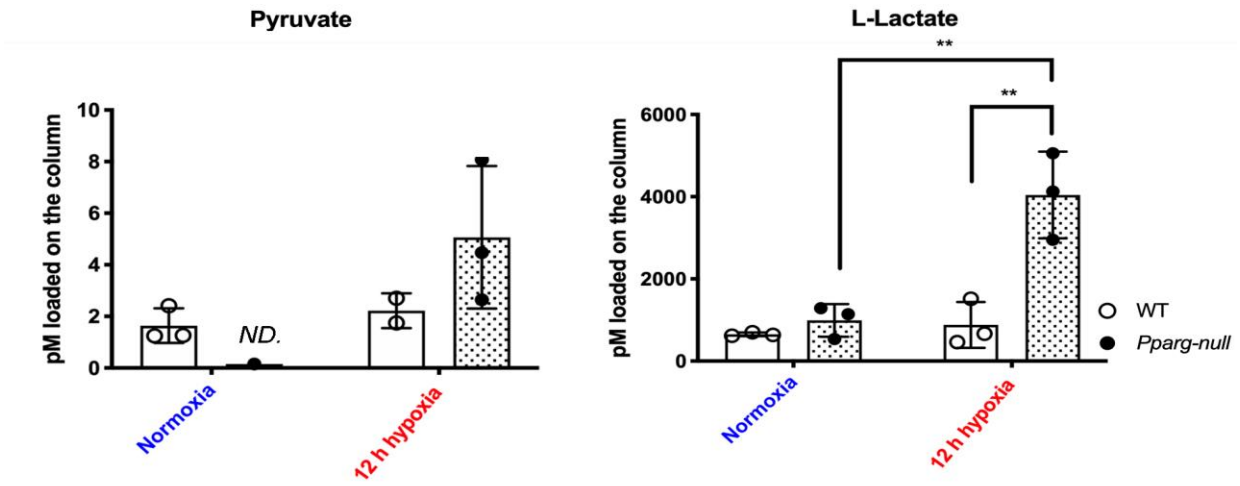

Figure 3-6- Pparg-null TSCs accumulate lactate in hypoxia

WT (GY11; open circles) and *Pparg*-null (GY9; closed circles) TSCs were cultured under hypoxic conditions for 12 h. Metabolism was immediately quenched by the addition of ice-cold 80% MeOH. Samples were sent to the University of Minnesota for untargeted aqueous phase metabolomic analysis. Values were analyzed using a two-way ANOVA and Tukey's multiple comparisons test. $P < 0.05$ was considered significant. ND = not determined. *Pparg*-null TSCs accumulate significantly more lactate in hypoxia than the WT counterparts.

3.2.2 The regulatory properties of lactate

The differential accumulation of intracellular metabolites in WT versus *Pparg*-null hypoxic TSCs further supported the burgeoning concept that PPARγ-mediated regulation of HIF1α and additional hypoxia-responsive proteins occurs at the level of lactate metabolism. JEG-

3 cells, a transformed human choriocarcinoma cell line, were used to interrogate the effects of intracellular lactate manipulation on the expression of key hypoxia-regulated proteins. First, JEG-3 cells were incubated with varying concentrations of exogenous L-lactate for 24 h under standard tissue culture conditions (Figure 7A). The highest concentration of L-lactate (100 mM) increased the levels of HIF1α, PPARγ, and NDRG1 proteins in normoxia (7A lane 4), suggesting that all three could be stabilized by excess cellular lactate, perhaps through a joint mechanism.

Inhibitors of lactate metabolism were used in parallel to compare the expression profiles of key hypoxia-regulatory proteins. JEG-3 cells were cultured under hypoxic conditions for 24 h

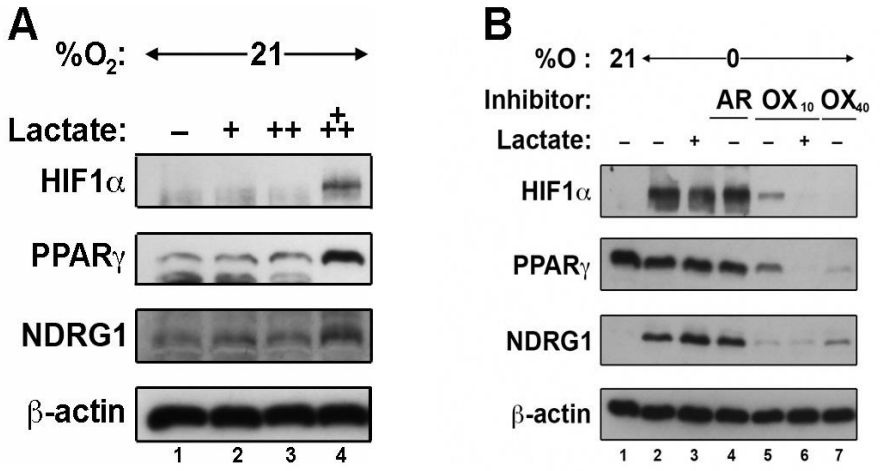

Figure 3-7 - Lactate alters the expression of hypoxia-regulated proteins

JEG-3 cells were cultured under standard (A) or hypoxic (B) conditions for 24 h in the presence or absence of various inhibitors +/– exogenous L-lactate. (A) Exogenous L-lactate positively regulates PPARγ, HIF1α, and NDRG1 under standard conditions; + - 25 mM, ++ - 50 mM, +++ - 100 mM. (B) PPARγ, HIF1α, and NDRG1 are negatively regulated by the LDH inhibitor oxamate (Ox); + - 50 mM lactate, 1 μM AR – AR-C155858 (MCT1/2 inhibitor;), Ox – 10 or 40 mM sodium oxamate (LDH inhibitor). β-actin confirms equal sample loading in all lanes.

in the presence or absence of various inhibitors of lactate metabolism ± 50 mM exogenous L-lactate (Figure 7B). HIF1α and NDRG1 protein were absent in normoxia (7B lane 1) and increased under acute hypoxic conditions (7B lane 2) as predicted. PPARγ protein levels were

relatively stable in hypoxia (7B lane 2) in contrast to WT TSCs (Figures 1 and 2). The expression of hypoxia-regulated proteins were unchanged with the addition of exogenous L-lactate or inhibition of lactate flux into the cell *via* MCT1/2 inhibitor AR-C15585 (AR) (7B lanes 3, 4). MCT1 is a high-affinity monocarboxylate transporter located on the basal plasma membrane of SynTs (fetal-facing) in the human term placenta and drives lactate into the cell (Nagi A et al., 2010; Settle P et al., 2004). Therefore, the addition of lactate or inhibition of transport into the cell did not alter the expression of hypoxia-responsive proteins.

Expression levels of HIF1α, PPARγ, and NDRG1 drastically declined in JEG-3 cells treated with the pan-LDH inhibitor sodium oxamate (Ox; 10 mM) (7B lane 5), and addition of exogenous L-lactate augmented the effect (7B lane 6). Levels of HIF1α, PPARγ, and NDRG1 protein were almost completely diminished in JEG-3 cells treated with 40 mM Ox (7B lane 7). JEG-3 cells treated with 40 mM Ox and supplemented with 50 mM exogenous L-lactate all died, precluding protein analysis.

Importantly, JEG-3 are cancerous by nature and thus may not accurately represent the hypoxic response of native trophoblasts. To further validate the findings in JEG-3 cells, WT TSCs were cultured under hypoxic conditions for 24 h in the presence or absence of various inhibitors of lactate metabolism ± 50 mM exogenous L-lactate (Figure 8). HIF1α, PPARγ, and NDRG1 were expressed by 24 h in hypoxia (lane 1). Neither the addition of exogenous L-lactate or treatment with the MCT1/2 inhibitor AR had an effect on the expression of hypoxia-responsive proteins (lanes 2, 3). Treatment with 10 mM Ox slightly attenuated HIF1α protein levels (lane 4) and this effect was mitigated with the addition of exogenous lactate (lane 5). In contrast, treatment with 40 mM Ox significantly decreased HIF1α protein levels (lane 6) and addition of lactate synergized

to further diminish HIF1α levels (lane 7). Overall PPARγ expression levels did not significantly change with inhibitor treatment (lanes 1-6). Although it is worthwhile to note that 40 mM, but not 10 mM, Ox significantly decreased PPARγ protein (lane 6). This effect was further augmented in the presence of exogenous L-lactate (lane 7). The response of NDRG1 to chemical inhibitors or exogenous lactate was much weaker than HIF1α or PPARγ. NDRG1 levels were slightly increased in response to 10 mM Ox (lane 4) and ameliorated by the addition of lactate (lane 5). The significance of this response is not clear at this time. Overall, these data suggest that the manipulation of intracellular lactate concentrations may have the same effect in both TSCs and JEG-3 cells, albeit with different sensitivity thresholds.

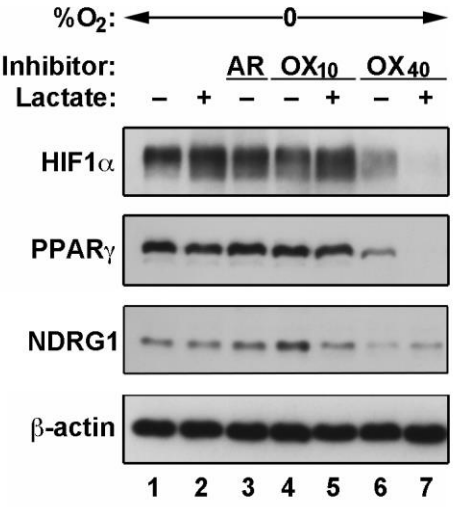

Figure 3-8- Response of TSCs to intracellular lactate modification

WT TSCs (GY11) were differentiated for 3 days and cultured under hypoxic conditions for 24 h in the presence or absence of various inhibitors of lactate metabolism +/– exogenous L-Lactate. PPAγ and HIF1α are negatively regulated by the LDH inhibitor Ox; + - 50 mM lactate, AR – 1 μM, Ox – 10 or 40 mM. β-actin confirms equal sample loading in all lanes.

3.2.2.1 Responses of hypoxia regulators to LDH inhibition

The differential regulation of hypoxia-responsive proteins to low (10 mM) and high (40 mM) Ox concentrations (Figure 7 and 8) was striking and warranted further investigation. The effects of Ox at three different concentrations – 10, 20, and 40 mM – was used to further define the dynamic regulation of hypoxia-responsive protein inhibition. JEG-3 cells were cultured under standard or hypoxic conditions from 6-48 in the presence or absence of varying concentrations of Ox. By 48 h in hypoxia untreated JEG-3 cells, as well as JEG-3 cells treated with 20 or 40 mM Ox, had died, obviating protein analysis (Figure 9). In contrast, JEG-3 cells treated with 10 mM Ox survived up to 48 h in hypoxia, suggesting that minor manipulations of the intracellular lactate pool translate to large scale effects ranging from variable protein expression to decreased cell viability.

As expected, HIF1α protein levels steadily increased in untreated WT cells (lanes 1-4) as predicted. Treatment with 10 mM Ox augmented protein levels of HIF1α at 24 and 48 h in hypoxia relative to control (lanes 4-9). In stark contrast, expression of HIF1α was significantly decreased by 6 h post hypoxia in cells treated with 20 mM Ox (lane 10). HIF1α levels were further reduced to near zero by 12 h (lane 11) and completely diminished by 24 h in hypoxia (lane 12). The increase of Ox concentration from 20 mM to 40 mM was sufficient to cease HIF1α induction all together (lanes 14-17). It's tempting to speculate that the decline of HIF1α levels (lanes 11, 12, 14-17) in cells treated with 20 mM and 40 mM contributed, to or directly caused, lethality.

PPARγ levels were stable throughout the course of hypoxia in untreated JEG-3 cells (lanes 1-4). Cells treated with 10 mM Ox increased PPARγ expression in normoxia (lane 5) relative to untreated WT cells. PPARγ expression peaked at 6 h, remained elevated by 24 h, and decreased by 48 h in hypoxia compared to untreated JEG-3 cells in acute hypoxic conditions (lanes 5-9).

Treatment with 20 and 40 mM Ox induced a similar, albeit accentuated, trend with PPARγ levels peaking at 6 h (lanes 11, 15), declining by 12 h (lanes 12, 16), and completely abolished by the 24th h of hypoxic exposure (lanes 13, 17).

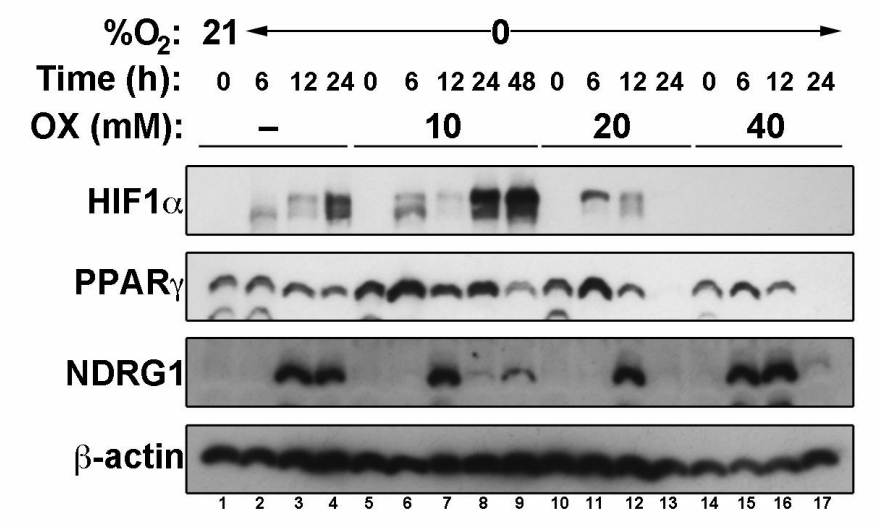

Figure 3-9- Refined analyses of the effects of lactate metabolism inhibitors

JEG-3 cells were treated with increasing concentrations of the LDH inhibitor Ox and culture in standard or hypoxic conditions for 6-48 h. Low [Ox] and high [Ox] exhibit unique effects on hypoxia-regulated proteins, suggesting differentiational LDH isozyme inhibition.

NDRG1 protein behaved as expected in untreated JEG-3 cells. NDRG1 levels were absent under standard tissue culture conditions (lane 1), increased by 12 h, and were sustained out to 24 h in hypoxia (lanes 3, 4). Unlike HIF1α and PPARγ, NDRG1 followed a similar expression pattern in cells treated with 10 mM and 20 mM Ox. Peak NDRG1 levels were observed at 12 h (lanes 7, 12) and declined to near zero by 24 h in hypoxia (lanes 8, 13). Interestingly, NDRG1 expression levels were slightly rescued by 48 h in hypoxia in JEG-3 cells treated with 10 mM Ox (lane 9). Treatment of cells with 40 mM Ox increased the NDRG1 induction timeline, with peak levels observed at 6 h in hypoxia (lane 15). Elevated expression levels were sustained at 12 h (lane 16)

and completely eradicated by 24 h (lane 17) in post-hypoxic exposure. Taken together, these data suggest that lactate metabolism, whether its rate of clearance or degradation to metabolic by products, has a distinctive quantitative and qualitative effect on the response of hypoxia-regulated proteins that warranted further investigation.

3.2.3 Lactate measurements and subsequent *in vitro* response

Previous data indicated that the regulation of lactate metabolism has a profound inhibitory role on key hypoxia-responsive proteins (Figures 7-9), yet the actual intracellular lactate concentrations in response to pharmacological manipulations were unclear. Importantly the pan-LDH inhibitor Ox suppresses the activity of both LHDA (lactate generation) and LDHB (lactate clearance). The dual-action inhibitory properties obscure true effects on the intracellular lactate milieu. To that end, key nodes of the experiment were repeated by culturing JEG-3 cells under either standard or hypoxic conditions for 6-12 h in the presence exogenous lactate, Ox, the PCX inhibitor phenylacetic acid (PA; 2.5 mM), and collecting parallel samples for either Western blot or intracellular lactate measurements.

Figure 10A demonstrates that while PPARγ levels remained relatively stable when cultured under standard or hypoxic conditions for 6-12 h, the levels of HIF1α protein drastically increased and NDRG1 levels slightly increased in response to the hypoxic stimulus (lanes 1-4). In contrast, the addition of 50 mM lactate in normoxia dramatically down-regulated PPARγ protein expression within 12 h (lane 6). The decline in PPAγ levels was accompanied by a significant increase in intracellular lactate accumulation (P = 0.0004) relative to untreated normoxic controls (Figure 10B). Paradoxically, PPARγ protein levels remained unchanged in hypoxic TSCs treated with exogenous lactate (lanes 7, 8). A possible interpretation of this observation is that unscheduled

lactate accumulation, in a manner that is not coordinated with oxygen deprivation and HIF1α pathway activation, suppresses PPARγ expression. Consistent with the earlier data (Figure 9), treatment of JEG-3 cells with 10 mM Ox did not influence the expression of PPARγ (10A lanes 9, 10), whereas 40 mM Ox near-completely abolished PPARγ levels by 12 h in hypoxia (lanes 11, 12). Importantly, intracellular lactate concentrations were decreased to a *similar* extent in JEG-3 cells cultured in the presence of either 10 mM or 40 mM Ox (Figure 10C). PPARγ expression was also negatively regulated by PA at 12 h post hypoxic exposure (lane 14). PA is metabolized *in vivo* into phenylacetyl CoA, a structural analog of acetyl CoA, and inhibits the enzymatic activity of PCX in an allosteric fashion (Zeczycki TN et al., 2010). PCX inhibition would cause a buildup of intracellular pyruvate, which allosterically activates LDHA and results in lactate production. Indeed, the addition of PA in hypoxia slightly increased the intracellular lactate levels, albeit not to a statistically significant manner (Figure 10C). These observed effects were largely recapitulated in WT mouse TSCs (Figure 10D), with two minor exceptions. First, in lactate-treated normoxic TSC cultures, PPARγ levels did not decline (lane 6). Second, 40 mM Ox resulted in PPARγ down-regulation as early as 6, rather than 12 h after hypoxic exposure.

HIF1α levels were not present JEG-3 reared under standard tissue culture conditions (Figure 10A lanes 1, 2, 5 6), and robustly induced by 6 h in hypoxia (lane 3). The addition of exogenous L-lactate reduced HIF1α levels by 6 h in hypoxia, and levels remained low at 12 h post-hypoxic exposure (lanes 7, 8). The addition of both 10 mM and 40 mM Ox completely diminished

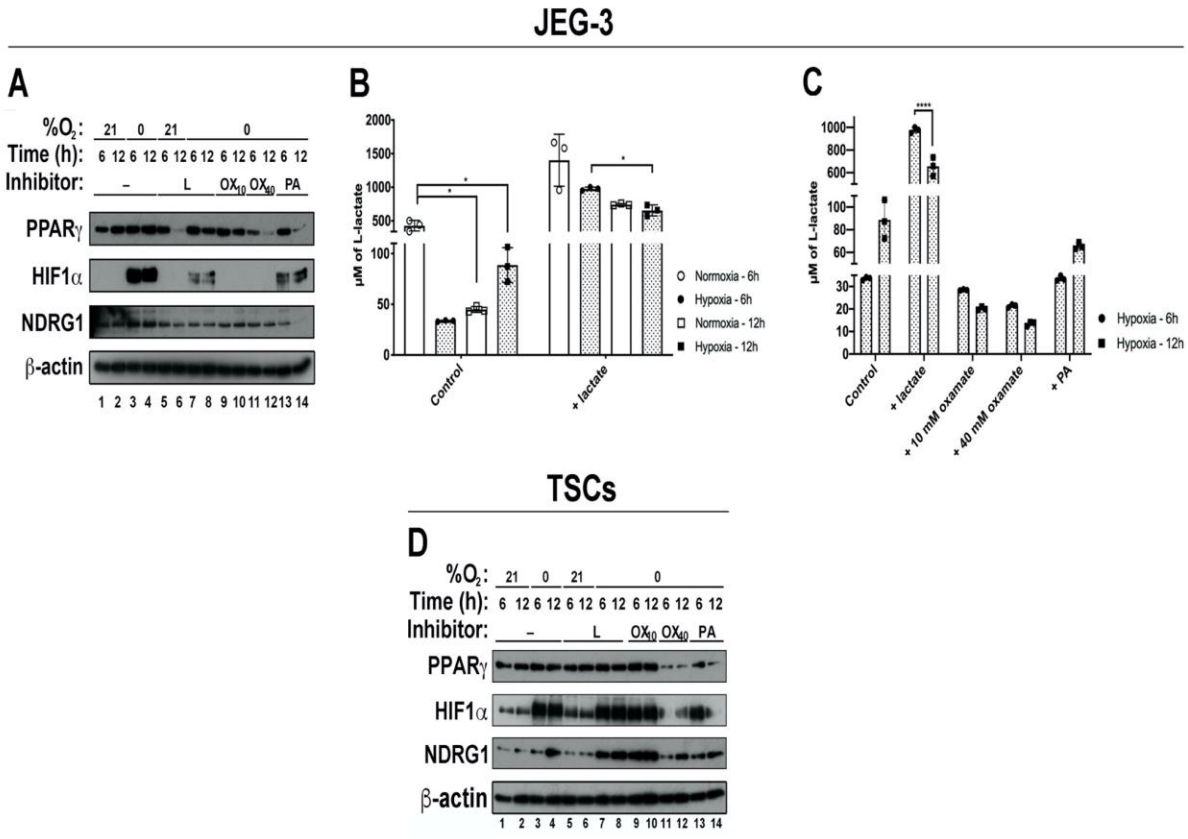

Figure 3-10- Intracellular lactate measurements and accompanying in vitro protein

JEG-3 cells (A) or WT TSCs (GY11; D) were cultured under standard or hypoxic conditions for 6-12 h in the presence or absence of exogenous L-lactate or inhibitors of lactate metabolism. Exogenous L-lactate – 50 mM; Low [Ox] – 10 mM; High [Ox] – 40 mM. Phenylacetic acid (PA – phenylacetic acid; 2.5 mM). (A) and (D) 40 mM Ox abolished HIF1α and PPARγ levels at both hypoxic time points. (B-C) JEG-3 cells were cultured as described and collected for intracellular [lactate] analysis. Briefly, samples were scraped in ice-cold 8% perchloric acid to quench metabolic processes and neutralized. Undiluted samples were analyzed using the Amplite Fluorimetric assay kit exactly according to manufacturer's instructions. Values were analyzed with two-way ANOVA and Tukey's multiple comparisons test. Some significance designations were omitted for clarity and exclusively stated in the text. $P < 0.05$ was considered significant.

HIF1α expression at all time points analyzed in hypoxic JEG-3 cells (lanes 9-12), consistent with results in Figure 9 (lanes 6, 7, 15, 16). This inconsistency may be the function of different culture conditions or cellular density. PA administration also reduced HIF1α levels at both 6 and 12 h of hypoxic exposure relative to untreated hypoxic cells (10A lanes 13, 14). Combined, these data provide a correlation that the intracellular lactate pool largely influences the expression of hypoxia-regulated proteins.

Unlike JEG-3 cells, in TSCs, addition of exogenous lactate, 10 mM Ox, or PA had no discernable effect on HIF1α levels at the 6^{th} or 12^{th} h of hypoxic exposure (Figure 10D, lanes 7-10, 13-14). However, similar to JEG-3 cells, HIF1α levels were decreased at both 6 and 12 h of hypoxia in the presence of 40 mM Ox (10D lanes 11-12). The basis for these differential effects of lactate metabolism inhibitors in TSCs versus JEG-3 cells could be attributable to the transformed nature of JEG-3 cells or the multi-lineage nature of differentiated TSC.

While NDRG1 levels were relatively unchanged at all time points analyzed, it is worthwhile to note that NDRG1 protein was present in normoxic JEG-3 cells in the absence of inhibitor treatment (10A lanes 1, 2). This discrepancy was unexpected, and may be a function of either culture density or the cancerous nature of JEG-3 cells and their altered metabolism. Treatment with PA completely eradicated NDRG1 levels by 12 h in hypoxia (10A lane 14). Whereas NDRG1 expression was relatively stable in JEG-3 cells irrespective of oxygen saturation, NDRG1 levels were increased in hypoxic TSCs by 12 h (10D lane 4). The addition of exogenous lactate further increased levels at both 6 and 12 h in hypoxia (10D lanes 7, 8), an effect not observed in JEG-3 cells. The addition of 10 mM Ox had no effect on NDRG1 expression (10D lanes 9, 10) although treatment with 40 mM Ox and PA significantly reduced NDRG1 protein (10D lanes 11-14).

Overall, the stochastic relationships between the effects of lactate and the various lactate metabolism inhibitors on intracellular lactate concentrations and levels of hypoxia-regulated proteins suggest that another downstream metabolite, or potentially a lactate derivative, rather than lactate itself, regulates hypoxic signaling in trophoblasts.

The results from Figure 10B show that, surprisingly, intracellular lactate levels in JEG-3 cells do not increase by 12 h in hypoxia. Therefore, the time frame was extended, and JEG-3 cells

were cultured under hypoxic conditions for 24h. Intracellular lactate levels increased slightly (Figure 11), although not to statistical significance, possibly attributable to one outlier. The response of hypoxia-regulated proteins, and accompanying intracellular lactate levels, to pharmacological inhibitors were further analyzed to investigate the effect of sustained hypoxic insult (Figure 12). JEG-3 cells were cultured under standard or hypoxic conditions for 24 h in the presence or absence of lactate metabolism inhibitors ± exogenous lactate. The addition of exogenous lactate in all conditions analyzed significantly increased intracellular lactate levels irrespective of pharmacological manipulation (Figure 12B).

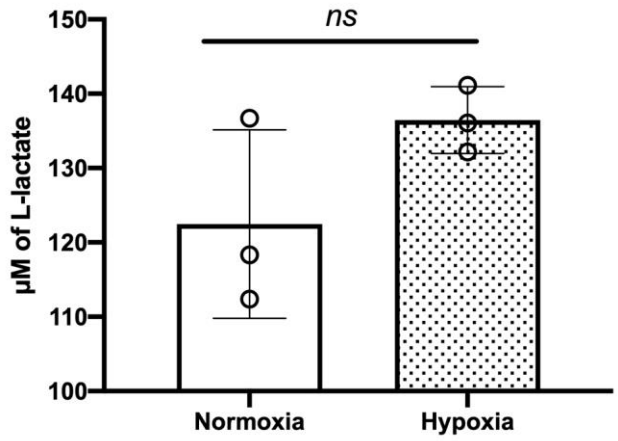

Figure 3-11 - Intracellular lactate concentrations in normoxic and hypoxic JEG-3 cells

Intracellular lactate levels were measured in JEG-3 cells cultured under standard or hypoxic conditions for 24 h. Values were analyzed with an unpaired t-test and Welch's correction. $P < 0.05$ was considered significant. Culture of JEG-3 cells under hypoxic conditions did not increase intracellular lactate accumulation.

The expression levels of PPARγ protein were relatively unchanged in response to stimulation with various inhibitors under normoxic conditions (Figure 12A), although treatment with 100 mM lactate decreased PPARγ protein (12A lane 2) consistent with results in figure 10A. In fact, the addition of 50 mM exogenous lactate was sufficient to decrease PPARγ protein in all

normoxic treatment groups, irrespective of inhibitor treatment (12A lanes 4, 6, 8, 10). PPARγ levels decreased by 24 h in hypoxia, but this effect could be mitigated with the addition of lactate (12A lanes 11, 12). The addition of 10 mM Ox increased the expression of PPARγ in hypoxic JEG-3 cells, consistent with results in Figure 9 (Figure 9 lane 8), while the addition of 10 mM Ox and exogenous lactate was sufficient to completely abolish expression (12A lanes 13, 14). The combinatorial effects of 10 mM Ox and 50 mM lactate increased intracellular lactate levels above baseline in hypoxia (Figure 12B), yet levels remained lower than with the addition of 50 mM lactate alone, as previously reported (Figures 7, 9, 10).

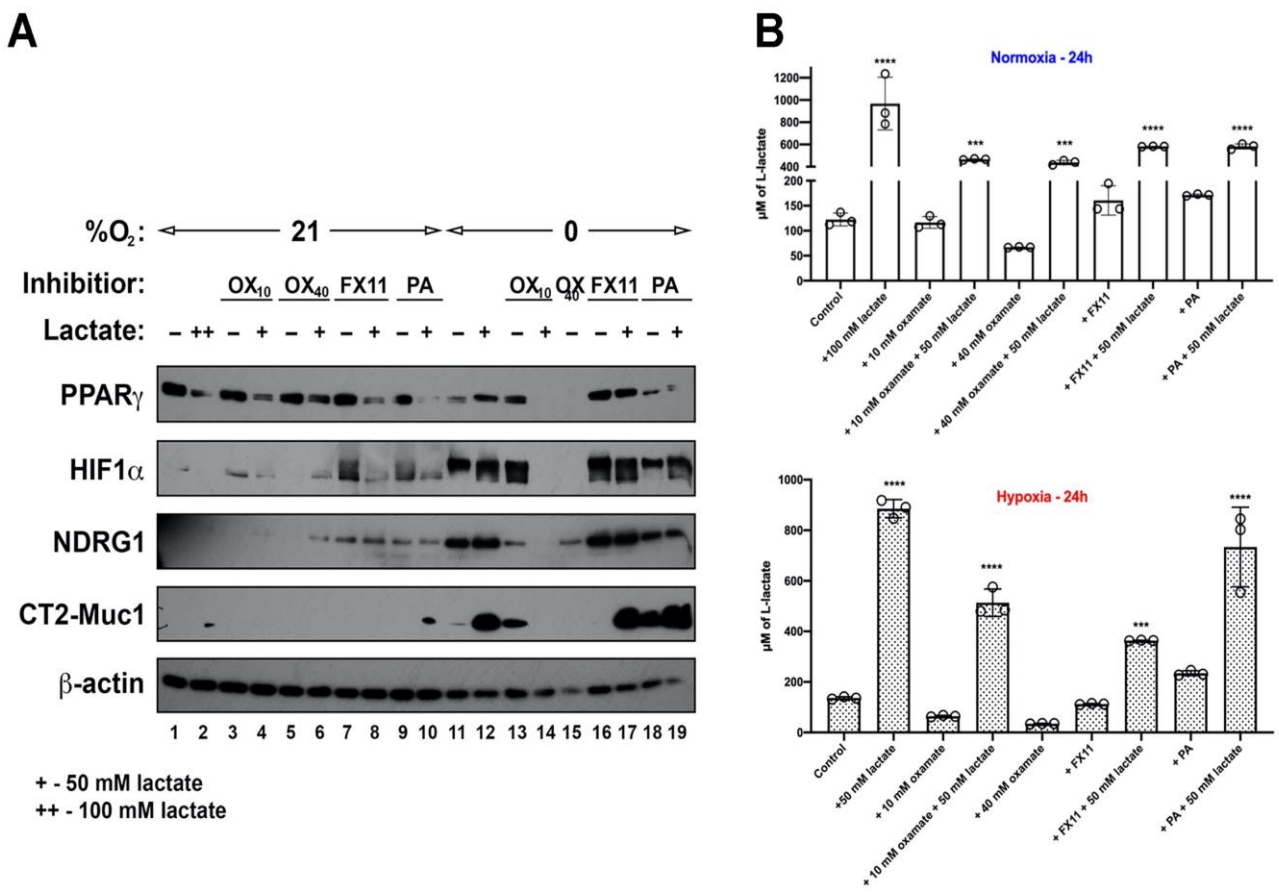

Figure 3-12- Protein and intracellular lactate response to sustained hypoxic insult

JEG-3 cells were cultured under standard or hypoxic conditions for 24 h in the presence or absence of exogenous L-lactate or inhibitors of lactate metabolism. Exogenous L-lactate + - 50 mM or ++ - 100 mM; Low [Ox] – 10 mM; High [Ox] – 40 mM. PA – 2.5 mM; FX11 – LDHA inhibitor – 10 µM. (A) 40 mM Ox abolished HIF1α and PPARγ levels, similar to results shown in Figure 10A. (B) JEG-3 cells were cultured as described and collected for intracellular [lactate] analysis. Values were analyzed with one-way ANOVA and Dunnett's multiple comparisons test. $P < 0.05$ was considered significant. All significance designations (*) are relative to baseline control. The addition of exogenous L-lactate increased intracellular levels in both normoxic and hypoxic conditions irrespective of inhibitor treatment.

The addition of 40 mM Ox and 50 mM lactate was sufficient to cause lethality, precluding protein analysis. The absence of PPARγ in JEG-3 cells treated with 40 mM Ox was coincident was a significant decrease in intracellular lactate levels (Figure 13A), indicating that ultra-precise regulation of lactate metabolism under conditions of acute hypoxia is required for the expression of PPARγ (Figure 12B and 13A). Treatment of JEG-3 cells with FX11 (FX), a selective, reversible, NADH competitive inhibitor of LDHA, did not result in a decline of intracellular lactate

levels in hypoxic JEG-3 cells (Figure 13B), and PPARγ expression was maintained (Figure 12A lane 16). Treatment of hypoxic JEG-3 cells with PA, irrespective of exogenous lactate, decreased PPARγ protein levels (12A lanes 18, 19). The addition of PA alone had no effect on intracellular lactate levels in hypoxia, while the combination of PA and exogenous lactate increased intracellular lactate accumulation (Figure 13C).

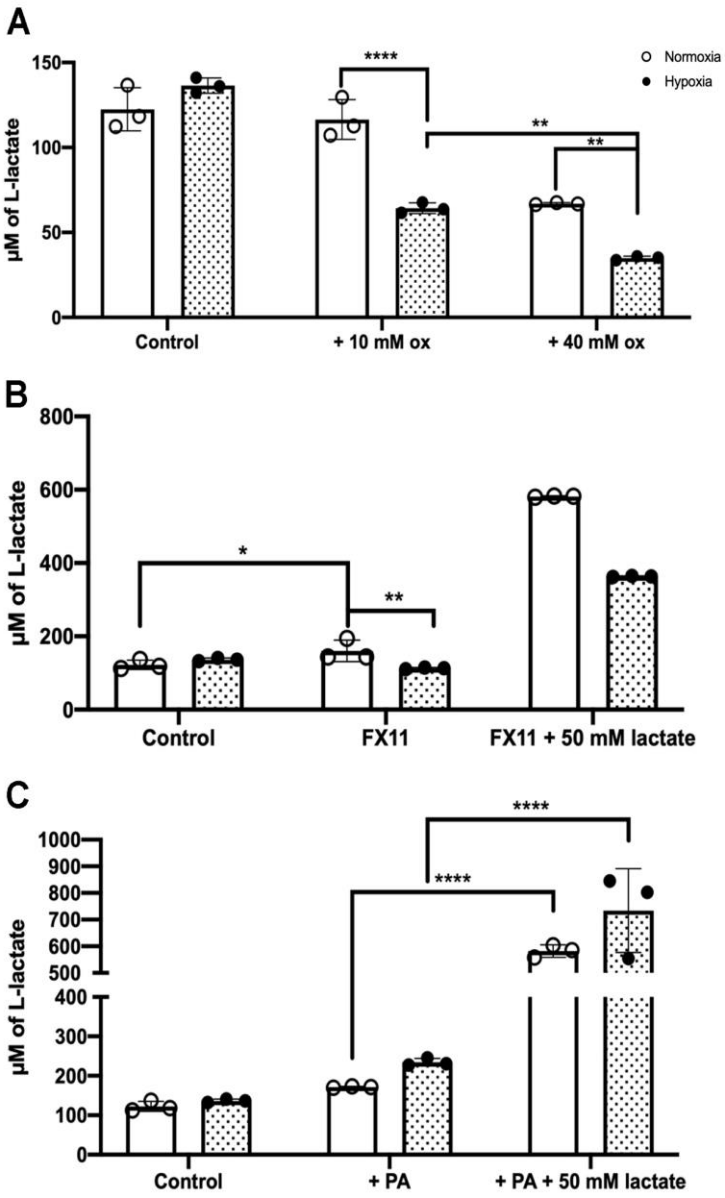

Figure 3-13- Effect of pharmacological inhibitors on intracellular lactate levels

JEG-3 cells were cultured under standard or hypoxic conditions for 24 h in the presence or absence of exogenous L-lactate or inhibitors of lactate metabolism and collected for intracellular [lactate] analysis.. Exogenous L-lactate - 50 mM; Low [Ox] – 10 mM; High [Ox] – 40 mM. PA – 2.5 mM; FX11 – 10 µM. Values were analyzed with a two-way ANOVA and Tukey's multiple comparisons test. $P < 0.05$ was considered significant. Inhibitors had varying effects on intracellular lactate accumulation.

HIF1α protein levels were largely absent in normoxic JEG-3 cells (Figure 12A) yet levels were increased when treated with either FX and PA in the absence of exogenous lactate (12A lanes

7 and 9). Intracellular lactate levels were slightly increased in normoxic cells treated with FX and PA (Figure 13B and C), potentially contributing to HIF1α accumulation in standard conditions. Singlet HIF1α protein is increased by 24 h in hypoxia as expected (12A lane 11). HIF1α levels were further increased with the addition of 50 mM exogenous lactate (12A lane 12) and 10 mM Ox (12A lane 13). Importantly, HIF1α levels were sustained in the presence *or* absence of high intracellular lactate concentrations (Figure 12B), indicating that additional regulation, either at the metabolite or protein level, is involved in maintaining HIF1α levels in hypoxia. Treatment of hypoxic JEG-3 cells with 10 mM Ox and exogenous lactate, or 40 mM Ox alone, completely abolished HIF1α protein levels (Figure 12A lanes 14, 15). In contrast, HIF1α levels were unchanged with the addition of FX irrespective of lactate supplementation (12A lanes 16, 17). Treatment with FX decreased lactate levels similar to that of 10 mM and 40 mM Ox (Figure 12B), further contributing to the notion that additional regulation of hypoxia-responsive proteins is at play. Singlet HIF1α protein was observed in JEG-3 cells treated with PA (12A lane 18) and the addition of lactate rescued the HIF1α doublet (12A lane 19). These data indicate that intracellular lactate, under normoxic conditions, can stabilize HIF1α, although the intimate details of this complex regulation, particularly under hypoxic conditions, remains elusive.

NDRG1 protein levels were remained at near zero in most normoxic conditions yet were slightly induced when cultured with the highest concentration of Ox and exogenous lactate (12A lane 6). Curiously, the addition of exogenous lactate alone (12A lane 2) was insufficient to increase NDRG1 levels despite higher intracellular lactate concentrations (Figure 12B). Additionally, treatment of normoxic JEG-3 cells with FX or PA, in the presence or absence of lactate, increased NDGR1 levels (12A lanes 7-10) despite drastically different intracellular lactate levels (Figure 13B, C). Robust NDRG1 induction was observed by 24 h in hypoxia (12A lane 11)

and sustained with the addition of 50 mM lactate (12A lane 12). The addition of 10 mM Ox decreased intracellular lactate levels in hypoxia (Figure 13A) and a coincident decline in NDRG1 protein level was observed (Figure 12A lane 13), consistent with results from Figure 9 lane 8. However, the addition of exogenous lactate was unable to ameliorate this decline (12A lane 14) despite increased intracellular lactate levels (Figure 12B). Treatment of hypoxic JEG-3 cells with 40 mM Ox caused a similar decline in NDRG1 protein (12A lane 15) and coincided with significant decrease in intracellular lactate levels relative to 10 mM Ox (Figure 13B). NDRG1 levels were relatively stable with the addition of FX or PA, irrespective of lactate supplementation, in hypoxia (12A lanes 16-19).

The expression of Muc1 in the presence or absence of various inhibitors of lactate metabolism was investigated to determine if intracellular lactate manipulation could sustain Muc1 levels in hypoxia (*see* Figures 1 and 2). Baseline normoxic expression of MUC1 was not observed in JEG-3 cells (Figure 12A lanes 1-10), potentially owing to their predominately hypertriploid or cancerous nature. Muc1 protein levels were significantly induced with 50 mM lactate supplementation by 24 h in hypoxia (12A lane 12). The addition of 10 mM Ox in hypoxia did not result in a significant decline in intracellular lactate production as compared to hypoxic controls (Figure 13A), yet was sufficient to cause a reduction in Muc1 protein levels (12A lane 13). The addition of exogenous lactate completely abolished protein levels, consistent with the regulation of additional hypoxia-responsive proteins (12A lane 14), and resulted in a significant increase of lactate accumulation relative to hypoxic controls (Figure 12B). Moreover, treatment with 40 mM Ox resulted in a complete shutdown of Muc1 protein, consistent with the levels of PPARγ and HIF1α (12A lane 15). This effect was recapitulated in hypoxic JEG-3 cells treated with FX (12A lane 16). Interestingly, both inhibitors reduced lactate levels as compared to hypoxic controls

(Figure 12B), yet were largely similar to the lactate concentration in hypoxic cells treated with 10 mM Ox, which permitted Muc1 expression (12A lane 13). MUC1 levels were rescued with the addition of FX and 50 mM lactate in hypoxic JEG-3 cells (12A lane 17) and levels were sustained with the addition of PA (12A lane 18). The addition of PA and exogenous lactate further augmented MUC1 levels (12A lane 19).

While the results presented herein are compelling, a clear trend between the expression of hypoxia-regulated proteins and intracellular lactate levels was largely absent. However, the "Goldilocks" effect of lactate accumulation on trophoblast hypoxic signaling suggests an important role for lactate metabolism and indicates that potentially all players in this pathway have not yet been identified.

3.3 I*n vivo* functions of *Ldhb*

The intricate quantitative and qualitative regulation of hypoxia-responsive proteins by lactate and its metabolites set the stage for the intriguing idea that lactate may be acting as a direct effector, or a precursor for one, in trophoblast hypoxic signaling. This notion is not exclusive to the placenta, as it was previously demonstrated that lactate-stabilized NDRG3 signals through the MAP kinase axis to promote VEGF-mediated angiogenesis (Lee DC et al., 2015). LDHB is responsible for the conversion of lactate to pyruvate and is one of the most robust targets of placental PPARγ. We reasoned that in the absence of PPARγ, lactate levels accumulate in trophoblasts and may contribute to the developmental defects observed in Pparg-null placentas. To directly approach this question, Ldhb-null mice were used to determine the effect of LDHB deficiency on placental development under steady state conditions and chronic hypoxic exposure.

3.3.1 *Ldhb*$^{\Delta/\Delta}$ targeting and validation

Ldhb$^{\Delta/\Delta}$ mice were generated before the start of this project by previous Barak lab members (Sungeun Lee and Srinivas R. Pallerla). *Loxp* sites flanking either side of exon 3 were inserted into the target allele using recombinant DNA technology (Figure 14A). Maternal sox2-Cre was crossed with *Ldhb*$^{fl/+}$ mice to globally delete the *Ldhb* floxed allele. *Ldhb*$^{\Delta/+}$ founders were backcrossed onto both B6 and 129 backgrounds for several generations before phenotypic analysis. Mice heterozygous for the mutation were crossed to generate WT, heterozygous, and null placentas. Western blot analysis of E18.5 placentas confirms robust expression of LDHB in WT, reduced expression in heterozygotes, and complete deficiency in null animals (Figure 14B).

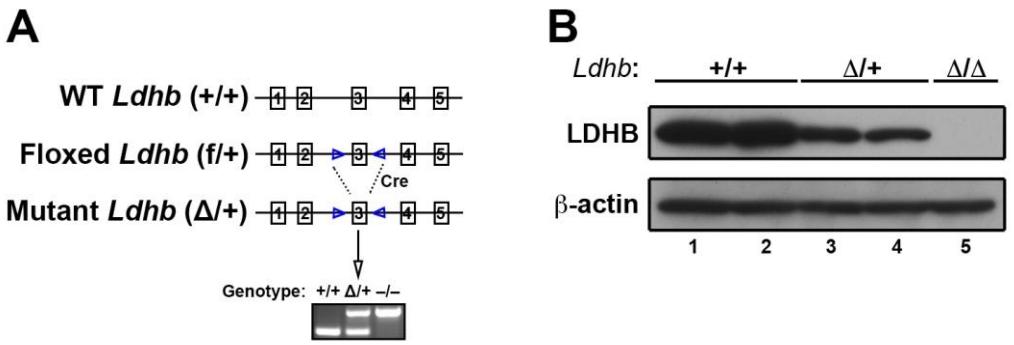

Figure 3-14- Ldhb targeting and validation

(A) Recombineering methodology was used to introduce *loxp* sites flanking exon 3 of the *Ldhb* gene. The final targeting vector was introduced into ES cells, clones were selected for the correct integration in the *Ldhb* locus, and homologous recombinant clones were used to generate *Ldhb*-null mice. (B) A Western blot of E18.5 placentas from WT and *Ldhb*-null embryos confirm the loss of LDHB protein in *Ldhb*-null placentas, as well as significant reduction in *Ldhb*-heterozygous placentas. β-actin confirms equal sample loading in all lanes.

3.3.2 Phenotypic analysis of *Ldhb*$^{\Delta/\Delta}$ mice

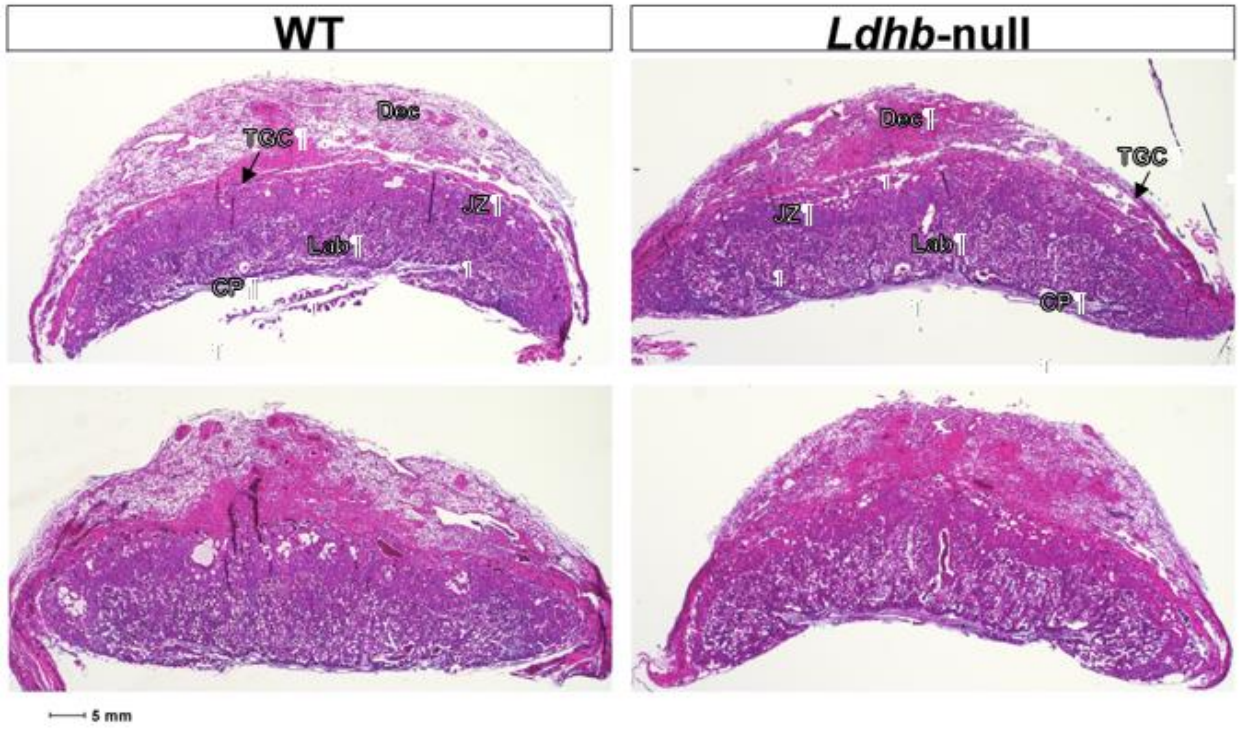

Figure 3-15 - Ldhb-null placentas display no gross abnormalities

Whole placentas (E12.5) were collected from WT and *Ldhb*-null embryos. Placentas were fixed in neutralized 4% PFA, dehydrated in a graded EtOH series, and embedded in paraffin wax. Midline cross sections (5 µm) were stained with H&E. Dec – maternal decidua; TGC – trophoblast giant cell; JZ – junctional zone; Lab – labyrinth; CP – chorionic plate. *Ldhb*-null placentas do not display any differences in gross morphology or cellular distribution.

Under normal husbandry conditions, *Ldhb*-null mice are born at the expected Mendelian frequency with no observable changes in viability, health, or fertility. Placentas collected from WT and *Ldhb*-null embryos at mid-gestation demonstrate that all placental layers are intact (i.e., chorion, labyrinth, JZ, and maternal decidua) and gross abnormalities in cellular distribution or layer formation are not detected (Figure 15). This indicates that LDHB is not essential for placental development or embryonic survival and growth under standard conditions.

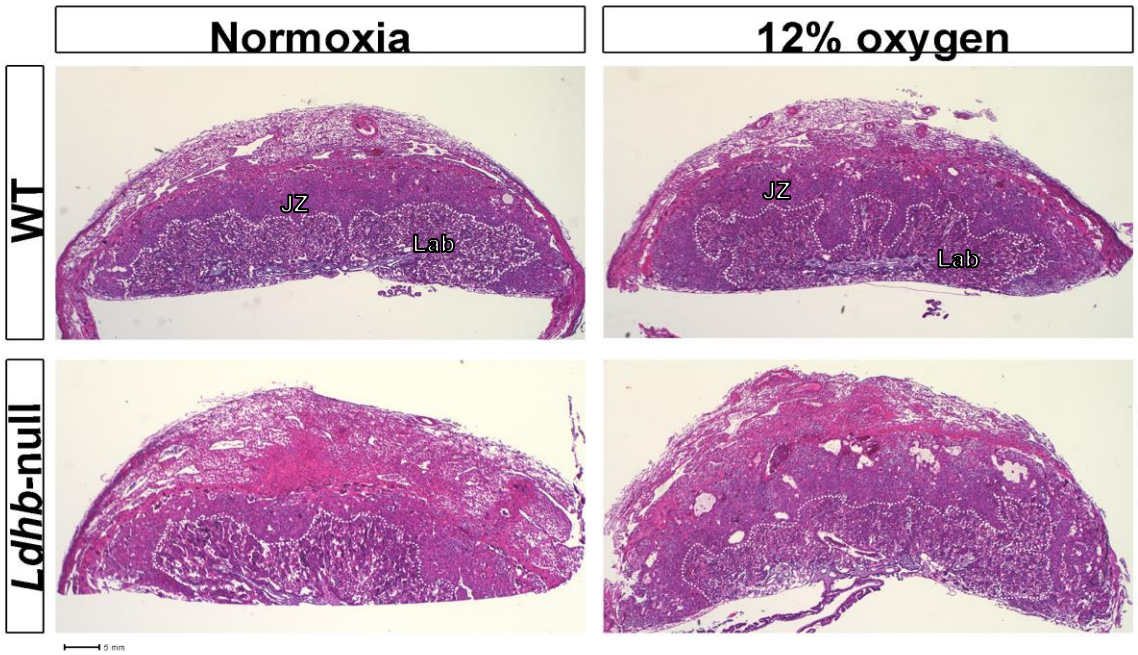

Figure 3-16- Hypoxic insult reduces labyrinth area in WT embryos

Dams pregnant with the product of heterozygous crosses were reared in 12% oxygen from E9.5 – 12.5. Whole placentas were collected from WT and *Ldhb*-null embryos. Placentas were fixed in neutralized 4% PFA, dehydrated in a graded EtOH series, and embedded in paraffin wax. Midline cross sections (5 µm) were stained with H&E. JZ – junctional zone; Lab – labyrinth. Outline designates Lab-JZ border. WT embryos reared in hypoxic conditions display an irregular Lab-JZ border and reduced total labyrinth volume.

To test whether LDHB has important functions during chronic hypoxic exposure, heterozygous dams and sire were mated and housed under standard conditions or placed under 12% oxygen from E9.5-E12.5 to determine the effect of chronic hypoxic exposure on placental development in *Ldhb*-null embryos (Figure 16). Whole placentas collected from WT and $Ldhb^{\Delta/\Delta}$ embryos from dams housed under normal ambient conditions were indistinguishable and displayed a typical labyrinth-JZ border. In contrast, WT placentas collected from embryos of hypoxic pregnancies displayed an irregular labyrinth-JZ border, possibly attributable to SpT invasion into the labyrinth or attenuated migration of SpT to the distal JZ, and *Ldhb* deficiency appeared to mitigate this effect.

3.3.3 Vascular analysis of *Ldhb*$^{\Delta/\Delta}$ placentas

While H&E staining is informative with respect to gross morphology and placental organization, in-depth information regarding labyrinth formation is difficult to deduce. Therefore, a reliable method to detect changes in the placental vascular architecture in response to genetic and environmental manipulation was critical for further investigation. Confocal area scans were used to determine the effect of *Ldhb* deficiency on vascular tree formation and gain deeper insight into the role of hypoxia during placental development. To that end, dams pregnant with *Ldhb*$^{\Delta/+}$ intercrosses were housed in 12% O_2 from E9.5-15.5 to simulate chronic hypoxic exposure. At E15.5 embryos and placentas were assessed for viability, weighed, and genotyped. There was relatively no change in embryonic or placental weight irrespective of genotype or hypoxic exposure. Placentas were subsequently cryoembedded in OCT for IF analysis. Midline sections were permeabilized and stained with α-CD31 (red; eBioScience) and α-Muc1 (green; ThermoFisher Scientific) to visualize the fetal blood vessels and maternal blood sinuses, respectively. Images were acquired on a Nikon A1 confocal microscope equipped with a motorized stage and 20x objective to collect stepwise images. The acquired image tiles were stitched together to generate a comprehensive overview of the vascular structure (Figure 17).

There were no significant differences in WT or *Ldhb*-null placentas collected from normoxic pregnancies with respect to total labyrinth volume or vascular organization. In contrast, the total labyrinth volume of hypoxic WT embryos placentas was significantly reduced compared to WT normoxic counterparts. *Ldhb* deficiency appeared to ameliorate this effect, suggesting that the absence of LDHB is protective in conditions of reduced oxygen saturation. Interestingly, the three hemochorial trophoblast layers of the labyrinth was intact in both WT and *Ldhb*$^{\Delta/\Delta}$ placentas collected from hypoxic pregnancies (Figure 17, inset), confirming an underlying developmental,

as opposed to structural, defect of WT hypoxic placentas. Because LDHB is responsible for converting lactate to pyruvate, it is tempting to speculate that the protective effect observed is due

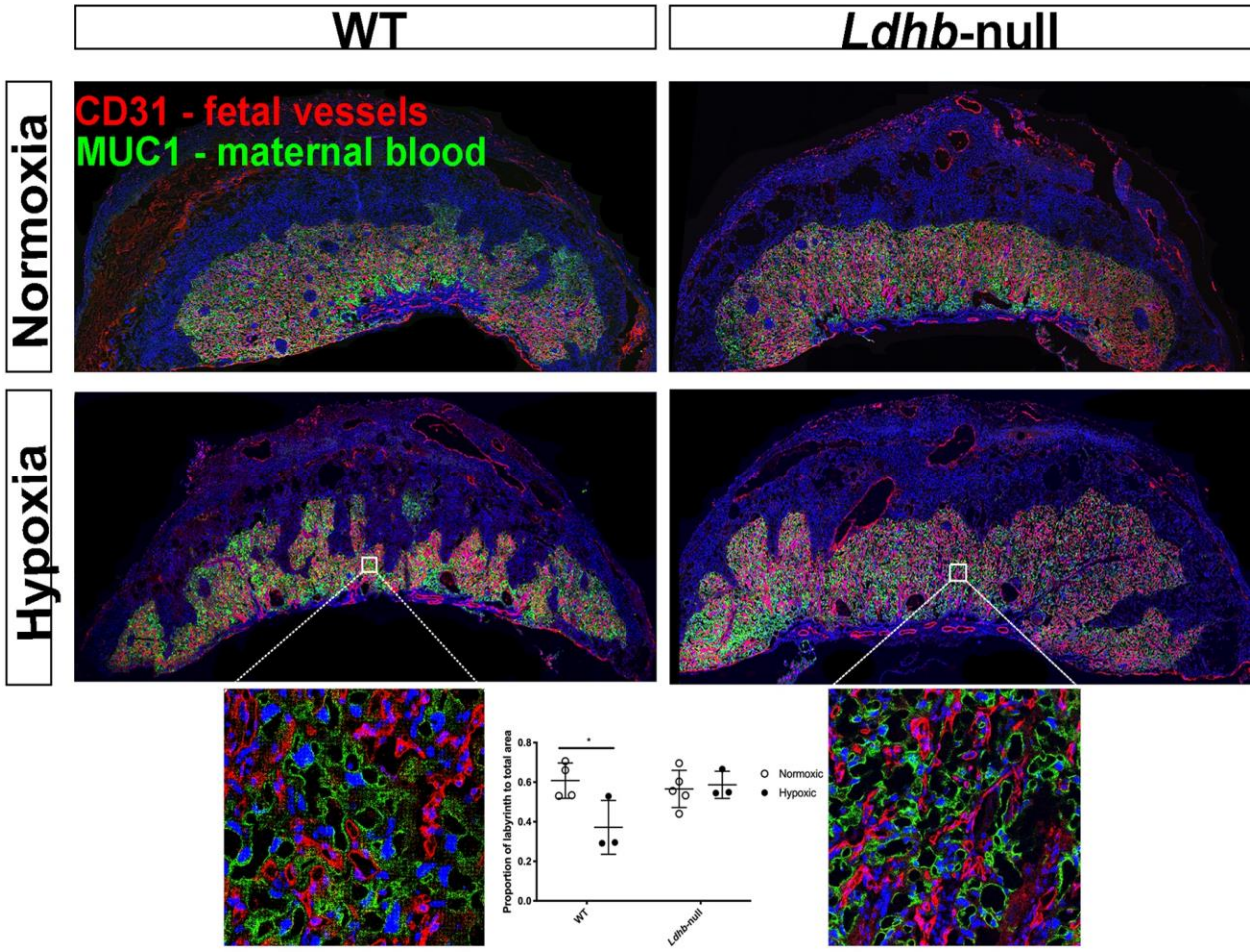

Figure 3-17- Ldhb deficiency mitigates vascular defects in hypoxic placentas

Ldhb$^{\Delta/+}$ dams pregnant with the product of heterozygous crosses were randomly allocated to either standard or hypoxic (12% O_2) conditions from E9.5-15.5 Midline serial sections of WT and *Ldhb*-null placentas were stained with α-CD31 and α-Muc1 to visualize the fetal vessels and maternal blood sinuses, respectively. Images were acquired on a Nikon Spectral A1 confocal microscope equipped with a 20x scanning objective and motorized stage to collect stepwise images. The acquired image tiles were stitched together to generate a comprehensive overview of the vascular tree. The total labyrinth area was quantified on whole area scans in the program Nis Elements. Inset depicts the intimate association of fetal vessels and maternal blood sinuses. Values were analyzed for significance with a two-way ANOVA and Tukey's multiple comparisons test. $P < 0.05$ was considered significant. Labyrinth growth was stunted in WT placentas reared in hypoxia, while *Ldhb* deficiency mitigated this effect.

to the accumulation of lactate, which may regulate factors that instruct trophoblast differentiation or promote fetal vessel angiogenesis.

3.4 *In vitro* genetic analyses of the trophoblast hypoxia-response pathway

The effect of Ldhb deficiency on development of the placental vascular tree in hypoxic pregnancies was striking (see Figure 17), and solidified the notion that lactate production and clearance may have profound effects on trophoblast hypoxic signaling and subsequent placental development. In addition, treatment of JEG-3 cells or TSCs with inhibitors of lactate metabolism revealed the complexities of intracellular lactate regulation and its effect on the expression of multiple hypoxia-responsive proteins in trophoblasts. Given the non-specific nature of chemical inhibitors, and potential confounding off-target effects, a more precise method of interrogation was required. To that end, CRISPR-Cas9 genetic engineering was used to delete key genes involved in the regulation of lactate metabolism in JEG-3 cells, including LDHB, PCX, PPARγ, and NDRG1, to further tease apart the regulatory properties of lactate in hypoxic trophoblasts.

3.4.1 Generating the KOs

To further delineate the PPARγ-HIF1α axis and determine the role of lactate metabolism in hypoxic trophoblasts, monoclonal cell lines with homozygous deletions of essential hypoxia-regulatory proteins were generated. A stable parent clone, containing dox-inducible Flag-Cas9 expression, was generated first and served as the foundation for all subsequent genetic modifications. To generate this clone, JEG-3 cells were transfected with a puro-resistant plasmid expressing the dox- dependent activator, rtTa, and TET-response element driven Flag-Cas9 (Figure 18). Individual puro-resistant colonies were selected, expanded, and incubated in the presence or absence of 1 μM dox. Western blot analysis was used to determine the extent of Cas9 induction post-stimulation.

As demonstrated in Figure 18, JEG clone 5.1, herein referred to as JEG 5.1, displayed undetectable levels of Flag-Cas9 at baseline, yet robust induction upon stimulation, and thus was chosen as the parent clone for further genetic modifications. JEG 5.1 primed with dox for two

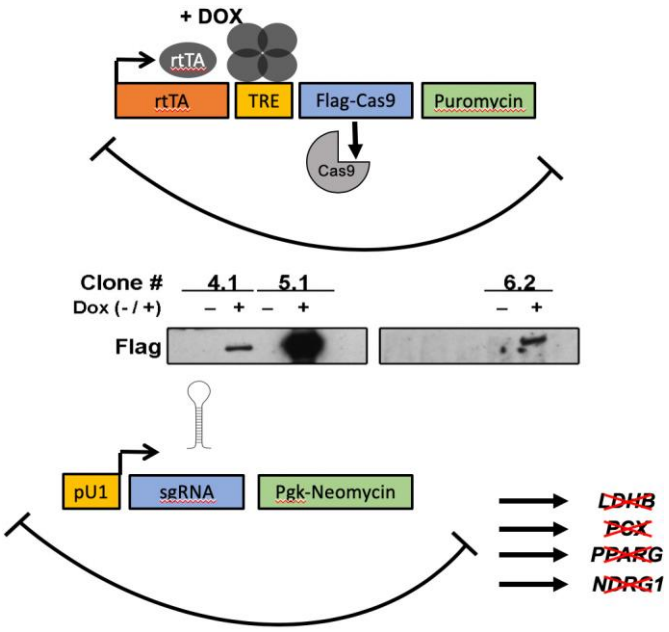

Figure 3-18- Generation of monoclonal cell lines with dox-inducible Cas9 expression

JEG-3 cells were transfected with a puro-resistant plasmid that expressed a dox-dependent activator of FLAG-Cas9. Individual puro-resistant clones were selected, expanded, and incubated in the presence or absence of 1 μM dox for two days and screened for the expression of Flag-Cas9 with α-FLAG M2 antibody. JEG 5.1 produced high levels of Flag-Cas9 when stimulated as compared to undetectable levels at baseline, and therefore was selected as the parent clone for all subsequent genetic modifications. Neo-resistant vectors containing guides directed against the target gene were subsequently transfected into JEG5.1, selected, and screened for appropriate genetic deletion.

days to induce Cas9 expression, and then co-transfected with multiple vectors expressing neo resistance and sgRNAs directed against the gene of interest. Colonies were selected with G418, expanded, and analyzed first by PCR to confirm deletion at both alleles of each gene and then by Western blot to confirm deficiency at the protein level. All plasmids, sgRNAs and analytical oligos used are listed in appendices A and B, respectively.

3.4.1.1 PPARγ$^{-/-}$ trophoblasts are not viable

sgRNAs were inserted in exons 6 and 7 of the human *PPARG* gene (Figure 19). Very few clones survived selection, and even fewer were viable at the validation stage, and as such only one clone was generated. *Pparg*-null JEG-3 cells proliferated at an extremely slow rate, exhibited reduced viability in culture, and had poor survival yield upon passaging. Due to their slow growing nature and overall reduced viability, these cells could not be experimentally tested in hypoxia or otherwise. However, this observation may provide useful insight into the role of placental PPARγ, as discussed later.

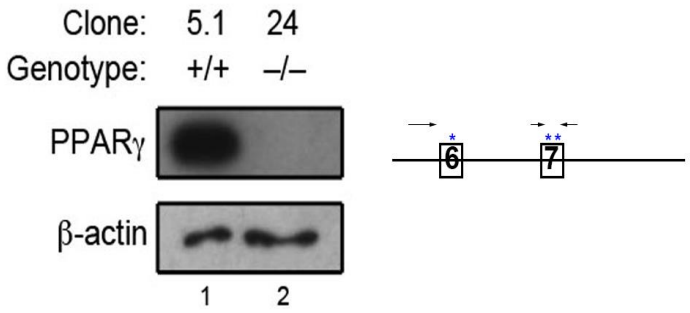

Figure 3-19- PPARG targeting and validation

Guides directed against exons 6 and 7 of the human *PPARG* gene were transfected into JEG 5.1 cells. A graphical representation of gene targeting is provided for clarity. (*) designate location of sgRNAs, and arrows represent the location of analytical oligos used for genotyping. Western blot analysis confirms the loss of PPARγ protein in clone #24.3. β-actin confirms equal sample loading in all lanes.

3.4.1.2 *LDHB* deletion has no effect in hypoxic trophoblasts

JEG 5.1 were transfected with guide RNAs targeted in exon 3, and introns 2 and 3, of the human *LDHB* gene as described above. Colonies were selected based on PCR analysis of both WT *LDHB* alleles, expanded, and analyzed for the expression of LDHB (Figure 20). LDHB protein was absent from all clones analyzed. *LDHB*$^{-/-}$ cells displayed no overt changes in cell cycle

regulation (i.e., proliferation), morphology, or overall cell vitality, and thus were further interrogated to determine their hypoxic phenotype.

LDHB$^{-/-}$ cells were cultured under standard or hypoxic conditions for 6-48 h in the presence or absence of 1 μM Rosi. LDHB protein was completely absent from clone #62.1, and slightly increased in parental JEG 5.1 cells in response to Rosi (Figure 21A and B) as expected (Shalom-Barak T et al., 2012). The expression of PPARγ was relatively stable at all time points analyzed and, surprisingly, was sustained by 72 h in hypoxia in both WT and *LDHB*-null cells. Consistent with previous results, PPARγ protein levels slightly declined in the presence of Rosi (Figure 21B), indicative of negative feedback regulation. HIF1α was undetectable in normoxic WT and *LDHB*-null cells (A – lane 1 and 7, B – lane 13 and 18) and remained stable throughout culture in hypoxia. Additionally, NDRG1 expression increased throughout the course of hypoxic exposure, and levels were somewhat reduced in the presence of Rosi (Figure 21B), as shown earlier, irrespective of the presence or absence of LDHB. Given these relatively unremarkable results, further *LDHB*-null clones were not analyzed.

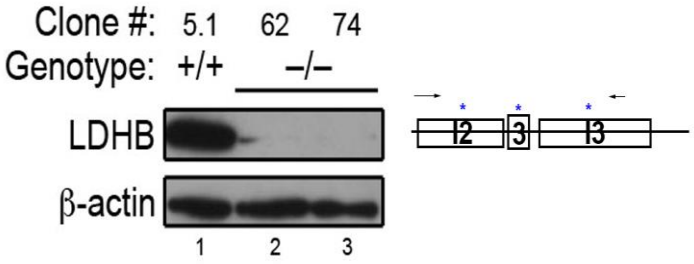

Figure 3-20- LDHB targeting and validation

JEG 5.1 cells were transfected with sgRNAs directed against introns 2 and 3, and exon 3, of the human *LDHB* gene. A graphical representation of gene targeting is provided for clarity. (*) designate location of sgRNAs, and arrows represent the location of analytical oligos used for genotyping. Western blot analysis confirms the loss of LDHB protein in 2 clones. β-actin confirms equal sample loading in all lanes.

3.4.2 PCX deletion negatively regulates hypoxia-responsive proteins

Plasmids containing sgRNAs directed at exon 3 of the *PC* locus were introduced in JEG 5.1 and subsequently selected, expanded, and analyzed for the expression of PCX protein. Western blot analysis confirms the loss of PCX in null clones (Figure 22). Morphology and lethality patterns were well conserved between WT and *PC*-null cells, yet $PC^{-/-}$ cells proliferated slower than the parental JEG 5.1 clone. Considering that PCX catalyzes the carboxylation of pyruvate to form OAA, which is a critical intermediate in multiple metabolic pathways (Jitrapakdee S et al., 1999). It is likely that the absence of PCX causes a decline in intracellular OAA, effectively inhibiting production of a key building blocks required for demanding metabolic processes such as cell division.

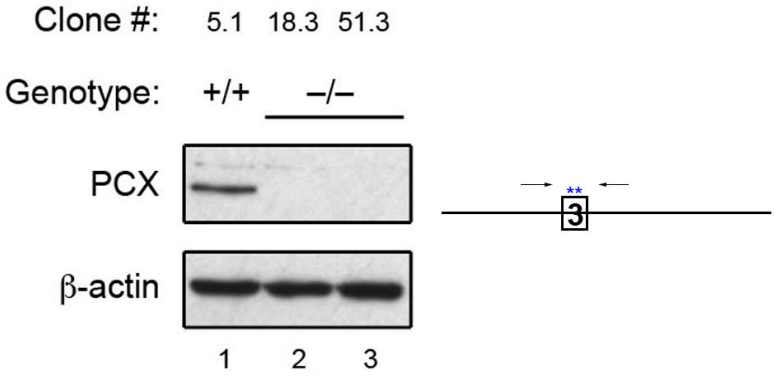

Figure 3-21 - Targeting and validation of PCX

Plasmids containing sgRNAs targeted towards exon 3 of the human *PC* gene were transfected into JEG 5.1. (*) designate location of sgRNAs, and arrows represent the location of analytical oligos used for genotyping. Clones were generated as described previously and analyzed for the expression of PCX by Western blot Western blot analysis confirms the loss of PCX in null clones. β- actin indicates equal sample loading in all lanes.

Despite decreased proliferation rates, *PC*-null cells were viable and therefore further interrogated to determine if PCX deficiency influences the expression of hypoxia-regulated

proteins. JEG 5.1 (control) or *PC*$^{-/-}$ cells were cultured under either standard or hypoxic conditions 6-48 h in the presence or absence of Rosi (Figure 23). *PC-null* cells died by 48 h in hypoxia, irrespective of Rosi addition, precluding protein analysis. Expression levels of PCX in JEG 5.1 were stable throughout most of the hypoxic time course and declined by 48 h, potentially attributable to a concurrent decline in PPARγ protein (lane 5). Rosi supplementation slightly increased PCX expression at all time points, as expected, as well as suppressed PPARγ levels, as shown before (lanes 5-10). PPARγ protein in *PC*-null cells were comparable to control (lanes 11-14) and were similarly suppressed by the addition of Rosi (lanes 15-18).

PCX deficiency had no apparent effect on the expression of HIF1α in null cells in the absence of Rosi, and its levels were sustained up to 24 h in hypoxia (lanes 11-14). In contrast, supplementation with Rosi suppressed HIF1α induction in *PC*-null cells (lanes 15-18) and

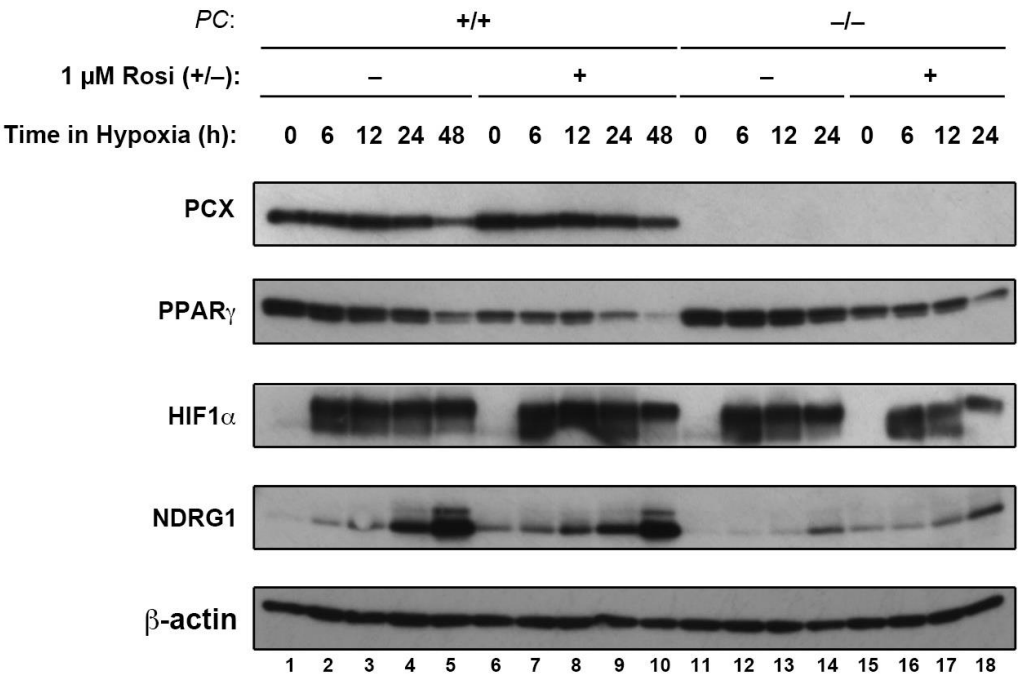

Figure 3-22- PCX deficiency decreasees NDRG1 expression in hypoxia

JEG 5.1 or *PC*$^{-/-}$ clone #18.3 were cultured under standard or hypoxic conditions for 6-48 h in the presence or absence of 1 µM Rosi. NDRG1 protein levels were significantly decreased in *PC*-null cells as compared to control (5.1). β-actin confirms equal sample loading in all lanes.

significantly hastened its decline by 24 h, reflected in complete suppression of the lower MW band of the HIF1α doublet (lanes 15-18).

Most importantly, PCX deletion had a profound influence on NDRG1 levels in hypoxic cultures. Induction was substantially blunted and delayed irrespective of Rosi supplementation, with a slight increase by the 24 h mark (lanes 14, 18). Rosi treatment slightly increased NDRG1 levels compared to the untreated counterparts (lane 18). This effect may correlate with the concomitant decline in PPARγ expression (lane 18), in line with the previously described properties of PPARγ as a negative regulator of NDRG1 expression.

3.4.3 NDRG1 deletion had no effect on the expression of hypoxia-regulated proteins

Guide RNAs directed towards exons 4 and 5 of the *NDRG1* gene were introduced in JEG 5.1 cells, and clones were selected based on their resistance to neo as described previously (*see section 3.4.1*). Since NDRG1 is typically exclusively present in hypoxic trophoblasts, clones were cultured under hypoxic conditions for 24 h to confirm deletion of NDRG1 protein. Indeed, *NDRG1*-null clones did not induce NDRG1 protein by 24 h in hypoxia as compared to JEG 5.1 (Figure 24). *NDRG1*-null cells displayed no differences in cell cycle regulation, gross morphology or overall cell viability in standard tissue culture conditions as predicted.

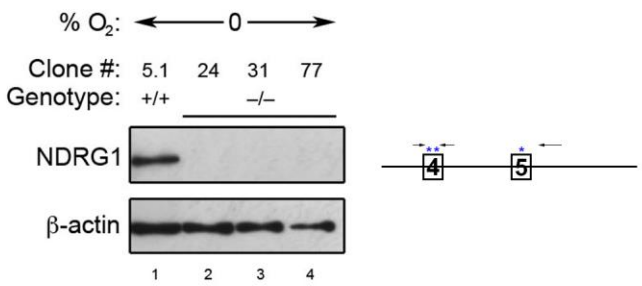

Figure 3-23- NDRG1 targeting and validation

JEG 5.1 cells were transfected with plasmids containing sgRNAs targeted towards exons 4 and 5 of the human *NDRG1* gene. (*) designate location of sgRNAs, and arrows represent the location of analytical oligos used for genotyping. JEG 5.1 and *NDRG1*-null cells were cultured under hypoxic conditions for 24 h. Western blot analysis confirmed the loss of NDRG1 protein in hypoxia as compared to its retention in the parent clone JEG 5.1. β-actin confirms equal sample loading in all lanes.

Surprisingly, NDRG1 deficiency had no effect on the expression kinetics of any hypoxia-regulated proteins despite what appeared to be a complete KO by Western blotting. The top band represents cross-reactivity of the polyclonal α-NDRG1 antibody (Figure 25).Because the

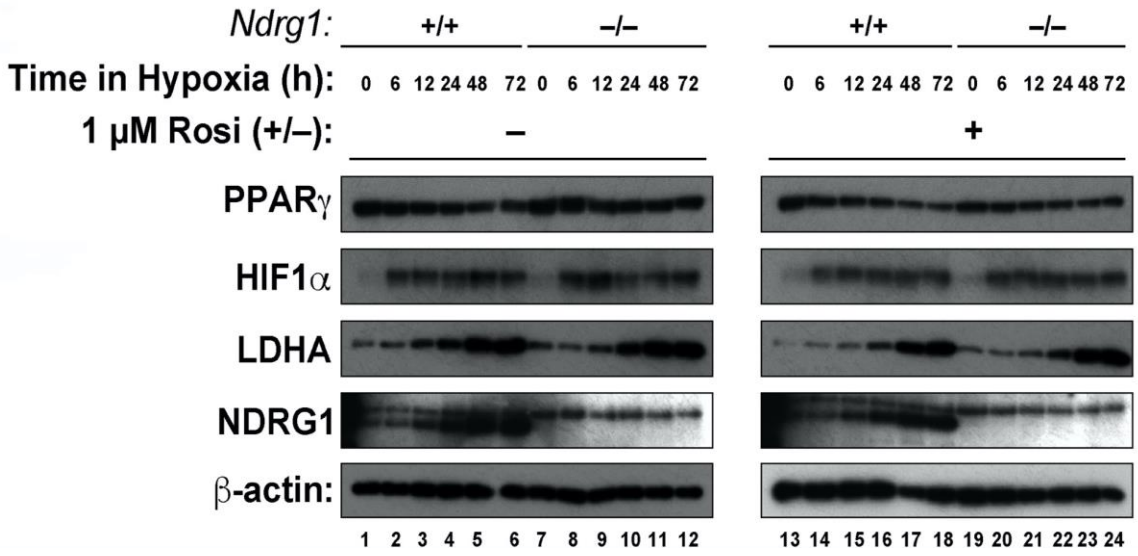

Figure 3-24- NDRG1 deficiency has no effect on the expression of hypoxia-regulated proteins

JEG 5.1 and *NDRG1*$^{-/-}$ clone #77.1 were reared under standard or hypoxic conditions from 6-72 h in the presence or absence of Rosi (1 μM). NDRG1 deletion did not affect the expression of any hypoxia-regulated proteins. β-actin confirms equal sample loading in all lanes.

stabilization of the NDRG family of proteins is reported to be positively regulated by lactate (Lee DC et al., 2015), the expression of LDHA was analyzed in addition to the standard suite of proteins tested in other KO lines. LDHA induction slightly lagged behind the hypoxia-induced induction of HIF1α, consistent with HIF-dependent regulation of LDHA in hypoxic trophoblasts (Kay HH et al., 2007). Moreover, time-dependent up-regulation of LDHA roughly coincided with the timing of NDRG1 upregulation in JEG 5.1, suggestive of close regulatory relationships and consistent with the expectation that increased lactate synthesis should further stabilize NDRG1 (Lee DC et al., 2015). However, LDHA levels and induction kinetics were roughly similar irrespective of NDGR1 status in the cells. Given the absence of dramatic effects in this *NDRG1*-null clone, additional null clones were not further analyzed.

3.4.4 MUC1 deletion has disparate effects on the expression of hypoxic proteins

MUC1$^{-/-}$ cells were generated as previously described (*see section 3.4.1*). Briefly, plasmids containing sgRNAs targeted towards exon 7, and introns 6 and 7, of the human *MUC1* gene were introduced in JEG 5.1 cells to selectively disrupt the C-terminal cytoplasmic tail (CT-2) domain.

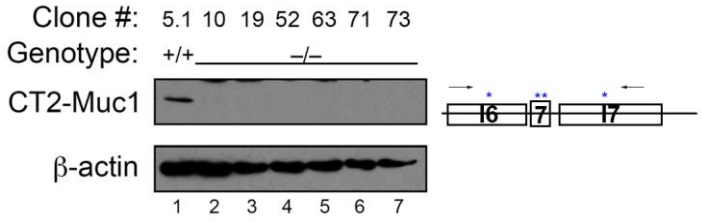

Figure 3-25- Muc1 targeting and validation

JEG 5.1 cells were transfected with plasmids containing sgRNAs targeted towards exon 7 and introns 6 and 7 of the human *MUC1* gene. (*) designate location of sgRNAs, and arrows represent the location of analytical oligos used for genotyping. Muc1 expression is completely abolished in null clones as confirmed by Western blot. β-actin confirms equal sample loading in all lanes.

The CT-2 domain is proteolytically cleaved from the holo-Muc1 protein, and is believed to regulate the signaling functions of Muc1 in both the cytoplasm and the nucleus (Brayman M et al., 2004). It was therefore targeted to ensure complete shutdown of downstream Muc1 signaling, although it is possible that other Muc1 variants containing the sialylated extracellular and transmembranal domains are still expressed in some KO combinations. Western blot analysis confirms the loss of Muc1-CT2 protein in the 6 clones generated, with the parental clone JEG 5.1 serving as a positive control (Figure 26). Similar to *PPARG*$^{-/-}$ cells, *MUC1*-null cells were slow-growing and died upon passaging, albeit to a lesser extent (~50% replating efficiency based on empirical observations). Although the placental function of Muc1 is currently unclear (Shalom-Barak T et al., 2004), this cellular defect, combined with recent reports that implicate Muc1 in HIF1α regulation (Chaika NV et al., 2012; Goudarzi H et al., 2013), enhanced the prospects that *MUC1*$^{-/-}$ cells would yield important information regarding the regulation of trophoblast hypoxic signaling.

JEG 5.1 and two distinct *MUC1*$^{-/-}$ clones were cultured under standard or hypoxic conditions for 6-48 h in the presence or absence of Rosi (Figure 27). Unlike the patterns observed in TSCs (Figures 1, 5 and Shalom-Barak T et al., 2004, 2012), in JEG 5.1 Muc1-CT2 was only induced by 24 h in hypoxia, and increased dramatically by the 48th h (lanes 4, 5, 9, 10, 24, 25, 29, 30). In another departure from TSCs, Rosi had no effect on Muc1-CT2 expression (lanes 9, 10, 29, 30). This striking discrepancy could reflect species-specific or lineage-specific differences between JEG-3 cells and TSCs. As expected, both *MUC1*-null clones were completely devoid of Muc1-CT-2 expression (lanes 11-20, 31-40).

Interestingly, a cross-reactive protein, migrating as an ~160 kDa band, was exclusively present in *MUC1*$^{-/-}$ clone #52.1 treated with Rosi at 6 and 12 h of hypoxic exposure (Figure 27

lanes 17-18). Although this is odd, considering that the α-Muc1 mAb targets the excised CT2 domain, the temporal regulation of this entity in hypoxia and its induction by Rosi akin to mouse Muc1 in TSCs (Shalom-Barak T et al., 2004; 2012) argues that this might be a *bona fide* alternative, uncleaved Muc1 isoform, which retained the corresponding epitope within the CT2 domain. Given the multiple possible CRISPR-mediated excision combinations with the four guide RNA sequences used to target *MUC1* in JEG 5.1 (Figure 26), it is possible that the gene excision product in this clone produced an in-frame, albeit truncated, version of Muc1 that retains expression and some function. This speculation is supported by the differential effects of the two tested *MUC1*-null clones on hypoxia-regulated proteins, as elaborated below.

In *MUC1*-null clone #73.1 cells, HIF1α levels were as high at the 48th h of hypoxic exposure as in JEG 5.1 cells (Figure 27 lanes 25, 30, 35). However, in the presence of Rosi clone #73.1 (right) exhibited a dramatic decrease in HIF1α levels by 48 h in hypoxia to below the detection threshold (lane 40). A possible interpretation of this odd observation is that Muc1 is part of a finely tuned network of positive and negative regulators of HIF1α stability in hypoxia downstream of PPARγ, and its deletion disturbs the balance of this putative network.

Compared to WT JEG 5.1 cells, *MUC1* deficiency accelerated the decline of PPARγ protein in hypoxia in both KO cell lines (Figure 27 lanes 11-15, 31-35) and the addition of Rosi augmented this effect (lanes 16-20, 36-40), suggesting that Muc1 is required for long-term sustenance of both HIF1α and PPARγ expression in hypoxia.

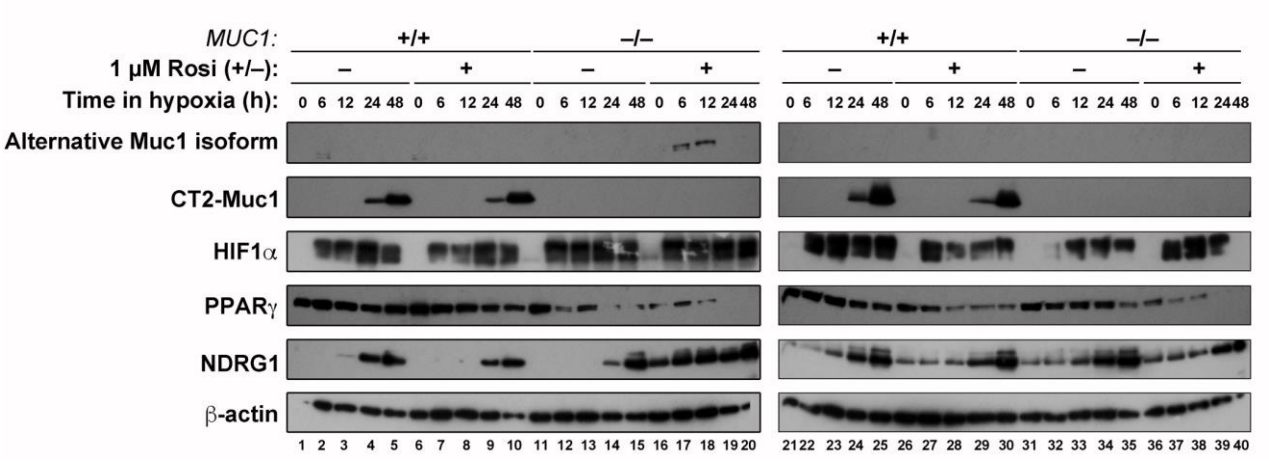

Figure 3-26- MUC1-null cells have differential effects on trophoblast hypoxic signaling

JEG 5.1 and *MUC1*$^{-/-}$ clone #52.1 (left) or clone #73.1 (right) were cultured under standard or hypoxic conditions from 6-48 h in the presence or absence of Rosi (1 μM). *MUC1*-null clones have differential effects on the regulation of hypoxia-responsive proteins. β-actin confirms equal sample loading in all lanes.

NDRG1 levels were similarly induced in untreated *MUC1*-null cells with expression observed by 24h in hypoxia (Figure 27 lane 14). Importantly, the addition of Rosi was sufficient to significantly promote the expression of NDRG1 levels in normoxic *MUC1*-null cells and sustain expression up to 48 h in hypoxia exclusively in *MUC1*$^{-/-}$ clone #52.1 (lanes 16-20). These data suggest that Muc1 may be the negative regulator of NDRG1, while PPARγ functions to simply regulate its expression, and by proxy, the expression of NDRG1. The expression of NDRG1 followed a similar pattern in JEG 5.1 and *MUC1*-null clone #73.1 cells, where expression was increased by 12 h in hypoxia, and Rosi had little to no effect.

4.0 Discussion

4.1 The PPARγ-HIF1α-lactate axis in hypoxic trophoblasts

This thesis describes the identification of a putative PPARγ-HIF1α signaling axis in hypoxic trophoblasts, whereby PPARγ is critical for their sustained HIF1α expression and prolonged survival. A simplified model of this presumed pathway is illustrated in Figures 28 and 29. Hours after hypoxic insult, the intracellular levels of HIF1α are increased in response to the

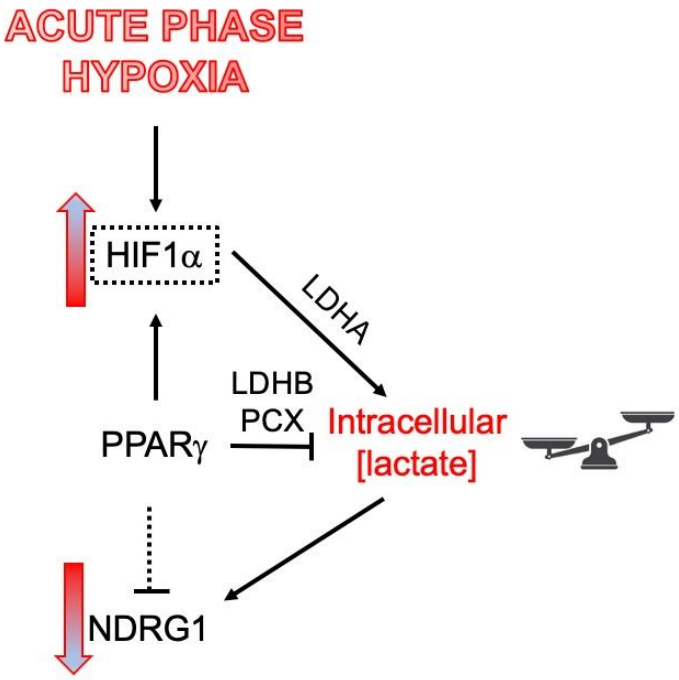

Figure 4-1- The potential role of PPARγ and its target genes under acute hypoxic conditions

Proposed model for acute phase hypoxia in trophoblasts

reduced hydroxylation capacity of its negative regulator, PHD2, resulting in an increase of free cytoplasmic HIF1α protein (Lee DC et al., 2015). Monomeric HIF1α subsequently translocates to

the nucleus where it forms an obligate heterodimer with ARNT, binds to its cognate response element in the promoters of regulated genes, and activates the transcription of target genes (Koh My et al., 2012). In the acute stage, the most relevant HIF1α target is LDHA and PDK1, which are responsible for the conversion of pyruvate to lactate and the reduction of pyruvate flux through the TCA cycle, respectively. The enzymatic activity of LDHA is critical for generating the reducing equivalents required for sustained glycolysis and for maintaining ATP production under hypoxic conditions. However, this reaction, in turn, increases intracellular lactate concentrations (Esterman A et al., 1997). As demonstrated here, PPARγ is critical for lactate clearance in acute phase hypoxia. This is reflected in the maintenance of basal lactate levels within the first 12 h of hypoxic exposure of WT TSCs, and the staggering accumulation of lactate in *Pparg*-null TSCs. This finding is fully consistent with the previous demonstration that PPARγ positively regulates two tandem enzymes, LDHB and PCX, that are synergistically responsible for lactate clearance (Shalom-Barak T et al., 2012).

Exogenous lactate supplementation of hypoxic trophoblasts resulted in a decline in HIF1α. As intracellular lactate overload can contribute to cellular acidosis and lethality, this finding suggests that the pathway evolved with a negative feedback safety switch, in which excessive lactate accumulation, directly or through an intermediate, reins in HIF1α. This thesis postulates that under acute hypoxic conditions, placental PPARγ suppresses intracellular lactate levels *via*

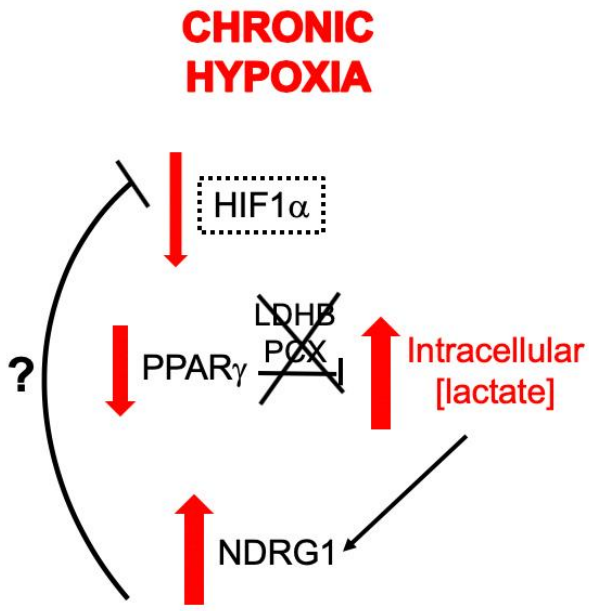

Figure 4-2- The potential role of PPARγ and its target genes under chronic hypoxic conditions

Proposed model for chronic hypoxia in trophoblasts.

positive regulation of LDHB and PCX, and functions as a countermeasure to maintain lactate concentrations at a relatively low level. As shown, the requirement for PPARγ to sustain HIF1α levels in the chronic hypoxic phase likely occurs at the protein level, as no direct regulation at the RNA level was observed. Based on the negative impact of high lactate concentrations on HIF1α levels, it is reasonable to hypothesize that this stabilizing effect is accomplished through the ability of PPARγ to rein in lactate accumulation. This long-term stabilization, in turn, is critical for the activation of downstream signaling pathways that enable cells to survive a more chronic insult by facilitating adaptive gene networks, such as cellular differentiation, energy metabolism, and angiogenesis (Liu W et al., 2012). Importantly, while PPARγ and HIF1a protein decay kinetics were accelerated in all WT TSC lines tested as compared to the GY11 clone ultimately chosen for in-depth analyses, the overall trends in the induction and regulation of hypoxia-responsive proteins

remained the same. This confirms that the direct regulation of HIF1α by PPARγ was not a clonal artifact. Importantly, treatment of WT and *Pparg*-null TSCs with $CoCl_2$ was unable to mimic the effects of acute oxygen deprivation on the expression of hypoxia-regulatory proteins, further defining a role for the morphogenetic properties of oxygen in trophoblast biology.

The flow of intracellular lactate levels in the early stages of hypoxia may also suppress NDRG1 levels. This hypothesis arises from the ability of lactate for physical stabilization and activation of the downstream signaling properties of its close homolog, NDRG3, whose lactate binding motif is 100% identical to that of NDRG1 (Lee DC et al., 2015). This notion is further validated by the observed inverse relationship between PPARγ and NDRG1. Thus, under acute hypoxic conditions, the primary function of placental PPARγ may be to quell trophoblast lactate accumulation, which promotes sustained HIF1α stabilization and suppresses NDRG1 levels. However, this is only one part of the story, as NDRG1 is regulated by both PPARγ and hypoxia, at least in part, at the transcriptional level.

As trophoblasts shift from acute to long-term hypoxic exposure (i.e., ≥24 h in hypoxia), PPARγ levels decline as previously published (Tache V et al., 2013), and as recapitulated here. This phenomenon was reported to be independent of both HIF and histone deacetylases (Tache V et al., 2013). The decline of PPARγ protein in long-term hypoxic trophoblast cultures, and hence the positive effect exerted on both LDHB and PCX, is concomitant with an increase in intracellular lactate concentrations and NDRG1 levels. It is tempting to hypothesize that the decreased activity of PPARγ and its target genes during chronic hypoxic exposure is directly responsible for the increased lactate accumulation, which subsequently leads to a rise in NDRG1 levels. The possibility that NDRG1, in turn, contributes to the decline of HIF1α levels during chronic hypoxia, as reported in this dissertation and by others (Lee DC et al., 2015), is as intriguing. One could

think of this phenomenon as "passing of the baton" as cells shift from acute hypoxia gene programs to more long-term adaptive gene networks, potentially driven by stabilized NDRG1, whose core function is still unknown (Choi SH et al., 2007; Shi XH et al., 2013; Larkin J et al., 2014).

4.1.1 Implications in placental development and disease

While the relative importance of PPARγ as an essential driver of placental development has been previously established (Barak Y et al., 1999), the *function* of placental PPARγ has yet to be elucidated. This dissertation establishes a direct relationship between PPARγ and HIF1α in hypoxic trophoblasts as described above, and further implicates lactate as a potential mediator of the trophoblast hypoxic response. Placentation initiates in a relatively hypoxic environment before establishment of the feto-placental vascular network (Weiss H et al., 2016). The fine-tuned regulation of inter-tissue oxygen levels is essential for successful pregnancy, as demonstrated by the KOs of *Hif1a, ARNT, and VHL* (Cowden Dahl KD et al., 2005; Kozak KR et al., 1997; Takeda K et al., 2006; Gnarra JR et al., 1997). In addition, previous studies have defined the role of oxygen sensing as a critical mediator of trophoblast differentiation (Tanaka S et al., 1998; Cowden Dahl KD et al., 2005). Given novel relationship between PPARγ and HIF1α established here, and the overall phenotypic similarities shared between *Pparg*-, *Hif1a*, and *Phd2*-null placentas, the notion that the PPARγ-HIF1α axis may be primarily influencing trophoblast differentiation, and thus underpinning the placental defects observed in *Pparg*-null placentas, is definitely plausible.

Indeed, Parast MM et al. (2009) previously demonstrated that under normoxic conditions *Pparg*-null TSCs fail to form the synTs that comprise the labyrinth and, rather, primarily differentiate into sTGCs, while hypoxic conditions reduced PPARγ expression levels independent of HIF1α activity and epigenetic regulation (Tache V et al., 2013). Conversely, transcriptional

profiling *in vivo* and *in vitro* suggested that *Pparg*-null placentas and TSCs may have reduced capacity to differentiate into sTGCs (Shalom-Barak T et al., 2012). The sTGCs form the first layer of the 3-cell trophoblast barrier in the mouse labyrinth and are in direct contact with the maternal blood (Rossant J et al., 2001). Therefore, it is tempting to speculate that the PPARγ-HIF1α axis ultimately functions as a first-line sensor the placenta to promote trophoblast proliferation in the absence of oxygen, and differentiation to sTGCs upon reoxygenation. Additionally, the complete vascularization failure of *Pparg*-null placentas, and its rescue by tetraploid complementation assays (Barak Y et al., 1999), indicates an underlying defect in trophoblast differentiation, as trophoblasts provide the framework into which the invading fetal vessels grow. In the absence of a road map, the fetal vessels fail to vascularize the labyrinth (Rossant J et al., 2001). Taken together, defects in the extended HIF pathway may ultimately underlie many of the placental and fetal defects associated with hypoxic insult during human pregnancy.

4.2 Potential functions of lactate

This thesis sheds a light on a previously unappreciated role of lactate in trophoblast hypoxic signaling. As shown here, *Pparg*-null TSCs accumulate significantly more lactate in hypoxia compared to the WT counterparts, consistent with a putative role in the hypoxic signaling of trophoblasts. Moreover, treatment of JEG-3 cells with 100 mM exogenous lactate under normoxic conditions increases the expression of HIF1α, PPARγ, and NDRG1, providing a potential explanation for the elevated NDRG1 levels in normoxic *Pparg*-null TSCs. Conversely, treatment of hypoxic JEG-3 cells or WT TSCs with inhibitors of lactate metabolism results in a near-complete shutdown HIF1α, PPARγ, and NDRG1 protein levels within 24 h, demonstrating the

bidirectional influence of oxygen tension on the effect of lactate on hypoxia-responsive proteins. It is noteworthy that PPARγ levels did not decline in hypoxic JEG-3 cells by 24 h in hypoxia. This could be attributable to the homogenous nature of JEG-3 cells, as opposed to the heterogenous cell populations in differentiated TSC cultures, and the likelihood that the expression of hypoxia-regulated proteins in alternative cell populations, such as sTGCs, could have differential sensitivity to acute oxygen deprivation. However, considering that the addition of exogenous lactate in combination with inhibitors of lactate metabolism to hypoxic trophoblasts further decreased, rather than promoted, the expression of HIF1α and additional proteins of interest, the role of lactate in the pathway is likely not as simplistic.

The intricate relationships between lactate and the expression of hypoxia regulated proteins were further exemplified in the confounding effects of varying concentrations of Ox on differential regulation of HIF1α. While treatment of hypoxic JEG-3 cells with 10 mM Ox enhanced the expression of HIF1α throughout the entirety of hypoxic exposure, higher Ox concentrations nearly abolished HIF1α expression completely. Part of this ambiguity stems from the dual-action pan-LDH inhibitor properties of Ox. Later studies reveled that treatment of hypoxic JEG-3 cells with 10 mM Ox slightly reduced the concentration of intracellular lactate by 12 h in hypoxia, albeit without statistical significance, while HIF1α levels were completely shut off. However, HIF1α levels were sustained by 12 h in hypoxia in WT TSCs treated with 10 mM Ox, potentially indicating that JEG-3 cells are more sensitive to intracellular lactate manipulation due to their cancerous nature. Treatment of JEG-3 cells with 40 mM Ox reduced intracellular lactate levels similar to that of 10 mM Ox yet diminished HIF1α levels by 6 h in hypoxia, prompting the notion that additional metabolites may be contributing to hypoxic protein regulation. The disparate effect of lactate-mediated hypoxic protein regulation was further exemplified by 24 h in hypoxia.

Importantly, HIF1α, PPARγ, and NDRG1 levels were sustained in the presence *or* absence of high intracellular lactate concentrations, indicating that additional regulation, either at the metabolite or protein level, is involved in regulating the expression of hypoxic proteins during acute oxygen deprivation.

While the results presented herein are intriguing, they still fall short of proving a clear causal link between the expression of hypoxia-regulated proteins and intracellular lactate levels. Disparate effects observed could be attributed to cellular acidosis, metabolic starvation, an undiscovered signaling intermediate, or differential metabolite regulation. However, the totality of the observations here indicate that dysregulation of lactate metabolism severely impairs the hypoxic response of trophoblasts, suggesting that lactate, or by-products of its metabolism, is an essential regulatory node in the pathway.

4.2.1 Additional metabolites measured

Consistent with the hypothesis that additional metabolites or by-products of lactate metabolism may be influencing the expression of key hypoxic proteins of interest, multiple aqueous-phase metabolites were measured in hypoxic WT and *Pparg*-null TSCs at 12 h in hypoxia with non-targeted metabolomic profiling (Appendix F). Citrate levels were relatively stable in WT and *Pparg*-null TSCs cultured under both normoxic and hypoxic conditions, strongly confirming that the marked intracellular lactate accumulation in hypoxic *Pparg*-null *versus* WT TSCs is significant and not an artifact of sample variability. Three different metabolites - acetyl CoA, α-ketoglutarate, and malic acid – exhibited a similar differential pattern, whereby their concentrations decreased precipitously in normoxic *Pparg*-null compared to WT TSCs, but was restored in hypoxic conditions to the same level as in WT TSCs. For acetyl CoA this reduction in

normoxic *Pparg*-null TSCs may indicate enhanced flux through the TCA cycle, decreased synthesis, or increased use as a substrate in anabolic reactions. Its recovery to normal levels when mutant cells were transitioned to a hypoxic environment may suggest that the hypoxia response pathway either halted processes that accelerate its depletion or activated alternative PPARγ-independent pathways for its synthesis. The similar pattern of alpha ketoglutarate is notable in that not only is it a key TCA cycle intermediate but is also an essential hydroxyl donor to the HIF1α-destabilizing modification by PHD2. In contrast, succinic acid accumulated in *Pparg*-null TSCs in both normoxia and hypoxia. This significance and underpinnings of this accumulation are not clear. All in all, these data are clearly indicative of differential cellular metabolism in *Pparg*-null *versus* WT TSCs, with more studies required for teasing apart the underlying mechanisms and physiological implications.

4.2.2 *Ldhb* in the placenta

Similar to the significant, albeit not fully resolved, role of lactate metabolism in hypoxic trophoblasts signaling, LDHB, and by proxy lactate metabolism and signaling, appeared to have an important role in hypoxic pregnancies. The vascular labyrinth of WT placentas from hypoxic pregnancies was smaller, with irregular labyrinth-JZ boundaries, suggestive of SpT migration defect, and *Ldhb* deficiency appeared to mitigate this effect and restore gross placental and vascular structures to those seen in normoxic pregnancies.

This evident discrepancy between WT and *Ldhb*-null placentas in hypoxic pregnancies suggests that similar to cultured trophoblasts, lactate metabolism is also a key regulator of the placental adaptative response to generalized hypoxia. Future understanding of the underlying mechanism may require detailed interrogation of hypoxia-regulated proteins and various analytes,

in particular lactate, pyruvate, and oxidative respiration intermediates, to verify whether these indeed change in *Ldhb*-null placentas. Nevertheless, these measurements might prove challenging. First, there is the technical caveat, which is a relatively lengthy placental dissection in ambient oxygen that may artificially erase hypoxia-driven differences by the time the samples are ready for analysis. Second, considering that not all placental trophoblasts have the same sensitivity to hypoxic insults, and not all trophoblast lineages express *Ldhb*, it is likely that cellular and molecular differences could be localized to hot-spot locations within the developing placenta, which will be lost in whole tissue analysis.

4.3 Lessons from CRISPR-Cas9-mediated KOs

To facilitate the dissection of the intricate PPARγ-HIF1α-lactate axis in trophoblasts, monoclonal JEG-3 human choriocarcinoma clones carrying constitutive CRISP-Cas9-mediated deficiencies in PPARγ and hypoxia-signaling genes were generated. Interrogated genes included *PPARG*, *LDHB*, *PC*, *NDRG1,* and *MUC1*. Initial attempts to generate a cleaner system consisting of clones with conditional, dox-inducible KOs failed, due to both the relatively low efficiency of Cas9-mediated deletion coupled with the aneuploid nature of JEG-3 cells. The default solution was to resort to clones with permanent deletion of each gene. There were two major disadvantages to this backup strategy. First, there is a theoretical risk that the lengthy selection process will be accompanied by random genetic deviations of individual clones, which will compromise comparison to "WT" JEG-3 cells. Second, if any of the targeted genes has essential functions in JEG-3 cells, clones deficient for this gene will be hard to obtain and investigate. With respect to the latter concern, it appears to have been realized with *PPARG*, and to a limited extent with

MUC1. Although this in itself is valuable information, investigation of the signaling functions of each line was hampered.

The deletion of *PPARG* in JEG 5.1 causes overt lethality, and therefore poor growth, resulting in poor survival of the majority of potential null clones and ultimately recovery of a single null clone that could not be expanded or preserved in any practical way. While disappointing from a standpoint of the failure to use this approach to study the effect of this KO on hypoxic signaling, this observation provided some potential clues of the role of PPARγ in the placenta. Because *Pparg* deficiency in TSCs is compatible with survival at both the differentiated and undifferentiated states, the initial observation that *PPARG* deficiency in JEG-3 cells results in complete lethality was surprising. Therefore, it is possible that PPARγ is required for survival of only certain trophoblast lineages, which may manifest as a slightly skewed differentiation population that has gone unnoticed previously. Gene expression data suggest broad failure of *Pparg*-null TSCs to express multiple markers of the sTGC lineage (Shalom-Barak T et al., 2012), and may lend support for this possibility. This idea was not thought of or tested prior to this dissertation. Another possibility is that PPARγ is essential in JEG-3 cells, potentially due to a need for its regulation of lactate metabolism, due to the cancerous nature of JEG-3 cells.

PC$^{-/-}$ and *MUC1*$^{-/-}$ JEG-3 cells provided the most informative insights into hypoxia-regulated proteins. Hypoxia-driven induction of NDRG1 was severely impaired in *PC*$^{-/-}$ cells. Similar to *PPARG*$^{-/-}$ cells, *MUC1*-null cells were slow-growing and died upon passaging, albeit to a lesser extent that permitted ~50% cell survival. Both *MUC1*-null clones generated were completely devoid of the CT-2 signaling domain, yet an alternative Muc1 product was exclusively present in *MUC1*$^{-/-}$ clone #52.1, and the temporal regulation of this truncated Muc1 product suggests that it may be a Muc1 isoform as opposed to background bands or cross-reactivity.

Because multiple guides directed against *MUC1* were inserted in JEG 5.1, it's entirely possible that this clone's unique combination of Cas9-directed genetic cuts produces a functional version of Muc1, potentially through an in-frame deletion, that is capable of influencing protein expression. Indeed, while the expression levels of NDRG1 were similarly induced in both untreated *MUC1*-null clones, the addition of Rosi was sufficient to significantly and exclusively promote the expression of NDRG1 levels in normoxic *MUC1*$^{-/-}$ clone #52.1 and sustain its expression in hypoxia. These data suggest that Muc1 may be the negative regulator of NDRG1, while PPARγ functions to simply regulate its expression. Alternatively, the Muc1 isoform in *MUC1*$^{-/-}$ clone #52.1 may function as a dominant negative, thereby increasing, as opposed to inhibiting, NDRG1 levels in hypoxia.

Interestingly, neither *LDHB* nor *NDRG1* deficiency had any significant effect on the expression of hypoxia-regulated proteins. These results were both surprising and disappointing, given the profound effect of *Ldhb* deficiency on the vascular development of hypoxic placentas, and the robust induction of NDRG1 in hypoxia, its established relationship with lactate (Lee DC et al., 2015), and inverse relationship with PPARγ. Still, these clones require further investigation into intracellular metabolite profiles both under normoxic and hypoxic conditions before definitely declaring the mutations asymptomatic.

In summary, this dissertation unearthed a complex regulation of HIF1α levels by placental PPARγ and its transcriptional targets and proposes a new role for lactate metabolism in the hypoxic response of trophoblasts.

Appendix A – Plasmids

Table 4 - Plasmids

Name	Ref #	Description	Origin
pCW-Cas9	1100	rtTA-Cas9 with 3x N-terminal FLAG tags	Addgene #50661
PLK05.sgRNA.EFS.GFP	1101	Empy sgRNA vector with a GFP reporter	Addgene #57822
sgRNA-neo	1573b	Empty sgRNA vector with a neo resistance cassette	This study
hPC E3 guide #1 sgRNA	1577	Guide RNAs directed against *PC*	This study
hPC E3 guide #2 sgRNA	1578		
hPPARG E6 guide #1 sgRNA	1595	Guide RNAs directed against *PPARG*	This study
hPPARG E7 guide #1 sgRNA	1596		
hPPARG E7 guide #2 sgRNA	1597		
hNDRG1 E4 guide #1 sgRNA	1598	Guide RNAs directed against *NDRG1*	This study
hNDRG1 E4 guide #4 sgRNA	1599		
hNDRG1 E5 guide #1 sgRNA	1600		
hLDHB I2 guide #1 sgRNA	1601	Guide RNAs directed against *LDHB*	This study
hLDHB E3 guide #1 sgRNA	1602		
hLDHB I3 guide #1 sgRNA	1603		
hMUC1 E7 guide #1 sgRNA	1604	Guide RNAs directed against *MUC1*	This study
hMUC1 E7 guide #5 sgRNA	1605		
hMUC1 I6 guide #1 sgRNA	1606		
hMUC1 I7 guide #1 sgRNA	1607		

** E = exon; I = intron*

Appendix B – sgRNAs and analytical oligos

Table 5 - sgRNAs and analytical oligos

Name	Ref #	Sequence	Origin
hPC E3 guide #1 FWD	1952	CACCGCAGGCCCGGAACACACGGA	This study
hPC E3 guide #1 Rev	1953	AAACTCCGTGTGTTCCGGGCCTGC	
hPC E3 guide #2 FWD	1954	CACCGAAGTTCCGAACAGTCCATGG	This study
hPC E3 guide #2 Rev	1955	AAACCCATGGACTGTTCGGAACTTC	
hPC sg analyze FWD	1998	CCA GGC ATC AGG AGG TAG ATG GTG	This study
hPC sg analyze REV	1999	CTGCTTTCTGCCGGTGCATCTG	
hPparg E6 guide #1 FWD	2028	CACCGAAGGCGAGGGCGATCTTGAC	This study
hPparg E6 guide #1 Rev	2029	AAACGTCAAGATCGCCCTCGCCTTC	
hPparg E7 guide #1 FWD	2032	CACCGCAGCCTCCACGGAGCGAAAC	This study
hPparg E7 guide #1 Rev	2033	AAACGTTTCGCTCCGTGGAGGCTGC	
hPparg E7 guide #2 FWD	2034	CACCGATGGGGTTCTCATATCCGA	This study
hPparg E7 guide #2 Rev	2035	AAACTCGGATATGAGAACCCCATC	
hPparg E6 sg Analyze FWD	2113	CCATCAGGTTTGGGCGGATGC	This study
hPparg E7 sg analyze FWD	2038	CCTGGGATGGCATTCACTGTGAG	
hPparg E7 sg analyze Rev	2039	CACCAAAAGGCTTTCGCAGGCTC	
hNdrg1 E4 guide #1 FWD	2059	CACCGCTGTTCACGTCACGCTGTGT	This study
hNdrg1 E4 guide #1 Rev	2060	AAACACACAGCGTGACGTGAACAGC	
hNdrg1 E4 guide #4 FWD	2061	CACCGTTCATGCCGATGTCATGGT	This study
hNdrg1 E4 guide #4 Rev	2062	AAACACCATGACATCGGCATGAAC	
hNdrg1 E5 guide #1 FWD	2065	CACCGCAACCCCCTCTTCAACTACG	This study
hNdrg1 E5 guide #1 Rev	2066	AAACCGTAGTTGAAGAGGGGGTTGC	
hNdrg1 E4 sg analyze FWD	2063	CGGATGCCATGAACCCCACATG	This study
hNdrg1 E4 sg analyze Rev	2064	CCAGAACAGCCCCAGGAAGTC	
hNdrg1 E5 sg analyze Rev	2070	CGACACCCAGTTTCCACCCTG	
hLdhb I2 guide #1 FWD	2040	CACCGACGCATCCTAGAGTGGCTTA	This study
hLdhb I2 guide #1 Rev	2041	AAACTAAGCCACTCTAGGATGCGTC	
hLdhb E3 guide #1 FWD	2042	CACCGGCTGATGAACTTGCTCTTG	This study
hLdhb E3 guide #1 Rev	2043	AAACCAAGAGCAAGTTCATCAGCC	
hLdhb I3 guide #1 FWD	2044	CACCGATCACTGATATGTCACTAAC	This study
hLdhb I3 guide #1 Rev	2045	AAACGTTAGTGACATATCAGTGATC	
hLdhb sg analyze FWD	2046	GGCCTACTCTTGAACTAAGCTGG	This study
hLdhb sg analyze Rev	2047	GTGTGGCAGTGTGGAGTGTGGAATAC	
hMuc1 E7 guide #1 FWD	2049	CACCGGCTACGATCGGTACTGCTA	This study
hMuc1 E7 guide #1 Rev	2050	AAACTAGCAGTACCGATCGTAGCC	
hMuc1 E7 guide #5 FWD	2051	CACCGAGTGCCGCCGAAAGAACTAC	This study
hMuc1 E7 guide #5 Rev	2052	AAACGTAGTTCTTTCGGCGGCACTC	
hMuc1 I6 guide #1 FWD	2053	CACCGCATGGAGTGCCTTCTACCGG	This study
hMuc1 I6 guide #1 Rev	2054	AAACCCGGTAGAAGGCACTCCATGC	
hMuc1 I7 guide #1 FWD	2055	CACCGAGGATTCTGAAGGGGGTACT	This study
hMuc1 I7 guide #1 Rev	2056	AAACAGTACCCCCTTCAGAATCCTC	
hMuc1 sg analyze FWD	2057	TGCCATTTCCTTTCTCTGCCCAG	This study
hMuc1 sg analyze Rev	2058	CGCCACTTCTCACCTCTTCCAAGC	

E = exon; I = intron

Appendix C – Cell lines

Table 6 - Cell lines

Name	Description	Origin
MEF	Primary mouse embryonic fibroblasts	Barak lab
GY11	WT primary mouse TSCs	Barak lab
TRF	WT primary mouse TSCs	Tanaka S et al., 1998
Clone 2	WT primary mouse TSCs	Kind gift from Dr. Tom Gridley
GY9	*Pparg*-null primary mouse TSCs	Barak lab
GY11	*Pparg*- null primary mouse TSCs	Barak lab
JEG-3	Human choriocarcinoma cell line	ATCC HTB-36
JEG 4.1, 5.1, 6.2	Contains a stable integration of rtTA-Cas9	This study
PPARγ$^{-/-}$ #24.3	JEG cell line deficient for PPARγ protein expression	This study
LDHB$^{-/-}$ #62.1, 74.1	JEG cell line deficient for LDHB protein expression	This study
PCX$^{-/-}$ #18.3, 51.3	JEG cell line deficient for PCX protein expression	This study
MUC1$^{-/-}$ #10.1, 19.1, 52.1, 63.1, 71.1, 73.1	JEG cell line deficient for Muc1 protein expression	This study
NDRG1$^{-/-}$ #24.1, 31.1, 77.1	JEG cell line deficient for NDRG1 protein expreesion	This study

Appendix D – Antibodies

Table 7- Antibodies

Host	Clonality	Target protein	Dilution	Company	Cat #
Rabbit	Monoclonal	HIF1α - WB	1:1000	Cell Signaling	14179S
Mouse	Monoclonal	HIF1α - IP	2 µg	ThermoFisher Scientific	MA1-16504
Rabbit	Monoclonal	PPARγ	1:1000	Cell Signaling	2443S
Rabbit	Polyclonal	NDRG1	1:1000 - WB; 5 µg - IP	ThermoFisher Scientific	42-6200
AH	Monoclonal	CT2-MUC1	1:1000 - WTB; 1:500 IF	ThermoFisher Scientific	HM-1630
Mouse	Monoclonal	LDHB	1:5000	ProteinTech	66425-1-Ig
Mouse	Monoclonal	PCX	1:1000	Santa Cruz Biotechnology	sc-365673
Rabbit	Monoclonal	LDHA	1:10000	Cell Signaling	3558S
Rabbit	Monoclonal	PHD2	1:1000	Cell Signaling	4835S
Rabbit	Monoclonal	PDK1	1:1000	Cell Signaling	5662S
Rabbit	Monoclonal	PPARδ	1:1000	Abcam	ab17866
Mouse	Monoclonal	FLAG	1:1000	Sigma	F1802
Mouse	Monoclonal	β-actin	1:10000	Cell Signaling	3700S
Rat	Monoclonal	CD31/PEACAM	1:50	eBioScience	14-0311

Appendix E – Ligands and chemicals

Table 8- Ligands and chemicals

Name	Description	Concentration	Company	Cat #
Rosiglitazone	PPARγ agonist	1 μM	Millipore Sigma	557366-M
LG100268	RXRα agonist	1 μM	Millipore Sigma	SML0279
L-165,041	PPARδ agonist	1 μM	Millipore Sigma	422175
L-lactate	exogenous lactate	25-100 mM	Millipore Sigma	71718
AR-C155858	MCT1/2 inhibitor	1 μM	MedChemExpress	HY-13248
Ox	LDHA/LDHB inhibitor	10-40 mM	Cayman Chemical Company	19057
PA	PCX inhibitor	2.5-5 mM	Millipore Sigma	W287806
FX11	LDHA inhibitor	10 μM	Calbiochem	427218

Appendix F – Additional metabolites measured

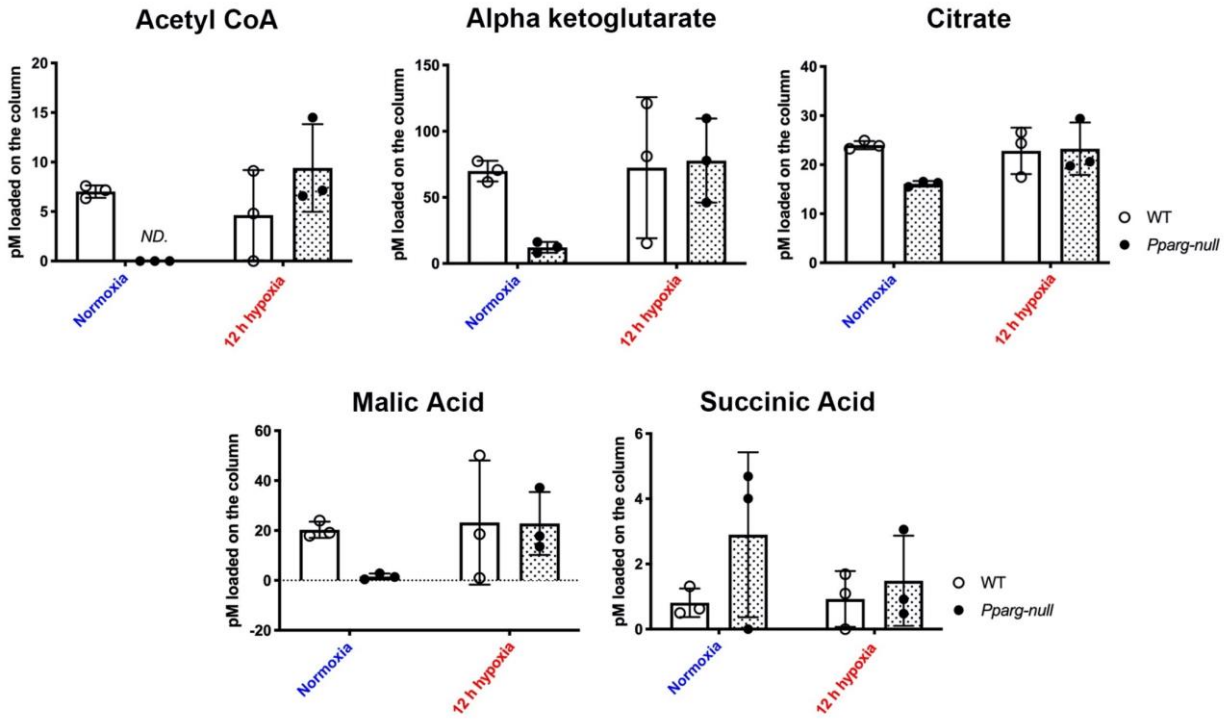

Figure A-1- Additional metabolites exhibit unique trends in *Pparg*-null cells

WT (GY11; open circles) and *Pparg*-null (GY9; closed circles) TSCs were cultured under hypoxic conditions for 12 h. Metabolism was immediately quenched and analyte profiles determined with metabolomic analysis. Values were analyzed using a two-way ANOVA and Tukey's multiple comparisons test. $P < 0.05$ was considered significant. ND = not determined. WT and *Pparg*-null TSCs displayed unique metabolic signatures at steady state and under hypoxic conditions.

Bibliography

Adams MJ, Buehner M et al. 1973. Structure-function relationships in lactate dehydrogenase. Proc Natl Acad Sci U S A. 70:1968-72.

Adelman DM, Gertsenstein M et al. 2000. Placental cell fates are regulated in vivo by HIF-mediated hypoxia responses. Genes Dev. 14:3191-203.

Arnold GL, Griebel ML, et al. 2001. Pyruvate carboxylase deficiency. Report of a case and additional evidence for the "mild" phenotype. Clin Pediatr (Phila). 40:519-21.

Barak Y, Nelson MC et al. 1999. PPARγ is required for placental, cardiac, and adipose tissue development. Mol Cell. 4:585-95.

Barak Y, Sadovsky Y, and Shalom-Barak T. 2008. PPAR signaling in placental development and function. PPAR Res. 2008:142802.

Barker, DJ. 2004. The developmental origins of adult disease. J Am Coll Nutr. 23:588S-95S.

Baumann MU, Zamudio S et al. 2007. Hypoxic upregulation of glucose transporters in BeWo choriocarcinoma cells is mediated by hypoxia inducible factor-1. Am J Physiol Cell Physiol. 293:477-85.

Blundell C, Tess ER et al. 2016. A microphysiological model of the human placental barrier. Lab Chip. 16:3065-73.

Brayman M, Thathiah A et al. 2004. MUC1 – a multifunctional cell surface component of reproductive tissue epithelia. Reprod Biol Endocrinol. 2:4.

Brett KE, Ferraro ZM, et al. 2014. Maternal-fetal nutrient transport in pregnancy pathologies: the role of the placenta. Int J Mole Sci. 15:16153-85.

Chaika NV, Gebregiworgis T et al. 2012. MUC1 mucin stabilizes and activates hypoxia-inducible factor 1 alpha to regulate metabolism in pancreatic cancer. Proc Natl Acad. 109:13787-92.

Chen B, Nelson DM et al. 2006. N-myc down-regulated gene 1 modulates the response of human term trophoblasts to hypoxic injury. J Biol Chem. 281:2764-72.

Chen DB and Zheng Jing. 2014. Regulation of placental angiogenesis. Microcirculation. 21:15-25.

Choi SH, Oh SY et al. 2007. Increased expression of N-myc downstream-regulated gene 1 (NDRG1) in placentas from pregnancies complicated by intrauterine growth restriction or preeclampsia. Am J Obstet Gynecol. 196:45.e1-7.

Christodoulou N, Weberling A et al. 2019. Morphogenesis of extra-embryonic tissues directs the remodeling of the mouse embryo at implantation. Nat Commun. 10:3557.

Cowden Dahl KD, Fryer BH et al. 2005. Hypoxia-inducible factors 1alpha and 2alpha regulate trophoblast differentiation. Mol Cell Bio. 25:10479-91.

Cross, JC. 2005. How to make a placenta: mechanisms of trophoblast cell differentiation in mice–a review. Placenta. 26, SupplA:S3-9.

Delorme-Axford E, Sadovsky Y, and Coyne, CB. 2014. The placenta as a barrier to viral infection. Annu Rev Virol. 1:133-46.

Desvergne B and Wahli W. 1999. Peroxisome proliferator-activated receptors: nuclear control of metabolism. Endocr Rev. 20:649-88.

Dunwoodie SL. 2009. The role of hypoxia in development of the mammalian embryo. Dev Cell. 17:755-73.

Edwards EM, Rattenbury J, et al. 1977. Enzyme activities in the sheep placenta during the last three months of pregnancy. Biochim Biophys Acta. 497:133-43.

Epstein AC, Gleadle JM et al. 2001. C. elegans EGL-9 and mammalian homologs define a family of dioxygenases that regulate HIF by prolyl hydroxylation. Cell. 107:43-564.

Esterman A, Greco MA et al. 1997. The effect of hypoxia on human trophoblast in culture: morphology, glucose transport, and metabolism. Placenta. 18:129-36.

Ferguson BS, Rogatzki MJ et al. 2018. Lactate metabolism: historical context, prior misinterpretations, and current understanding. Eur J Appl Physiol. 118:691-728.

Firth JF, Ebert BL et al. 1994. Oxygen-regulated control elements in the phosphoglycerate kinase 1 and lactate dehydrogenase A genes: similarities with the erythropoietin 3’ enhancer. Proc Natl Acad Sci U S A. 91:6496-500.

Fournier T, Tsatsaris V et al. 2007. PPARs and the placenta. Placenta. 28:65-76.

Fraisl P, Mazzone M et al. 2009. Regulation of angiogenesis by oxygen and metabolism. Dev Cell. 16:167-79.

Garcia-Cazorla A, Rabier D et al. 2006. Pyruvate carboxylase deficiency: metabolic characteristics and new neurological aspects. Ann Neurol. 59:121-7.

Gardner DK and Leese HJ. 1988. The role of glucose and pyruvate transport in regulating nutrient utilization by preimplantation mouse embryos. Development. 104:423-9.

Genbacev O, Joslin R et al. 1997. Hypoxia alters early gestation human cytotrophoblast differentiation/invasion in vitro and models the placental defects that occur in preeclampsia. J Clin Invest. 97:540-50.

Gnarra JR, Ward JM et al. 1997. Defective placental vasculogenesis causes embryonic lethality in VHL-deficient mice. PNAS. 94:9102-7.

Goudarzi H, Iizasa H et al. 2013. Enhancement of in vitro cell motility and invasiveness of human malignant pleural mesothelioma cells through the HIF-1α-MUC1 pathway. Cancer Lett. 339:82-92.

Hayashi M, Sakata M et al. 2004. Induction of glucose transporter expression through hypoxia-inducible factor 1alpha under hypoxic conditions in trophoblast-derived cells. J Endocrinol. 183:145-54.

Hemberger M and Cross JC. 2001. Genes governing placental development. Trends Endocrinol Metab. 12:162-8.

Hung TH, Skepper JN et al. 2002. Hypoxia-reoxygenation: a potent inducer of apoptotic changes in the human placenta, and possible etiological factor in preeclampsia. Circ Res. 90:1274-81.

Iyer NV, Kotch LE et al. 1998. Cellular and developmental control of O_2 homeostasis by hypoxia-inducible factor 1 alpha. Genes Dev. 12:149-62.

Jaakkola P, Mole DR et al. 2001. Targeting of HIF-alpha to the von Hippel-Lindau ubiquitylation complex by O2-regulated prolyl hydroxylation. Science. 292:468-72.

Jitrapakdee S and Wallace JC. 1999. Structure, function, and regulation of pyruvate carboxylase. Biochem J. 340:1-16.

Kay HH, Zhu S, and Tsoi S. 2007. Hypoxia and lactate production in trophoblast cells. Placenta. 28:854-60.

Kidron D, Bernhein J, and Aviram R. 2009. Placental findings contributing to fetal death, a study of 120 stillbirths between 23 and 40 weeks gestation. Placenta. 30:700-4.

Kim JW, Tchernyshvov I et al. 2006. HIF-1-mediated expression of pyruvate dehydrogenase kinase: a metabolic switch required for cellular adaptation to hypoxia. Cell Metab. 3:177-85.

Kliewer SA. Forman BM et al. 1994. Differential expression and activation of a family of murine peroxisome proliferator-activated receptors. Proc Natl Acad Sci U S A. 91:7355-9.

Knott JG and Paul S. 2014. Transcriptional regulators of the trophoblast lineage in mammals with hemochorial placentation. Reproduction. 148:R121-36.

Koh MY and Powis G. 2012. Passing the baton: the HIF switch. Trends Biochem Sci. 37:364-72.

Kozak KR, Abbott B et al. 1997. ARNT-deficient mice and placental differentiation. Dev Biol. 191:297-305.

Kumar EB, Vigi RI et al. 2007. Endothelial cell response to lactate: PAR modification of VEGF. J Cell Physiol. 211:477-85.

Larkin J, Chen B et al. 2014. NDRG1 deficiency attenuates fetal growth and the intrauterine response to hypoxic injury. Endocrinology. 155:1099-106.

Lavery DN and Mcewan IJ. 2005. Structure and function of steroid receptor AF1 transactivation domains: induction of active conformations. Biochem J. 391:449-64.

Lawn JE, Blencowe H et al. 2016. Still births: rates, risk factors, and acceleration toward 2030. Lancet. 387:587-503.

Lee DC, Sohn HA et al. 2015. A lactate-induced response to hypoxia. Cell. 161:595-609.

Lewis RM, Cleal JK, and Hanson MA. 2012. Review: Placenta, evolution, and lifelong health. Placenta. 33, Suppl:S28-42.

Liu W, Shen SM et al. 2012. Targeted genes and interacting proteins of hypoxia inducible factor-1. Int J Biochem Mol Biol. 3:165-78.

Livak KJ and Schmittgen TD. 2001. Analysis of relative gene expression data using real-time quantitative PCR and the $2^{-\Delta\Delta C_T}$ Method. Methods. 25:402-8.

Lu H, Forbes RA et al. 2002. Hypoxia-inducible factor 1 activation by aerobic glycolysis implicate the Warburg effect in carcinogenesis. J Biol Chem. 277:23111-5.

Maekawa M, Sudo K, et al. 1994. Population screening of lactate dehydrogenase deficiencies in Fukuoka Prefecture in Japan and molecular characterization of three independent mutations in the lactate dehydrogenase-B(H) gene. Human Genet. 93:74-6.

Maltepe E and Fisher SJ. 2015. Placenta: the forgotten organ. Annu Rev Cell Dev Biol. 31:523-52.

Maxwell PH, Wiesener MS et al. 1999. The tumor suppressor protein VHL targets hypoxia-inducible factors for oxygen-dependent proteolysis. Nature. 399:271-5.

McCarthy FP, Delany AC et al. 2013. PPAR-γ - - a possible drug target for complicated pregnancies. Br J Pharmacol. 168:1074-85.

Meirhaeghe A, Boreham CA et al. 2007. A possible for the PPARG Pro12Ala polymorphism in preterm birth. Diabetes. 56:494-98.

Nagi A, Takebe K et al. 2010. Cellular expression of the monocarboxylate transporter (MCT) family in the placenta of mice. Placenta. 31:126-33.

Nash WG and O'Brien SJ. 1982. Conserved regions of homologous G-banded chromosomes between orders in mammalian evolution: carnivores and primates. Proc Natl Acad Sci U S A. 79:6631-5.

Ohh M, Park CW et al. 2000. Ubiquitination of hypoxia-inducible factor requires binding to the beta-domain of the von Hippel-Lindau protein. Nat Cell Biol. 2:423-7.

Ornoy A, Salamon-Arnon, et al. 1981. Placental findings in spontaneous abortions and stillbirths. Teratology. 24:243-252.

Parast MM, Yu H et al. 2009. PPARgamma regulates trophoblast proliferation and promotes labyrinthine trilineage differentiation. PLoS One. 4:e8055.

Pastor-Soler NM, Sutton TA et al. 2015. Muc1 is protective during kidney ischemia-reprofusion injury. Am J Physiol Renal Physiol. 308:F1452-62.

Ptacek I, Sebire NJ et al. 2014. Systematic review of placental pathology reported in association with stillbirth. Placenta. 35:552-62.

Rodesch F, Simon P et al. 1992. Oxygen measurements in endometrial and trophoblastic tissues during early pregnancy. Obstet Gynecol. 80:283-85.

Rossant J and Cross JC. 2001. Placental development: lessons from mouse mutants. Nat Rev Genet. 2:538-48.

Rossant J and Tam PP. 2009. Blastocyst lineage formation, early embryonic asymmetries, and axis patterning in the mouse. Development. 136:701-13.

Schaiff WT, Barak Y, and Sadovsky Y. 2006. The pleiotropic function of PPARγ in the placenta. Mol Cell Endocrinol. 249:10-5.

Semenza GL, Roth PH et al. 1994. Transcriptional regulation of genes encoding glycolytic enzymes by hypoxia-inducible factor 1. J Biol Che,. 269:23757-63.

Settle P, Mynett K et al. 2004. Polarized lactate transporter activity and expression in the syncytiotrophoblast of the term human placenta. Placenta. 25:496-504.

Sferruzzi-Perri AN and Camm EJ. 2016. The programming power of the placenta. Front Physiol. 7:33.

Shalom-Barak T, Liersemann J et al. 2018. Ligand-dependent corepressor (LCoR) is a rexinoid-inhibited peroxisome proliferator-activated receptor γ-retinoid X receptor α coactivator. Mol Cell Biol. 38:pii:e00107-17.

Shalom-Barak T, Nicholas JM et al. 2004. Peroxisome proliferator-activated receptor γ controls *Muc1* transcription in trophoblasts. Mol Cell Biol. 24:10661-9.

Shalom-Barak T, Zhang X et al. 2012. Placental PPARγ regulates spatiotemporally diverse genes and a unique metabolic network. Dev Biol. 372:143-55.

Shi XH, Larkin JC et al. 2013. The expression and localization of N-myc downstream-regulated gene 1 in human trophoblasts. PLoS One. 8:e75473.

Shukla SK, Purohit V et al. 2017. MUC1 and HIF-1alpha signaling crosstalk induces anabolic glucose metabolism to impart gemcitabine resistance to pancreatic cancer. Cancer Cell. 32:71-87.e7.

Simmons DG and Cross JC. 2005. Determinants of trophoblast lineage and cell subtype specification in the mouse placenta. Dev Biol. 284:12-24.

Simon MC and Keith B. 2008. The role of oxygen availability in embryonic development and stem cell function. Nat Rev Mol Cell Biol. 9:285-96.

Stanek J. 2013. Hypoxic patterns of placental injury: a review. Arch Pathol Lab Med. 137:706-20.

Stern HJ, Nayar R, et al. 1995. Prolonged survival in pyruvate carboxylase deficiency: lack of correlation with enzyme activity in cultured fibroblasts. Clin Biochem. 28:85-9.

Sudo K, Maekawa M, et al. 1994. Premature termination mutations in two patients with deficiency of lactate dehydrogenase H(B) subunit. Clin Chem. 40:1567-70.

Tache V, Ciric A et al. 2013. Hypoxia and trophoblast differentiation: a key role for PPARγ. Stem Cells Dev. 22:2815-24.

Takatani T, Takaoka N, et al. 2001. A novel missense mutation in human lactate dehydrogenase B-subunit gene. Mol Genet Metab. 73:344-8.

Takeda K, Ho VC et al. 2006. Placental but not heart defects are associated with elevated hypoxia-inducible factor α levels in mice lacking prolyl hydroxylase domain protein 2. Mol Cell Biol. 26:8336-46.

Takeno T and Li SS. 1989. Structure of the human lactate dehydrogenase B gene. Biochem J. 257:921-4.

Tanaka S, Kunath T et al. 1998. Promotion of trophoblast stem cell proliferation by FGF4. Science. 282:2072-5.

Tanis RJ, Neel JV, et al. 1977. Two more “private” polymorphisms of Amerindian tribes: LDHb GUA-1 and ACP1 B GUA-1 in the Guaymi in Panama. Am J Hum Genet. 29:419-30.

Tesser RB, Scherholz PL et al. 2010. Trophoblast glycogen cells differentiate early in the mouse ectoplacental cone: putative role during placentation. Histochem Cell Biol. 134:83-92.

Tontonoz P, He E et al. 1995. PPAR gamma 2 regulates adipose expression of the phosphoenolpyruvate carboxykinase gene. Mol Cell Biol. 15:351-7.

Tsoi SC, Zheng J et al. 2001. Differential expression of lactate dehydrogenase isozymes (LDH) in human placenta with high expression of the LDH-A(4) isozyme in the endothelial cells of pre-eclampsia villi. Placenta. 22:317-22.

Tuuli MG, Longtime MS et al. 2011. Review: oxygen and trophoblast biology – a source of controversy. Placenta. 32:S109-18.

Wahli W. 2002. Peroxisome proliferator-activated receptors (PPARs): from metabolic control to epidermal wound healing. Swiss Med Wkly. 132:83-91.

Wakabayashi H, Tsuchiya M, et al. 1996. Hereditary deficiency of lactate dehydrogenase H-subunit. Intern Med. 35:550-4.

Wang GL, Jiang BH et al. 1995. Hypoxia-inducible factor 1 is a basic-helix-loop-helix PAS heterodimer regulated by cellular O2 tension. Proc Natl Acad Sci U S A. 92:5510-4.

Wei W and Hu YY. 2014. Expression of hypoxia-regulated genes and glycometabolic genes in placenta from patients with intrahepatic cholestasis of pregnancy. Placenta. 35:732-6.

Weiss H, Dundl M et al. 2016. The trophoblast plug during early pregnancy: a deeper insight. Histochem Cell Biol. 146:749-56.

Woods L, Perez-Harcia V, and Hemberger M. 2018. Regulation of placental development and its impact on fetal growth – new insights from mouse models. Front Endocrinol (Lausanne). 9:570.

Zamudio S, Wu Y et al. 2007. Human placental hypoxia-inducible factor-1alpha expression correlates with clinical outcomes in chronic hypoxia in vivo. Am J Pathol. 170:2171-9.

Zeczycki TN, Maurice MS et al. 2010. Inhibitors of pyruvate carboxylase. Open Enzym Inhib J. 3:8-26.